Comparison of Classical Dynamical Predictions for Low-Speed, Weak-Gravity, and Low-Speed Weak-Gravity Chaotic Systems

Liang Shiuan-Ni

M. Sc.

School of Science
Monash University
Sunway Campus, Malaysia

Submitted in fulfillment of the requirements
for the degree of Doctor of Philosophy

June 2012

Table of contents

Table of contents ii

Abstract iv

General declaration vi

Acknowledgements ix

1. Introduction 1
- 1.1 Low-speed chaotic dynamical system 1
- 1.2 Weak-gravity and low-speed weak-gravity chaotic dynamical systems 4
- 1.3 Objectives of the research 6
- 1.4 Methodology 7

Thesis chapter declaration 11

2. Low-speed chaotic dynamical system (I) - Kicked particle 12
- 2.1 Introduction 12
- 2.2 Calculation 13
- 2.3 Results - Statistical predictions 18
  - 2.3.1 Mean, standard deviation and probability distribution 18
  - 2.3.2 Momentum diffusion 35

Thesis chapter declaration 48

3. Low-speed chaotic dynamical system (II) - Scattering system 49
- 3.1 Introduction 49
- 3.2 Calculation 50
- 3.3 Results - Statistical predictions: Mean, standard deviation, probability distribution, mean dwell time, reflection and transmission coefficients 52

Thesis chapter declaration **65**

4. Low-speed weak-gravity chaotic dynamical system - Bouncing ball system **66**

4.1 Introduction 66

4.2 Newtonian and relativistic free-fall motion 67

4.3 Derivation of the special-relativistic and general-relativistic maps 71

4.4 Calculation 73

4.5 Results 78

4.5.1 Single-trajectory predictions 78

4.5.2 Statistical predictions: Mean, standard deviation and probability distribution 92

5. Summary and Discussion **110**

References **113**

Appendix – Publication list and reprints **121**

Abstract

There are three fundamental classical theories which can be used to study the motion of dynamical systems: Newtonian mechanics (**NM**), special-relativistic mechanics (**SRM**) and general-relativistic mechanics (**GRM**). It is conventionally believed that (i) the predictions of SRM are well approximated by those of NM in the low-speed limit, (ii) the predictions of GRM are well approximated by those of SRM in the weak-gravity limit, and (iii) the predictions of GRM are well approximated by those of NM in the low-speed weak-gravity limit. In my research project, numerically-accurate predictions of the theories were compared in the three limits for chaotic dynamical systems to check the validity of the conventional beliefs. The results of this study have overturned the conventional beliefs: for each limit, I showed that the two predictions can rapidly disagree completely. This new conceptual understanding of the relationships between the predictions of the theories for low-speed, weak-gravity, and low-speed weak-gravity chaotic dynamical systems implies that physicists and engineers must replace the theories they have conventionally been using to study these systems with the more general theories. In particular, NM must be replaced by SRM for low-speed systems, SRM must be replaced by GRM for weak-gravity

systems, and NM must be replaced by GRM for low-speed weak-gravity systems. These paradigm shifts could potentially lead to new understanding and discoveries in these systems.

General Declaration

In accordance with Monash University Doctorate Regulation 17/ Doctor of Philosophy and Master of Philosophy (MPhil) regulations the following declarations are made:

I hereby declare that this thesis contains no material which has been accepted for the award of any other degree or diploma at any university or equivalent institution and that, to the best of my knowledge and belief, this thesis contains no material previously published or written by another person, except where due reference is made in the text of the thesis.

This thesis includes three original papers: two published and one submitted for publication in peer-reviewed journals. The core theme of the thesis is comparison of classical dynamical predictions for low-speed, weak-gravity, and low-speed weak-gravity chaotic systems. The ideas, development and writing up of all the papers in the thesis were the principal responsibility of myself, the candidate, working within the School of Science under the supervision of Associate Professor Lan Boon Leong.

The inclusion of co-authors reflects the fact that the work came from active

collaboration between researchers and acknowledges input into team-based research.

In the case of chapters 2, 3 and 4, my contribution to the work involved the following:

Thesis chapter	Publication title	Publication status	Nature and extent of candidate's contribution
2	Statistical Predictions for the Dynamics of a Low-Speed System: Newtonian Versus Special-Relativistic Mechanics	Published *PLoS ONE*	Conceived and designed the experiments, performed the experiments, analyzed the data, contributed materials/analysis tools and wrote the manuscript. 70 %
3	Newtonian Versus Special-Relativistic Statistical Predictions for the Dynamics of a Low-Speed Scattering System	submitted *PLoS ONE*	
4	Comparison of Newtonian and Special-Relativistic Trajectories with the General-Relativistic Trajectory for a Low-Speed Weak-Gravity System	Published *PLoS ONE*	

I have renumbered sections of submitted or published papers in order to generate a consistent presentation within the thesis.

Notice 1

Under the Copyright Act 1968, this thesis must be used only under the normal conditions of scholarly fair dealing. In particular no results or conclusions should be extracted from it, nor should it be copied or closely paraphrased in whole or in part without the written consent of the author. Proper written acknowledgement should be made for any assistance obtained from this thesis.

Notice 2

I certify that I have made all reasonable efforts to secure copyright permissions for third-party content included in this thesis and have not knowingly added copyright content to my work without the owner's permission.

Liang Shiuan-Ni

4 June 2012

Acknowledgements

I take this opportunity to record my gratitude to the following:

Associate Professor Lan Boon Leong, my supervisor who not only called my attention to Nonlinear Dynamics and Chaos, but also gave me invaluable advice and full support during this research. Under his guidance, I gained an insight about performing numerically-accurate calculations and learned how to produce high-quality research papers.

Professor Tung Roh-Suan and Professor Chen Chiang-Mei for sharing with me their knowledge about general-relativistic free fall motion of a particle. Without their advice, my work on this part would become more difficult.

Ms. Tong Siew Peng, Ms. Bawani Veeriah and Ms. Kan Wen Ni – the mamas of the school research offices for making everything run smoothly by lending their hands to me whenever I encountered any administrative problem during my candidature.

Also, Associate Professor Woo Ko Choong, Associate Professor Raymond Ooi Chong Heng and Associate Professor Lim Yau Yan for being the review panel members of my oral presentations.

Last but not least, I am grateful to my family and friends for their patience,

encouragement and love.

Liang Shiuan-Ni

June 2012

Chapter 1
Introduction

There are 3 fundamental classical theories in physics which can be used to study the motion of a dynamical system: Newtonian mechanics (**NM**), special-relativistic mechanics (**SRM**) and general-relativistic mechanics (**GRM**). Over the last one hundred years, physicists have conventionally believed that the 3 fundamental theories are *generally* related as follows (Einstein,1961; Lapidus, 1972b; Ford and Mantica, 1992; McComb, 1999; Hartle, 2003):

(1) NM is the *low-speed* limit of SRM;

(2) SRM is the *weak-gravity* limit of GRM;

(3) NM is the *low-speed weak-gravity* limit of GRM.

1.1 Low-speed chaotic dynamical system

(Relationship #1:) It is conventionally believed (Einstein,1961; Ford and Mantica, 1992; Corben and Stehle, 1994; McComb, 1999) that if the speed of a dynamical system remains low, i.e. much less than the speed of light c, then the dynamics predicted by SRM stays well approximated by the dynamics predicted

by NM for the same parameter(s) and initial conditions.

In recent times, much progress has been made in studying the special-relativistic dynamics of nonlinear systems, where gravity does not play a role in the dynamics of the system, for example, an electron in a time-varying electric field in a plasma (Chernikov *et al*., 1989; Nomura *et al*., 1992), the relativistic kicked harmonic oscillator (Longcope and Sudan, 1987; Karimabadi and Angelopoulos, 1989; Ashkenazy and Horwitz, 2000; Horwitz and Ashkenazy, 2000), transport properties in the relativistic periodically kicked rotor (Matrasulov *et al*., 2005), the diffusive ionization of a relativistic hydrogen-like atom (Matrasulov, 1999), and the relativistic motion of a particle acted upon by a constant force (Lapidus, 1972a). The research work in (Lapidus, 1972a) compared the equations of the Newtonian and special-relativistic trajectories without studying the closeness between the two trajectories numerically.

Although dynamical systems where gravity is not involved in the dynamics have been studied in the framework of SRM, the numerical comparison between the closeness of the Newtonian and special-relativistic predictions for low-speed chaotic dynamical systems has never been done before until the recent work of Lan (2006, 2007, 2008, 2009a, 2009b; Lan and Cheng, 2010; Lan and Borondo, 2011). Since 2006, Lan (2006, 2007, 2008, 2009a, 2009b; Lan and Cheng, 2010;

Lan and Borondo, 2011) has showed numerically with three prototypical chaotic dynamical systems that, although the system is moving at a low speed, the Newtonian and special-relativistic trajectories of the same parameters and initial conditions can rapidly diverge and become completely different from each other if the trajectories are chaotic.

The first counterexample chaotic dynamical system is (Lan, 2006, 2009b) a model Hamiltonian system – the periodically delta-kicked particle. Lan found that the Newtonian and special-relativistic trajectories eventually become completely different regardless of whether the trajectories are chaotic or non-chaotic. The breakdown of agreement between the two trajectories is, however, much faster in the chaotic case compared to the non-chaotic case because the difference between the two trajectories grows exponentially in the former case but linearly in the latter case.

Similar rapid breakdown of agreement was also found numerically in the second counterexample: a model dissipative system (Lan, 2007, 2008, 2009a; Lan and Cheng, 2010), if the trajectories are chaotic. However, if the trajectories are non-chaotic, there is no breakdown of agreement between the two trajectories.

The third counterexample is a model scattering system (Lan and Borondo, 2011). Similar rapid breakdown of agreement was also found numerically in this

third counterexample. For this scattering system (Lan and Borondo, 2011), the rapid breakdown of agreement is due to a sufficiently-long exponential growth of the difference between the two trajectories in the scattering region when the scattering is chaotic.

The surprising finding in (Lan, 2006, 2007, 2008, 2009a, 2009b; Lan and Cheng, 2010; Lan and Borondo, 2011) for Relationship #1 raises the fundamental question of whether, for low-speed chaotic dynamical systems, Relationship #1 is true for other predictions besides the trajectory.

1.2 Weak-gravity and low-speed weak-gravity chaotic dynamical systems

(Relationship #2:) When gravity plays a role in the dynamics of a system but only weakly, i.e. gravitational potential $<< c^2$ (Davies, 1992), it is conventionally believed (Einstein, 1961; Lapidus, 1972b) that the dynamical prediction of GRM is well approximated by the prediction of SRM for the same parameter(s) and initial conditions.

(Relationship #3:) If the speed of a dynamical system is low, i.e., $v << c$, and gravity plays a role in the dynamics but is weak, it is conventionally believed

(Einstein, 1961; Lapidus, 1972b) that the dynamics predicted by GRM is well approximated by the dynamics predicted by NM for the same parameter(s) and initial conditions.

In recent times, much progress has been made in studying the relativistic dynamics of nonlinear systems, where gravity plays a role in the dynamics of the systems. For example, the non-chaotic pendulum (Erkal, 2000) has been studied numerically in the context of SRM, where the special-relativistic period was close to the Newtonian period when the speed of the system was low. Another example is the study of the relativistic non-chaotic motion of a free particle in a uniform gravitational field (Lapidus, 1972b; Desloge, 1990) in the context of SRM and GRM. The research work in (Lapidus, 1972b; Desloge, 1990) compared the equations of the Newtonian, special-relativistic and general-relativistic trajectories without studying the closeness among the trajectories numerically.

Although dynamical systems where gravity is involved in the dynamics have been studied in the frameworks of SRM and GRM, in my literature search, I have not found any research work which compares the closeness of the dynamical predictions of NM (SRM) and GRM for low-speed weak-gravity (weak-gravity) chaotic dynamical systems numerically. The finding in (Lan, 2006, 2007, 2008, 2009a, 2009b; Lan and Cheng, 2010; Lan and Borondo, 2011) for Relationship #1

casts a long shadow of doubt on the validity of Relationship #3 (#2) for trajectory predictions for low-speed weak-gravity (weak-gravity) chaotic dynamical systems. Furthermore, the finding in (Lan, 2006, 2007, 2008, 2009a, 2009b; Lan and Cheng, 2010; Lan and Borondo, 2011) also raises the fundamental question of whether, for low-speed weak-gravity (weak-gravity) chaotic dynamical systems, Relationship #3 (#2) is true for other predictions besides the trajectory.

1.3 Objectives of the research

The objectives of my research is to determine whether

(1) the statistical predictions of SRM for a low-speed system are always well approximated by the NM predictions,

(2) the single-trajectory and statistical predictions of GRM for a weak-gravity system are always well approximated by the SRM predictions,

(3) the single-trajectory and statistical predictions of GRM for a low-speed weak-gravity system are always well approximated by the NM predictions,

if the system is chaotic. The statistical predictions which will be studied are the means, standard deviations and probability distributions of position and momentum, the momentum diffusion, the mean dwell time, and the reflection and

transmission coefficients - these quantities are determined from an ensemble of trajectories.

1.4 Methodology

To address the 3 objectives of the research, it is imperative that the predictions of the theories are numerically calculated accurately for comparison. The strategy I have adopted to achieve this is to only study chaotic dynamical systems where the equations of motion are reducible to mappings for the trajectory.

To address objective #1, the chaotic dynamical system for my research must meet the following criteria:

(1) gravity does not play a role in the dynamics of the system since gravity is not involved in Relationship #1 and, thus, objective #1,

(2) the mapping for the trajectory should be simple and can be studied easily to obtain accurate numerical results.

The chaotic kicked particle previously studied by Lan (2006, 2009b) meets the above criteria. For this spatially bounded Hamiltonian system, the Newtonian and special-relativistic maps are known as the standard map (Casati *et al.*, 1979;

Chirikov, 1979) and the relativistic standard map (Chernikov *et al*., 1989; Nomura *et al*., 1992) respectively.

I have also addressed objective #1 for the chaotic scattering system introduced by Beeker and Eckelt (1993). For this spatially unbounded system, the Newtonian map (Beeker and Eckelt, 1993) and special-relativistic map (Lan and Borondo, 2011) are also known. By studying the predictions for this chaotic scattering system, besides the mean, standard deviation and probability distribution, one can also study the predictions for other statistical quantities, such as mean dwell time, transmission and reflection coefficients, which cannot be studied for the chaotic kicked particle.

To address objectives #2 and #3, the chaotic dynamical system for my research must meet the following criteria:

(1) gravity plays a role in the dynamics of the system since gravity is involved in Relationships #2 and #3 and, thus, objectives #2 and #3,

(2) the Newtonian, special-relativistic and general-relativistic mappings for the trajectory should not be too difficult to solve numerically.

The bouncing ball system (Tufillaro *et al*., 1986; Tufillaro *et al*., 1992), where gravity governs the motion of the ball in between its impacts with a vertically oscillating 'table', meets the criteria above. The Newtonian map (Tufillaro *et al*.,

1986) for this bounded system is known, but the special-relativistic map and general-relativistic map are not known and so I had to derive them in my research project. In order to derive the general-relativistic map, I had to study and derive and solve the general-relativistic equations of motion for a free particle in a gravitational field due to a uniform sphere, which is the most challenging part of my thesis.

The accuracy of the single-trajectory and statistical quantity calculations were determined by the standard method (Lichtenberg and Lieberman, 1983) of comparing the less-accurate calculation with the more-accurate calculation. Each statistical quantity was calculated from an ensemble of trajectories.

Table 1 gives a summary of the dynamical quantities and the chaotic dynamical systems that were studied in my research project.

Table 1. Summary of the dynamical quantities and the chaotic dynamical systems that are studied in my research project.

Limit		(i) Low-speed		(ii) Weak-gravity (iii) Low-speed weak-gravity
Theories involved		(i) NM vs. SRM		(ii) SRM vs. GRM (iii) NM vs. GRM
System		Kicked particle	Scattering system	Bouncing ball system
Dynamical quantity	Single trajectory	√	√	o
	Mean trajectory	o	o	o
	Standard deviation	o	o	o
	Probability distribution	o	o	o
	Momentum diffusion	o		
	Mean dwell time		o	
	Transmission coefficient		o	
	Reflection coefficient		o	

Note: √ means that the dynamical quantity has already been studied by other researchers. o means that the dynamical quantity was studied in my research project.

Thesis Chapter Declaration

Monash University

Declaration for Thesis Chapter 2

Declaration by candidate

In the case of Chapter 2, the nature and extent of my contribution to the work was the following:

Nature of contribution	Extent of contribution (%)
Conceived and designed the experiments, performed the experiments, analyzed the data, contributed materials/analysis tools and wrote the manuscript.	70%

The following co-authors contributed to the work. Co-authors who are students at Monash University must also indicate the extent of their contribution in percentage terms:

Name	Nature of contribution	Extent of contribution (%) for student co-authors only
Dr. Lan Boon Leong	Supervisory role - Conceived and designed the experiments, analyzed the data, contributed materials/analysis tools and wrote the manuscript.	

Candidate's Signature		**Date**

Declaration by co-authors
The undersigned hereby certify that:

(1) the above declaration correctly reflects the nature and extent of the candidate's contribution to this work, and the nature of the contribution of each of the co-authors.
(2) they meet the criteria for authorship in that they have participated in the conception, execution, or interpretation, of at least that part of the publication in their field of expertise;
(3) they take public responsibility for their part of the publication, except for the responsible author who accepts overall responsibility for the publication;
(4) there are no other authors of the publication according to these criteria;
(5) potential conflicts of interest have been disclosed to (a) granting bodies, (b) the editor or publisher of journals or other publications, and (c) the head of the responsible academic unit; and
(6) the original data are stored at the following location(s) and will be held for at least five years from the date indicated below:

Location(s)	School of Science, Sunway Campus

		Date
Signature		

Chapter 2
Low-Speed Chaotic Dynamical System (I) - Kicked Particle

2.1 Introduction

In this chapter, I extend the Newtonian special-relativistic comparison for the low-speed periodically-delta-kicked particle from *single-trajectory* predictions (Lan, 2006) to *statistical* predictions – in particular, the mean, standard deviation and probability density function of the position and momentum – which are calculated from the same parameters and initial ensemble of trajectories. Calculating these statistical quantities directly from an ensemble of trajectories is far easier than solving the Newtonian and special-relativistic Liouville's equations numerically to first obtain the phase-space probability density functions.

Furthermore, momentum diffusion in Hamiltonian systems has been studied (Chirikov, 1979; Karney, 1983; Chernikov *et al*., 1990; Afanasiev *et al*., 1991; Chaĭkovsky and Zaslavsky, 1991; Ishizaki *et al*.,1991; Ishizaki *et al*., 1993; Ishizaki and Mori, 1997; Zaslavsky *et al*., 1997; Ishizaki and Mori, 1998; Lebœuf, 1998; Zheng and Kobe, 2006) extensively using Newtonian mechanics and it is

known that it can be anomalous. Considerable effort has been made recently to understand anomalous diffusion in Hamiltonian systems – see, for example, the article by Altmann and Kantz (2008) and the review by Zaslavsky (2002). However, a comparison of Newtonian and special-relativistic predictions for *low-speed* momentum diffusion has not been done. In this chapter, I also compare the low-speed momentum diffusion predicted by the two theories for the periodically-delta-kicked particle. Details of the kicked particle and numerical calculation are presented next (Sec. 2.2), followed by the discussion of the results (Sec. 2.3).

2.2 Calculation

The model Hamiltonian system is a one-dimensional system where the particle is subjected to a sinusoidal potential which is periodically turned on for an instant. The Newtonian equations of motion for the periodically-delta-kicked particle are easily integrated exactly (Casati *et al*., 1979; Chirikov, 1979) to yield a mapping, which is known as the standard map, of the dimensionless scaled position X and dimensionless scaled momentum P from just before the nth kick to just before the $(n+1)$th kick:

$$P_n = P_{n-1} - \frac{K}{2\pi}\sin(2\pi X_{n-1}) \tag{2.1}$$

$$X_n = (X_{n-1} + P_n) \bmod 1 \tag{2.2}$$

where n = 1,2,…, and K is a dimensionless positive parameter. For the standard map, the transition from weak (local) chaos to strong (global) chaos occurs at $K \approx 0.917$.

The special-relativistic equations of motion are also easily integrated exactly, producing a mapping known as the relativistic standard map (Chernikov *et al*., 1989; Nomura *et al*., 1992) for the dimensionless scaled position X and dimensionless scaled momentum P from just before the nth kick to just before the (n+1)th kick:

$$P_n = P_{n-1} - \frac{K}{2\pi}\sin(2\pi X_{n-1}) \tag{2.3}$$

$$X_n = \left(X_{n-1} + \frac{P_n}{\sqrt{1+\beta^2 P_n^2}} \right) \bmod 1 \tag{2.4}$$

where n = 1,2, …, and β, like K, is a dimensionless positive parameter. Since

$$\frac{v}{c} = \frac{\beta P}{\sqrt{1+(\beta P)^2}}\,, \tag{2.5}$$

$\beta P << 1$ implies $v << c$ (i.e., low speed), where v is the particle speed and c is the speed of light. Ciubotariu *et al*. (2002) have studied a dissipative version of the relativistic standard map to see how weak damping changes the phase-space structure around the origin described by the relativistic standard map; they did not

however compare the dynamical predictions of their dissipative *relativistic* standard map with the predictions of the dissipative *non-relativistic* standard map.

For both theories, the ensemble of trajectories is initially Gaussian distributed in position and momentum with means $\langle X_0 \rangle$ and $\langle P_0 \rangle$, and standard deviations σ_{X_0} and σ_{P_0}:

$$\rho(X_0, P_0) = \frac{1}{2\pi\sigma_{X_0}\sigma_{P_0}} \exp\left[-\frac{(X_0 - \langle X_0 \rangle)^2}{2\sigma_{X_0}^2} - \frac{(P_0 - \langle P_0 \rangle)^2}{2\sigma_{P_0}^2} \right]. \tag{2.6}$$

Each trajectory in the Newtonian (special-relativistic) ensemble is time-evolved using the standard map (relativistic standard map). For each theory, the mean trajectory, i.e., mean position and mean momentum, just before each kick is calculated from the ensemble of trajectories. First, the mean trajectory is calculated using 10^6 trajectories, where the accuracy of the double-precision calculation is determined by comparison with the quadruple-precision calculation. The mean trajectory is then recalculated using 10^7 trajectories with the same accuracy determination. Finally, the accuracy of the mean trajectory is determined by comparing the 10^6-trajectories calculation with the 10^7-trajectories calculation. The position and momentum standard deviations and probability density functions are calculated in the same manner.

As for the momentum diffusion, the statistical quantity that is typically used to study momentum diffusion is (Chirikov, 1979; Chernikov *et al*., 1990; Ishizaki

et al., 1991; Ishizaki *et al*., 1993; Lebœuf, 1998; Zheng and Kobe, 2006) the mean square momentum displacement (MSMD)

$$\left\langle \left(\Delta P_n\right)^2 \right\rangle \equiv \left\langle \left(P_n - P_0\right)^2 \right\rangle, \tag{2.7}$$

where <…> is an average over an ensemble of trajectories. The MSMD [Eq. (2.7)] can be expressed as the following sum:

$$\left\langle \left(\Delta P_n\right)^2 \right\rangle = \sum_{j=0}^{n-1} C_j(0) + 2\sum_{i=1}^{n-1}\sum_{j=0}^{n-1-i} C_j(i), \tag{2.8}$$

where

$$C_j(i) \equiv \left\langle u_j u_{j+i} \right\rangle$$

is the correlation of the momentum difference $u_j \equiv P_{j+1} - P_j$ and it is a function of kick i, and $i, j = 0,1,\ldots$. For the Newtonian standard map [Eqs. (2.1) and (2.2)] and the relativistic standard map [Eqs. (2.3) and (2.4)] , the correlation function is given by

$$C_j(i) = K^2 \left\langle \sin\left(2\pi X_j\right) \sin\left(2\pi X_{j+i}\right) \right\rangle \Big/ 4\pi^2 \,. \tag{2.9}$$

Eq. (2.8) can be rewritten as

$$\left\langle \left(\Delta P_n\right)^2 \right\rangle = \left\langle \left(\Delta P_{n-1}\right)^2 \right\rangle + C_{n-1}(0) + 2\sum_{i=1}^{n-1} C_{n-1-i}(i). \tag{2.10}$$

Eq. (2.10) shows that the MSMD at kick n can be rewritten as the MSMD at kick (n-1) plus a sum involving correlation functions $C_{n-1-i}(i) \equiv \left\langle u_{n-1-i} u_{n-1} \right\rangle$ where i = 0,1,…, n-1. I will refer to Eq. (2.10) at the end of the results section.

In previous studies (Chirikov, 1979; Ishizaki *et al*., 1991; Zheng and Kobe,

2006) of momentum diffusion in the Newtonian standard map, an initially non-localized semi-uniform ensemble, where the initial positions are uniformly distributed and the initial momentums are all the same, is used in the numerical calculation of the MSMD. Previous studies (Ishizaki *et al*., 1991; Zheng and Kobe, 2006) of the Newtonian standard map have shown that, for parameter K where accelerator mode islands exist, the MSMD has a power law dependence on the kick n: Dn^{α} where $1 < \alpha < 2$. In this case, the diffusion is termed anomalous. In contrast, for parameter K where there is no accelerator mode island, the diffusion is normal – the MSMD grows linearly (Chirikov, 1979; Ishizaki *et al*., 1991; Zheng and Kobe, 2006).

In my calculations, besides the initially non-localized semi-uniform ensemble, I also use an initially localized ensemble where the initial positions and momentums are both Gaussian distributed (see Eq. (2.6)) with means $\langle X_0 \rangle$ and $\langle P_0 \rangle$, and standard deviations σ_{X_0} and σ_{P_0}. The accuracy of the MSMD is determined in the similar way to the mean trajectory, however, to obtain a higher accuracy for the MSMD, the 30-significant-figure calculation is used instead of the double-precision calculation.

2.3 Results - Statistical predictions

2.3.1 Mean, standard deviation and probability distribution

In this section, I will present three examples to illustrate the general results. In the first example, the map parameters are $K = 7.0$ and $\beta = 10^{-7}$. The Newtonian and special-relativistic ensembles are both initially Gaussian distributed in phase space with means $\langle X_0 \rangle = 0.5$ and $\langle P_0 \rangle = 99.9$, and standard deviations $\sigma_{X_0} = \sigma_{P_0} = 10^{-10}$, and thus initially localized in the chaotic 'sea' in phase space. Fig. 2.1 shows that the Newtonian mean position and mean momentum agree with the special-relativistic mean position and mean momentum for the first 16 kicks only, the two mean trajectories are completely different from kick 17 onwards.

The breakdown of agreement between the Newtonian and special-relativistic mean trajectories in Fig. 2.1 can be understood as follows. In either the Newtonian or special-relativistic case, the position and momentum standard deviations grow (Fox and Elston, 1994; Lan, 1994), on average, exponentially initially because the trajectories in the ensemble are chaotic. But as long as the position standard deviation remains small ($<<1$), the mean trajectory is (Fox and Elston, 1994; Lan, 1994) well-approximated by the single trajectory with the

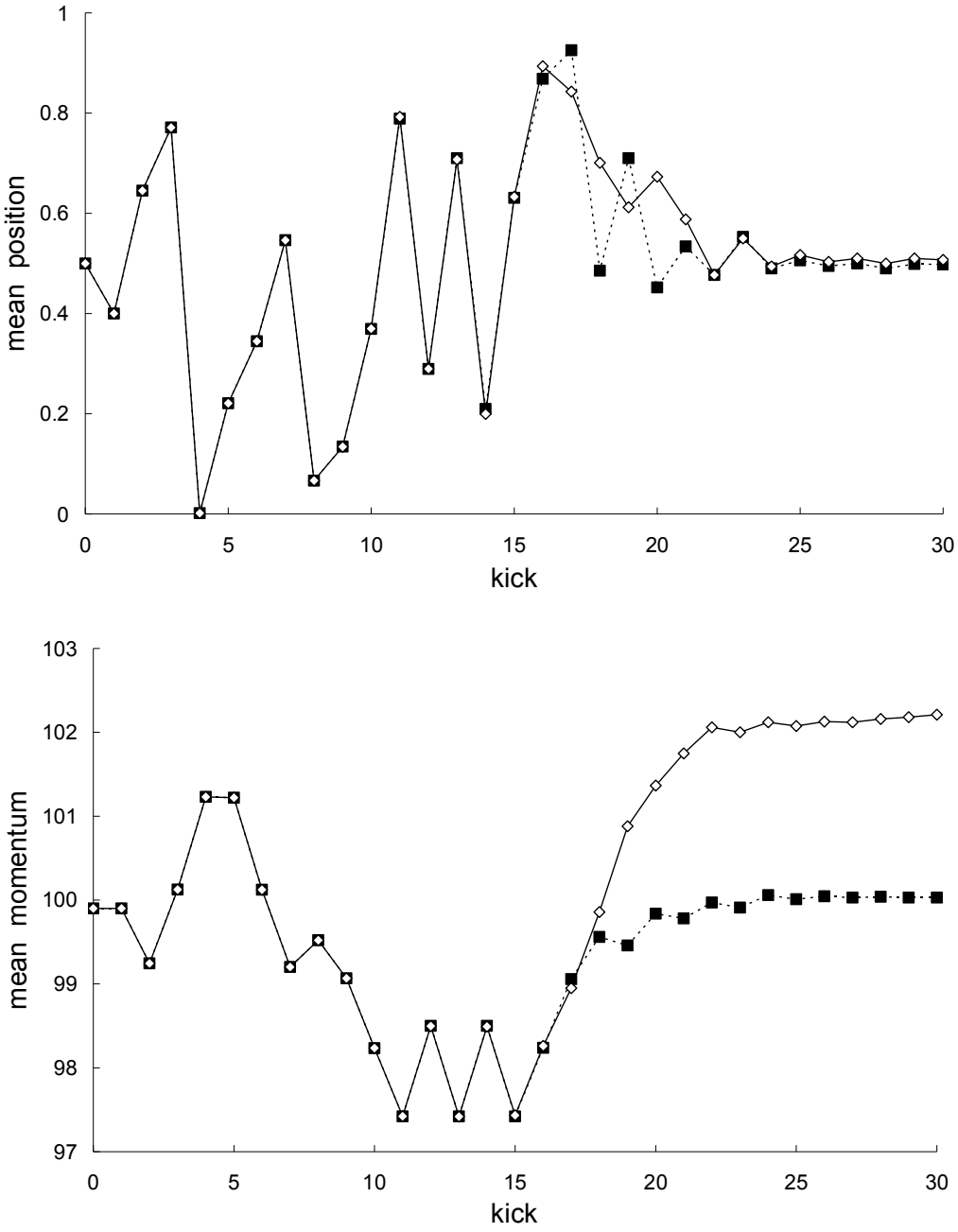

Figure 2.1. Newtonian (squares) and special-relativistic (diamonds) mean positions (top plot) and mean momentums (bottom plot) for the first example.

same initial conditions as the mean trajectory. The agreement between the single trajectory and mean trajectory breaks down when the position standard deviation saturates (Fox and Elston, 1994; Lan, 1994), that is, when the position probability density becomes delocalized over the entire position interval, which triggers the delocalization of the momentum probability density. Fig. 2.2 shows that the Newtonian and special-relativistic position standard deviations saturate at kick 19. In each theory, before the saturation of the position probability density, the exponential growth constants of the standard deviations are about 1.0, which are

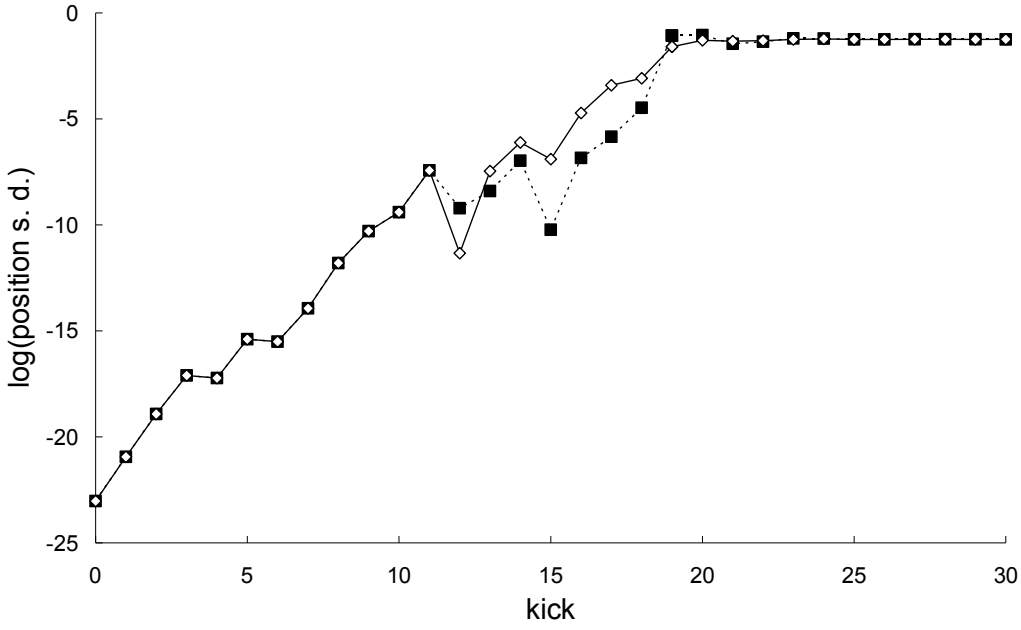

Figure 2.2. Natural-log of the Newtonian (squares) and special-relativistic (diamonds) position standard deviations for the first example.

close to the Lyapunov exponent of 1.27 for the single trajectory. Thus, in either the Newtonian (see Fig. 2.3) or special-relativistic (see Fig. 2.4) case, the mean trajectory is well-approximated by the single trajectory for the first 18 kicks only. The complete disagreement between the Newtonian and special-relativistic mean trajectories at kick 17 and kick 18 is therefore due to the complete disagreement of the Newtonian single trajectory and the special-relativistic single trajectory, which are both chaotic with Lyapunov exponent of 1.27, from kick 17 onwards. Since the position and momentum difference between the chaotic Newtonian and special-relativistic single trajectories grows exponentially at a rate approximately given by the Lyapunov exponent (Lan, 2006), we can estimate when the agreement between the two single trajectories breaks down and thus when the two mean trajectories breaks down. In particular, the position difference between the two single trajectories with the same initial conditions is 4.99×10^{-9} after 1 kick and, assuming that the exponential growth constant is 1.27, it grows to 0.1 (the maximum possible position difference is 1) after 14 kicks, which is close to the actual 17 kicks.

Furthermore, the difference between the Newtonian and special-relativistic mean trajectories grow exponentially up to kick 18 (see Fig. 2.5) because the

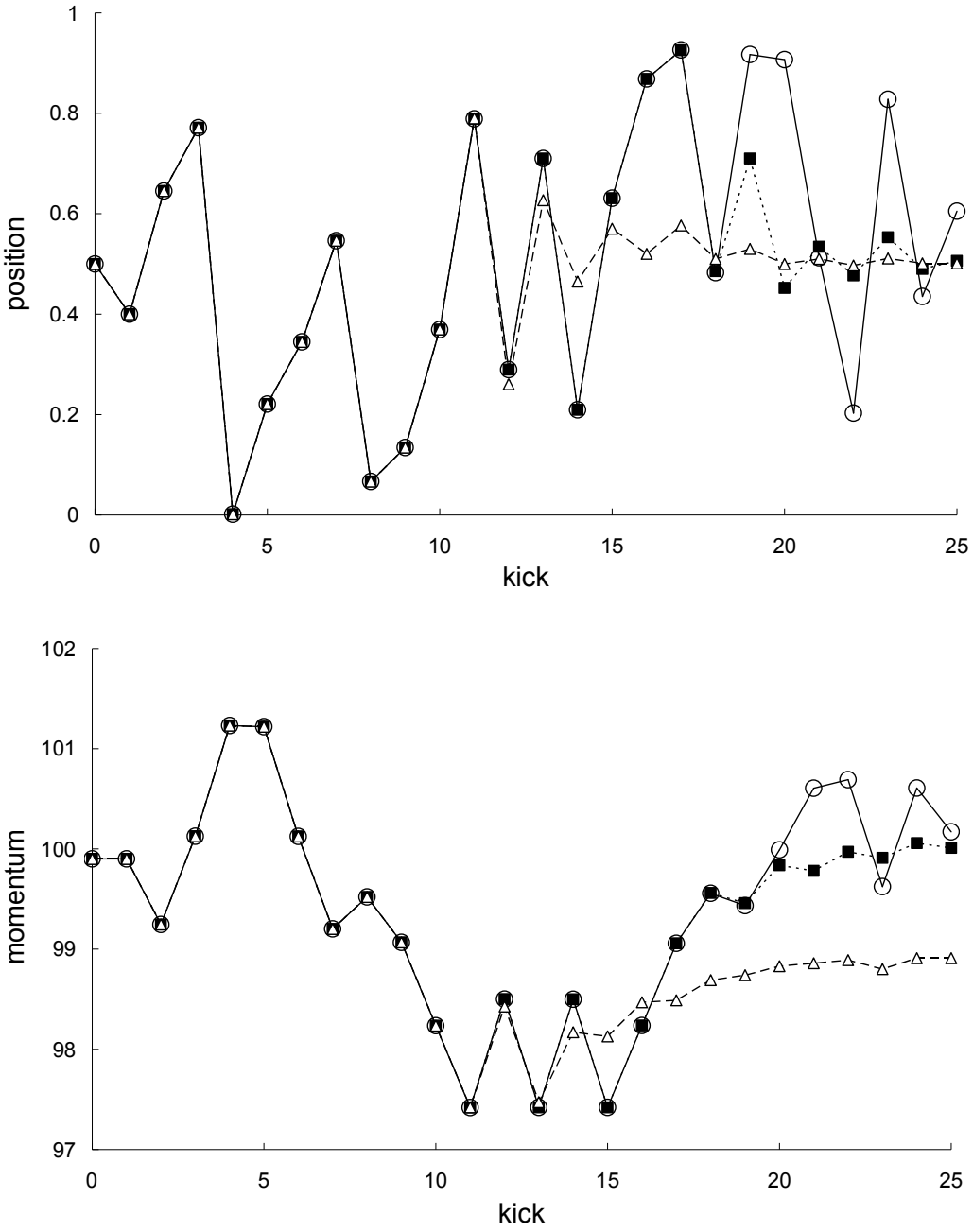

Figure 2.3. Newtonian single trajectory (circles), Newtonian mean trajectory for the first example (squares), and Newtonian mean trajectory for the second example (triangles): positions (top plot) and momentums (bottom plot).

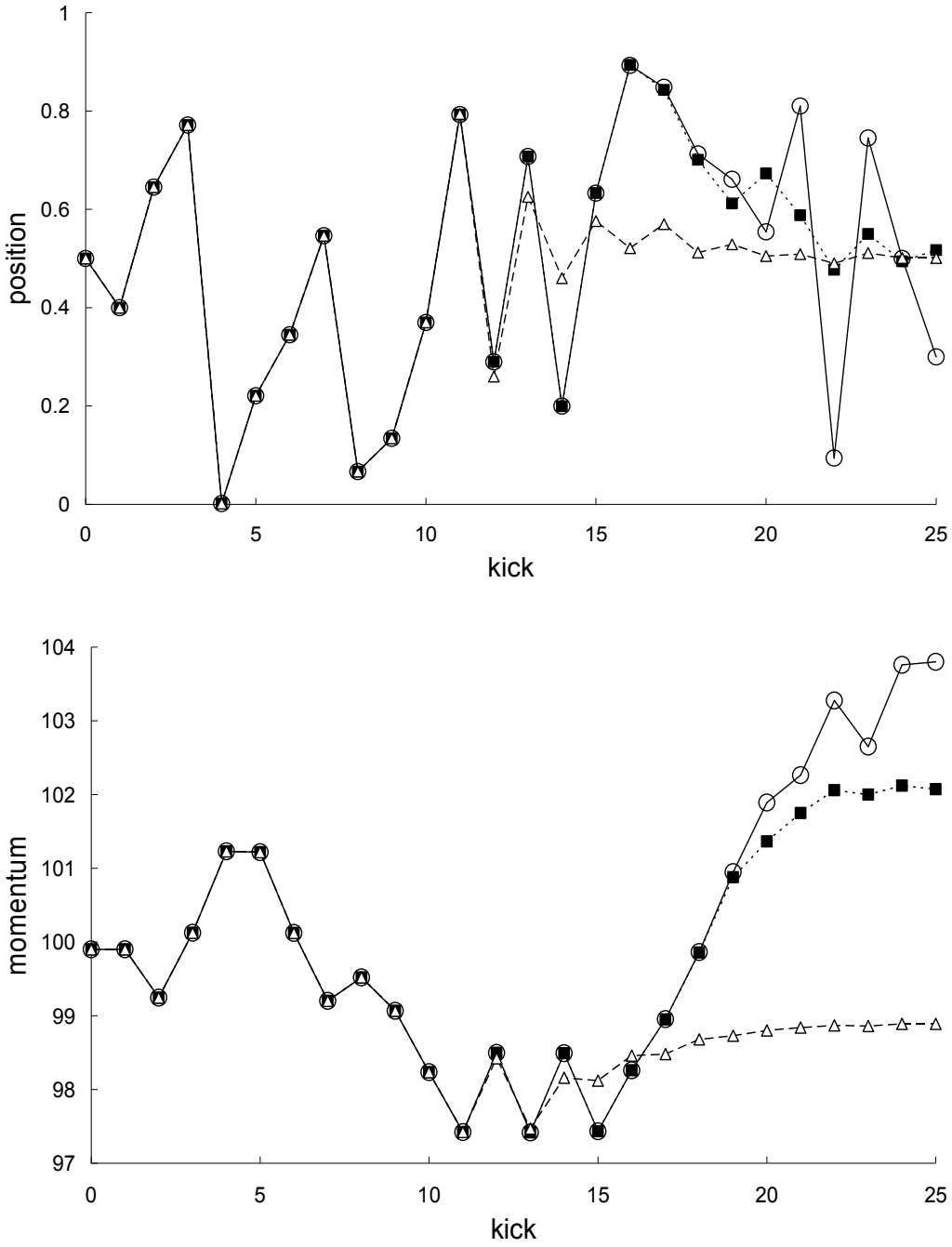

Figure 2.4. Special-relativistic single trajectory (circles), special-relativistic mean trajectory for the first example (squares), and special-relativistic mean trajectory for the second example (triangles): positions (top plot) and momentums (bottom plot).

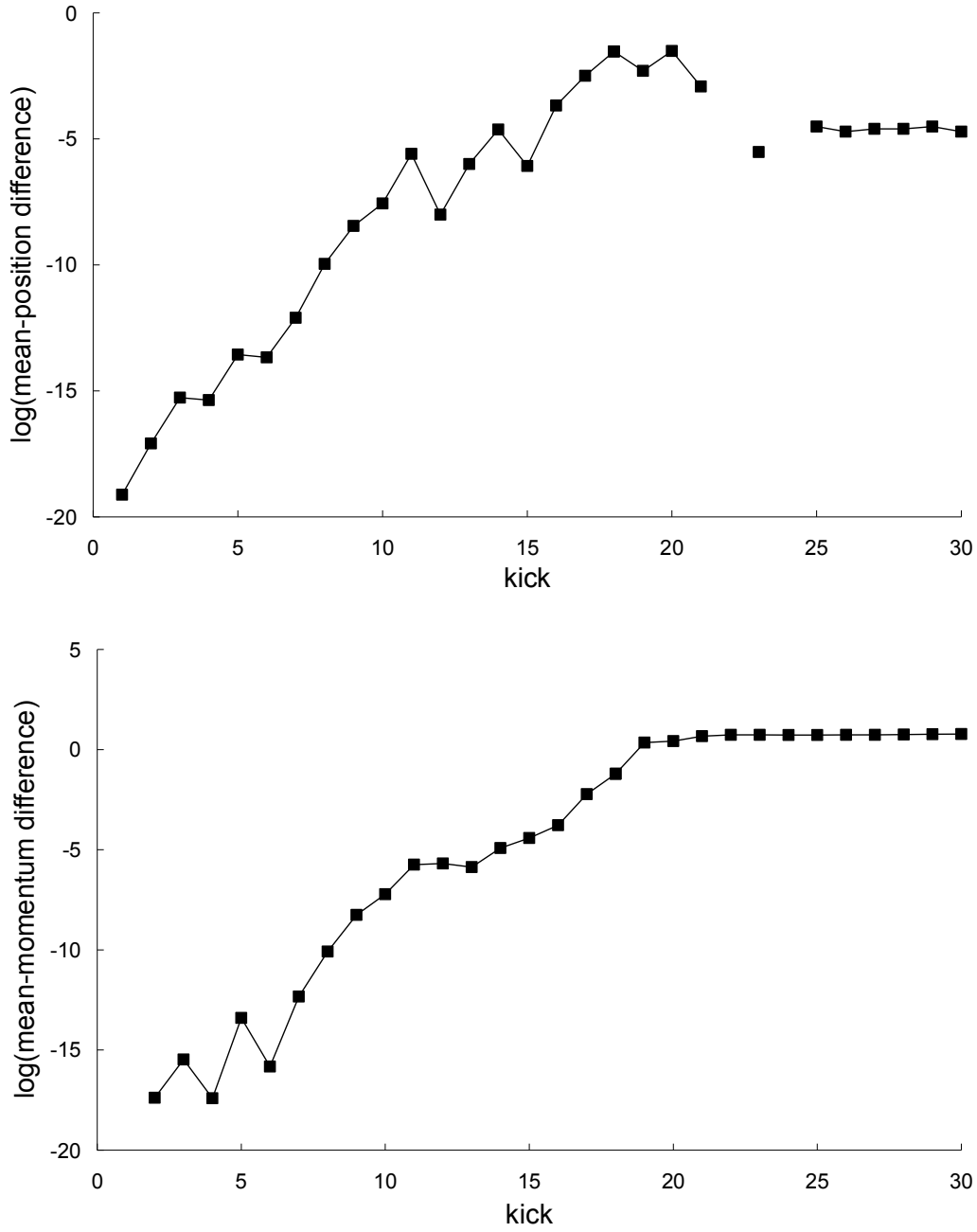

Figure 2.5. Natural-log of the absolute value of the difference between the Newtonian and special-relativistic mean positions (top plot) and mean momentums (bottom plot) for the first example. The mean-position differences at kick 22 and 24 cannot be resolved with the accuracy I have for the Newtonian and special-relativistic mean positions at those kicks.

difference between the Newtonian and special-relativistic chaotic single trajectories grow (Lan, 2006) exponentially. Hence, the breakdown of agreement between the Newtonian and special-relativistic mean trajectories is rapid because of the exponential growth of the difference between the two mean trajectories.

Figure 2.2 and Fig. 2.6 show that the position and momentum standard deviations predicted by the two theories also do not always agree. The breakdown of agreement occurs at kick 12. This rapid breakdown of agreement is, see Fig. 2.7, due to the exponential growth of the difference between the Newtonian and special-relativistic standard deviations, for both position and momentum, up to kick 12. In Fig. 2.7, the exponential growth constants of the position and momentum standard-deviation differences, which are measured from kick 10 to kick 19 (the accuracy of the standard-deviation differences before kick 10 cannot be resolved with the accuracy I have for the standard deviations), are 1.36 and 1.38 respectively. These growth constants are slightly larger than the Lyapunov exponents of 1.27 for the Newtonian and special-relativistic single trajectories.

Together, Fig. 2.1, Fig. 2.2 and Fig. 2.6 show that the agreement between the statistical predictions of the two theories, Newtonian and special relativistic, for the position and momentum means and standard deviations breaks down from

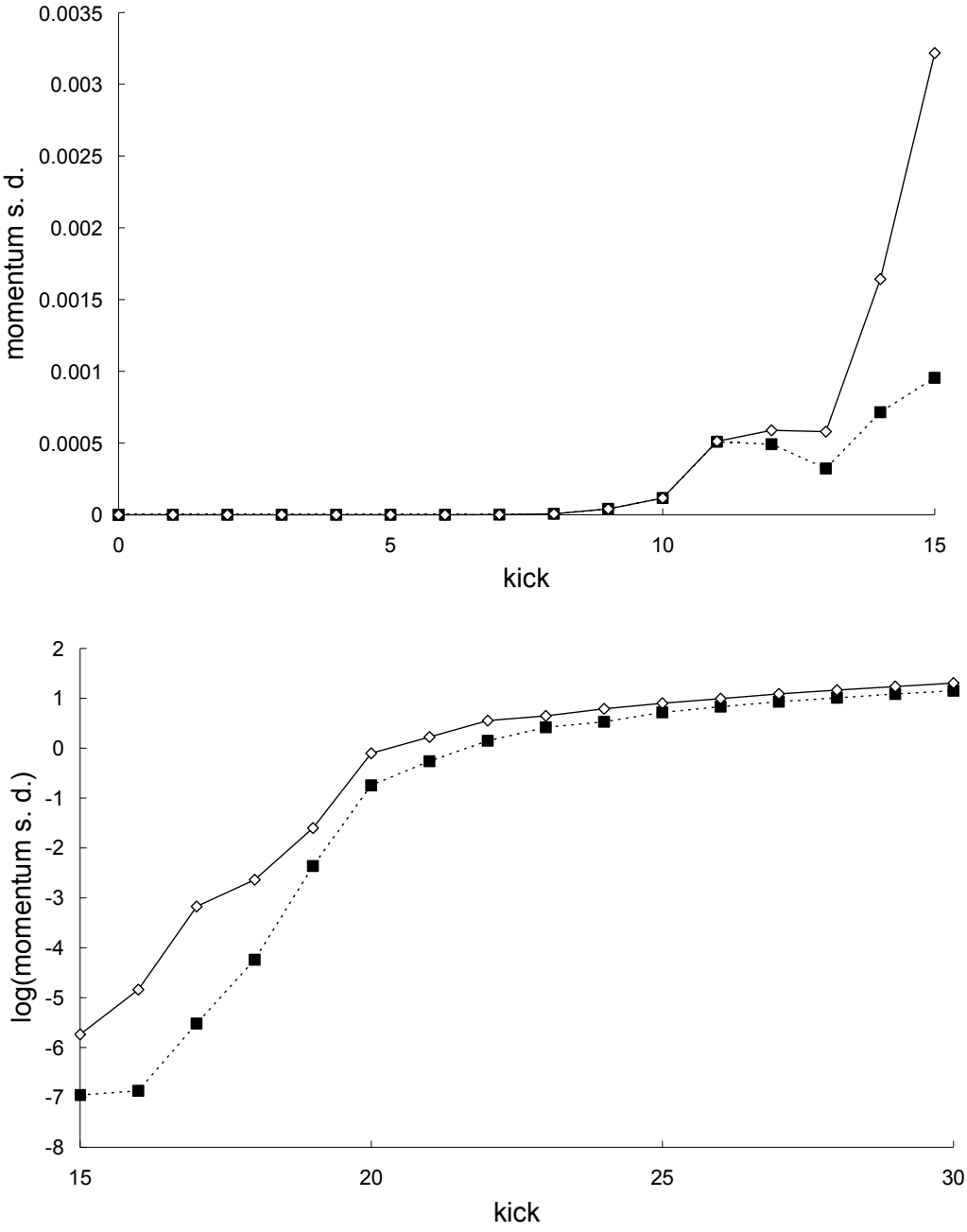

Figure 2.6. Newtonian (squares) and special-relativistic (diamonds) momentum standard deviations for the first example: first 15 kicks (top plot), kick 15 to 30 (bottom plot). The Newtonian and special-relativistic momentum standard deviations in the bottom plot are completely different from each other - they appear to be close from kick 25 onwards because the natural log of the standard deviations is plotted.

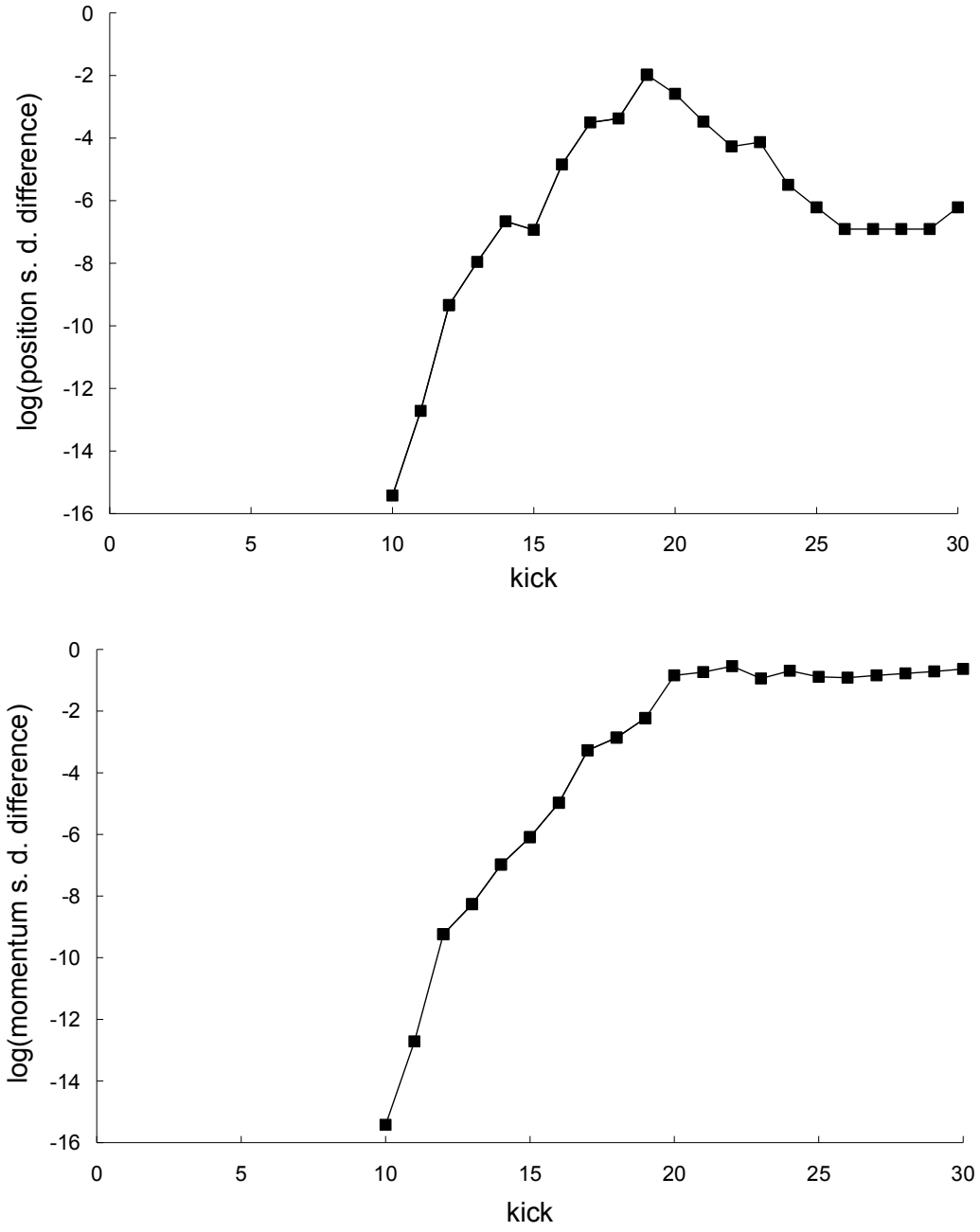

Figure 2.7. Natural-log of the absolute value of the difference between the Newtonian and special-relativistic position standard deviations (top plot) and momentum standard deviations (bottom plot) for the first example. The standard-deviation differences from kick 1 to 9 cannot be resolved with the accuracy I have for the Newtonian and special-relativistic standard deviations at those kicks.

kick 12 onwards even though the mean particle speed is low, only 0.001% of the speed of light since $\beta = 10^{-7}$. Fig. 2.8 shows the different Newtonian and special-relativistic position and momentum probability densities at kick 17.

In the second example, the parameters and initial means are the same as those in the first example but the initial standard deviations are larger: $\sigma_{X_0} = \sigma_{P_0} = 10^{-8}$. In this case, Fig. 2.9 shows there is no breakdown of agreement between the mean trajectory predictions of the two theories. In addition, Fig. 2.10 shows there is also no breakdown of agreement between the position and momentum standard deviations predicted by the two theories.

The results in Fig. 2.9 and Fig. 2.10 for the second example can be understood as follows. Fig. 2.3 and Fig. 2.4 show that the single trajectory is close to the mean trajectory for the first 12 kicks only, in either the Newtonian or special-relativistic case. Thus, for the first 12 kicks, the Newtonian and special-relativistic mean trajectories are close because the Newtonian and special-relativistic single trajectories are close (recall, the agreement between the two single trajectories only breaks down at kick 17). Furthermore, the Newtonian and special-relativistic standard deviations are, like the means, still very close at kick 13 when the position standard deviations saturate. In other words, the

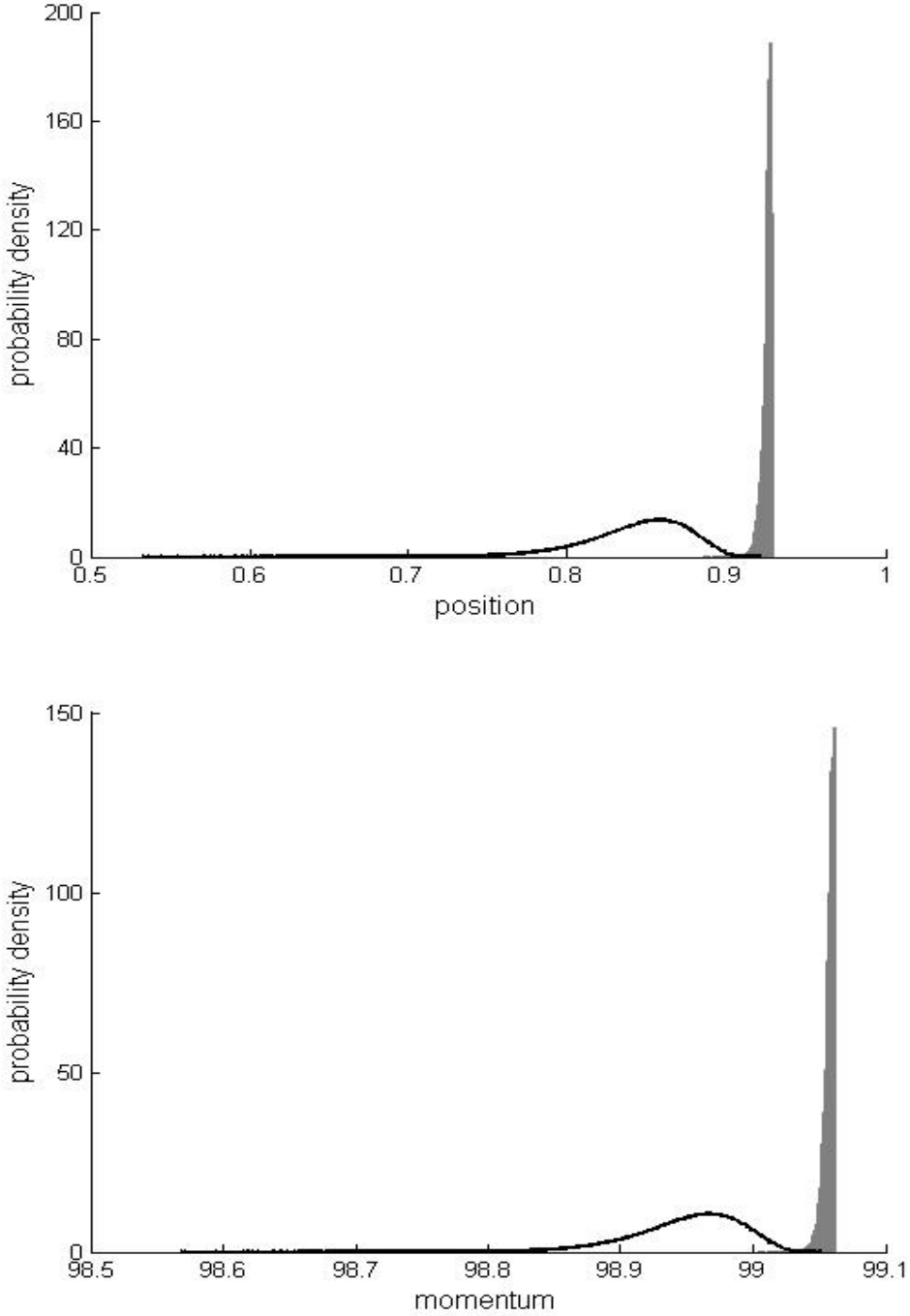

Figure 2.8. Newtonian (shaded grey) and special-relativistic (bold line) position (top plot) and momentum (bottom plot) probability densities for the first example at kick 17.

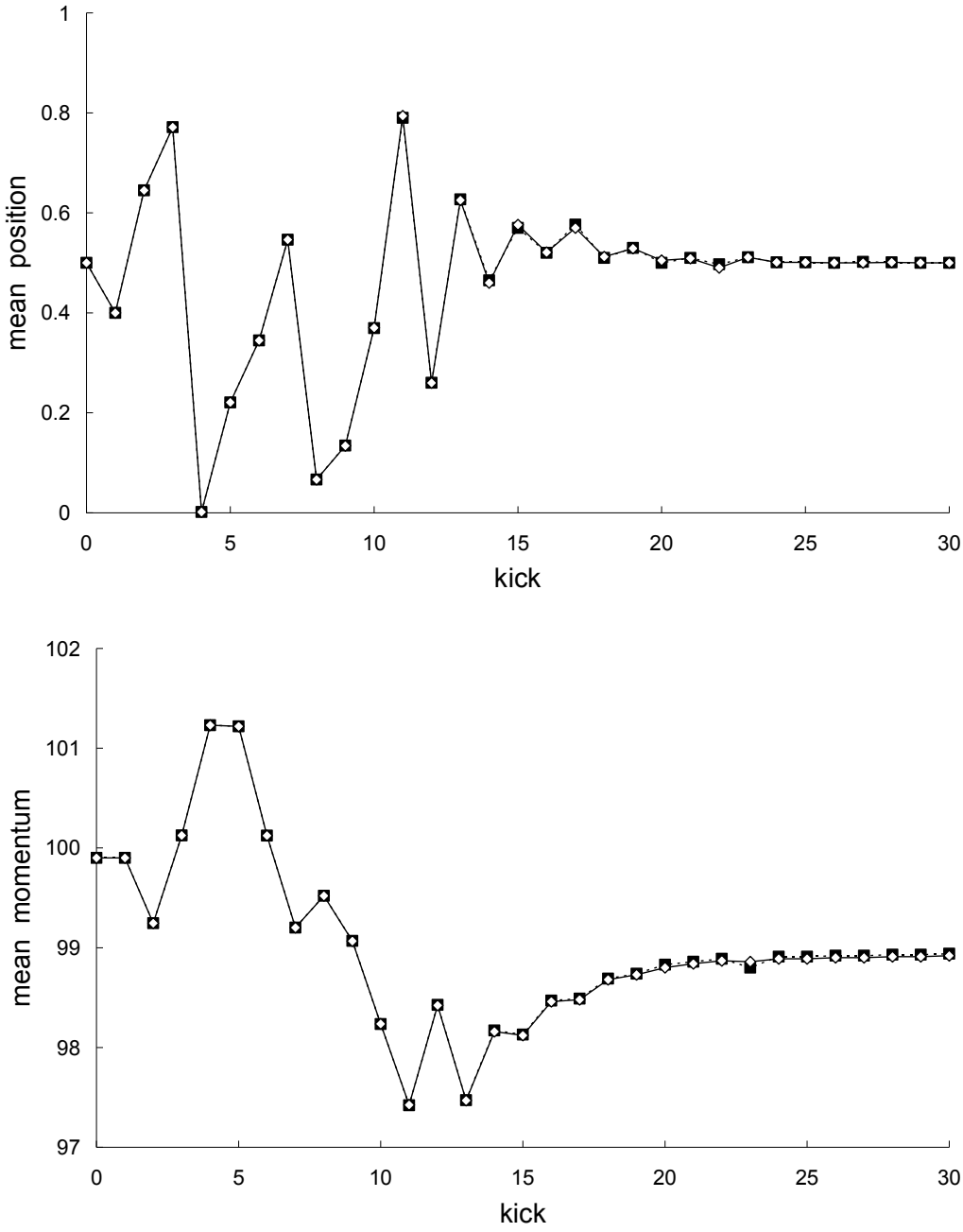

Figure 2.9. Newtonian (squares) and special-relativistic (diamonds) mean positions (top plot) and mean momentums (bottom plot) for the second example.

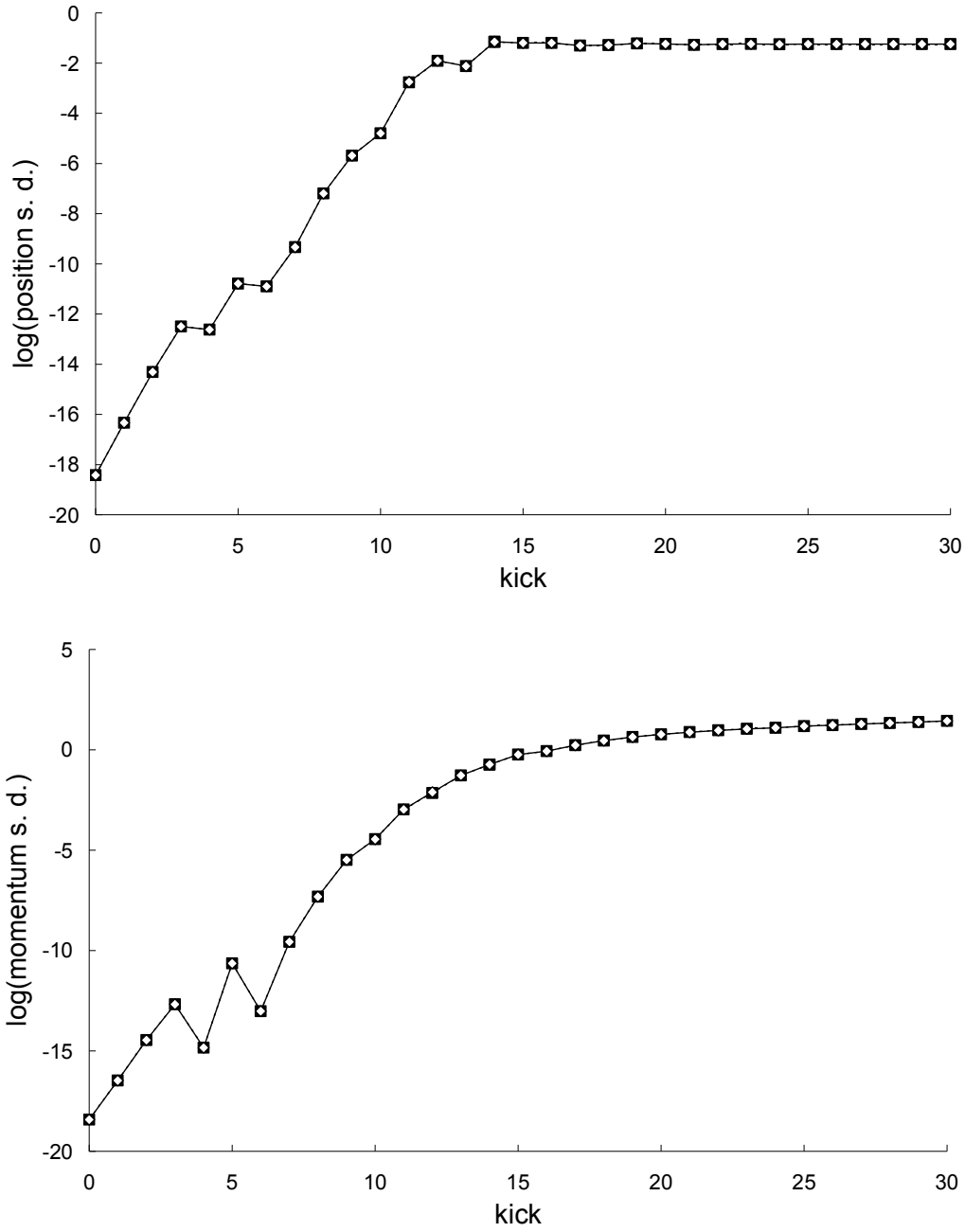

Figure 2.10. Natural-log of the Newtonian (squares) and special-relativistic (diamonds) position standard deviations (top plot) and momentum standard deviations (bottom plot) for the second example.

Newtonian and special-relativistic position and momentum probability densities are essentially the same at kick 13. I have found that the agreement between the statistical predictions of the two theories for the position and momentum means and standard deviations does not break down for an ensemble of trajectories which is initially uniformly distributed (delocalized) in position. Thus, in this example, because the Newtonian and special-relativistic position probability densities are essentially the same and delocalized at kick 13, the statistical predictions of the two theories continue to be close for subsequent kicks.

The results illustrated by the two examples above were also found for other values of the K parameter: 0.9, 3.86, 6.4717, 6.9115 and 10.053.

Recall, in the first example (with smaller initial standard deviations), the Newtonian and special-relativistic position standard deviations saturate *after* the agreement between the Newtonian and special-relativistic single trajectories breaks down. However, in the second example (with larger initial standard deviations), the Newtonian and special-relativistic position standard deviations saturate *before* the agreement between the Newtonian and special-relativistic single trajectories breaks down. The first and second examples therefore show that in order for the statistical predictions of the two theories to break down, the initial Gaussian ensemble must be sufficiently well-localized in phase space, that

is, the initial standard deviations must be sufficiently small such that the Newtonian and special-relativistic position standard deviations saturate *after* the agreement between the Newtonian and special-relativistic single trajectories breaks down.

If the initial ensemble is localized in the chaotic 'sea' in phase space, in the first example for instance, the agreement between the Newtonian and special-relativistic single trajectories (the initial conditions of the two single trajectories are the same, equal to the initial mean position and mean momentum) breaks down rapidly because the difference between the single trajectories grows (Lan, 2006) exponentially. In contrast, if the initial ensemble is localized in the non-chaotic 'island' in phase space, the difference between the Newtonian and special-relativistic single trajectories only grows (Lan, 2006) linearly, and therefore it takes a very long time for the agreement between the single trajectories to break down. This means that the breakdown of agreement between the statistical predictions of the two theories, Newtonian and special-relativistic, is very fast in the chaotic case, as we saw in the first example, but very slow in the non-chaotic case.

As an example of the non-chaotic case (this is my third example), for map parameters $K = 0.9$ and $\beta = 10^{-7}$, the agreement between the Newtonian and

special-relativistic single trajectories with initial conditions $X_0 = 0.7$ and $P_0 = 99.9$ takes about 10^8 kicks (Lan, 2006) to break down. The Newtonian and special-relativistic statistical predictions can thus agree for a very long time. Indeed, for initial standard deviations $\sigma_{X_0} = \sigma_{P_0} = 10^{-9}$, the means still agree to 6 and 9 significant figures respectively for position and momentum at kick 1000. At the same kick, the accuracies I have for both the Newtonian and special-relativistic standard deviations are 3 and 4 significant figures respectively for position and momentum – the Newtonian and special-relativistic standard deviations are the same, 2.67×10^{-7} for position and 2.446×10^{-7} for momentum, within these accuracies. Similar results were found for other non-chaotic cases for other values of the parameter K, 0.5 and 1.5.

Finally, the breakdown of agreement between the Newtonian and special-relativistic statistical predictions for the periodically-delta-kicked particle at low speed can be further understood from a broader perspective by comparing the Newtonian Liouville's equation for the phase-space probability density function $\rho(X,P,t)$

$$\frac{\partial\rho(X,P,t)}{\partial t} = -\left[\frac{P}{T}\right]\left[\frac{\partial\rho}{\partial X}\right] + \left[\frac{K}{2\pi T}\sin(2\pi X)\sum_{j=-\infty}^{\infty} T\delta(jT-t)\right]\left[\frac{\partial\rho}{\partial P}\right] \qquad (2.11)$$

with its special-relativistic counterpart

$$\frac{\partial\rho(X,P,t)}{\partial t}=-\left[\frac{P}{T\left(1+\beta^2P^2\right)^{1/2}}\right]\left[\frac{\partial\rho}{\partial X}\right]+\left[\frac{K}{2\pi T}\sin(2\pi X)\sum_{j=-\infty}^{\infty}T\delta(jT-t)\right]\left[\frac{\partial\rho}{\partial P}\right],$$

(2.12)

where the infinite sum in both equations is the series of periodic delta kicks with period T. For low speed, $\beta P << 1$, therefore

$$\frac{1}{\left(1+\beta^2P^2\right)^{1/2}}\approx 1-\frac{1}{2}\beta^2P^2 \tag{2.13}$$

in Eq. (2.12). The breakdown of agreement between the Newtonian and special-relativistic statistical predictions is therefore essentially due to the small $\beta^2P^2/2$ term in Eq. (2.12).

2.3.2 Momentum diffusion

In this section, I will present three examples to illustrate the general results. In all the examples presented here, the parameter β in the relativistic standard map [Eqs. (2.3) and (2.4)] is small, 10^{-7}, and so the mean speed is low, at most about 0.001% of the speed of light.

If the initial ensemble is semi-uniformly distributed, where the initial positions X_0 are uniformly distributed between 0 and 1 and all initial momentums are P_0, then there is generally no breakdown of agreement between the Newtonian

and special-relativistic MSMD, which grow either linearly or as a power law from the outset. An example (this is my first example) is given in Fig. 2.11 for P_0 = 99.9 and K = 10.053, where the two MSMD grow linearly at close rates.

In the second example, K is also 10.053, but the ensemble is initially Gaussian localized in phase space with means $\langle X_0 \rangle$ = 0.5 and $\langle P_0 \rangle$ = 99.9, and standard deviations $\sigma_{X_0} = \sigma_{P_0} = 10^{-12}$. Fig. 2.12 shows that the Newtonian and special-relativistic predictions for the MSMD are very close and fluctuating for

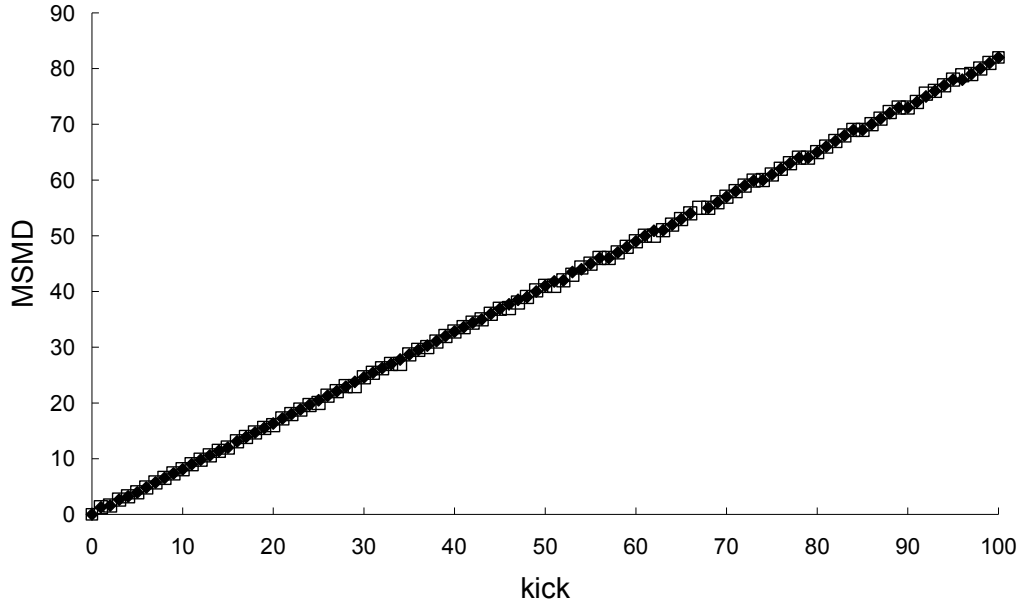

Figure 2.11. Newtonian (squares) and special-relativistic (diamonds) MSMD in the first example where the initial ensemble is semi-uniformly distributed. MSMD which cannot be resolved in accuracy is not plotted.

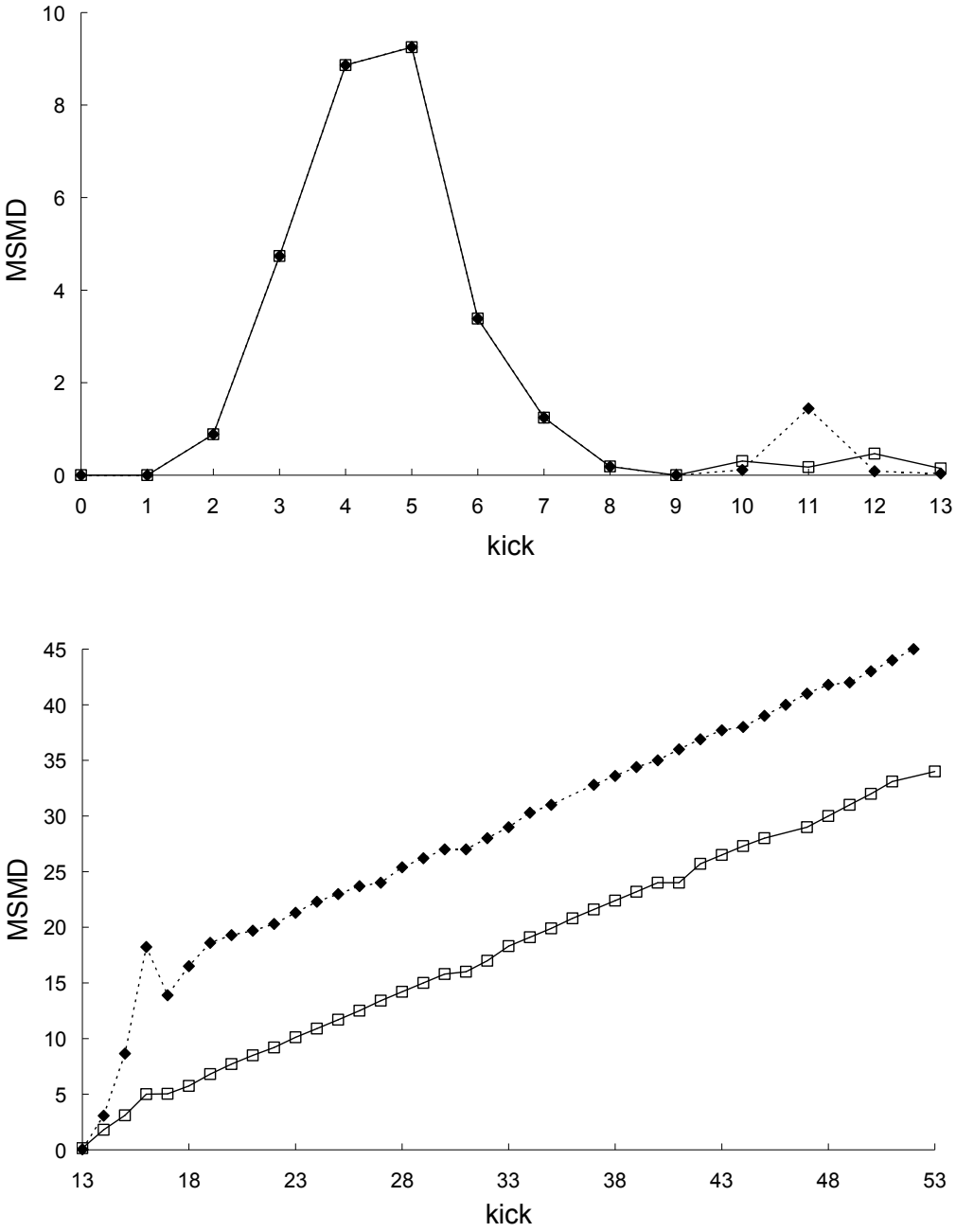

Figure 2.12. Newtonian (squares) and special-relativistic (diamonds) MSMD in the second example for the first 13 kicks (top plot) and from kick 13 to kick 53 (bottom plot). MSMD which cannot be resolved in accuracy is not plotted.

the first 9 kicks, but, from kick 10 onwards, the MSMD predicted by the two theories disagree with each other completely.

In the third example, the map parameter K and the means of the initial Gaussian ensemble are the same as those in the second example but the initial Gaussian ensemble is broader in both position and momentum with $\sigma_{X_0} = \sigma_{P_0} = 10^{-7}$. In contrast to the result in the second example, Fig. 2.13 shows that there is no breakdown of agreement between the Newtonian and special-relativistic MSMD in this case.

In the second example, the Newtonian and special-relativistic position probability densities are delocalized in the entire position interval at kick 13 and kick 15 respectively. In the third example, the position probability densities are both delocalized at kick 8. The MSMD results in the second and third examples before the position probability densities are delocalized can be understood as follows. In each theory, before the delocalization of the position probability density, the MSMD

$$\left\langle \left(P_n - P_0 \right)^2 \right\rangle \equiv \sigma_{P_n}^2 + \left\langle P_n \right\rangle^2 - 2\left\langle P_n P_0 \right\rangle + \sigma_{P_0}^2 + \left\langle P_0 \right\rangle^2 \tag{2.14}$$

is dominated by

$$\left\langle P_n \right\rangle^2 - 2\left\langle P_n P_0 \right\rangle + \left\langle P_0 \right\rangle^2, \tag{2.15}$$

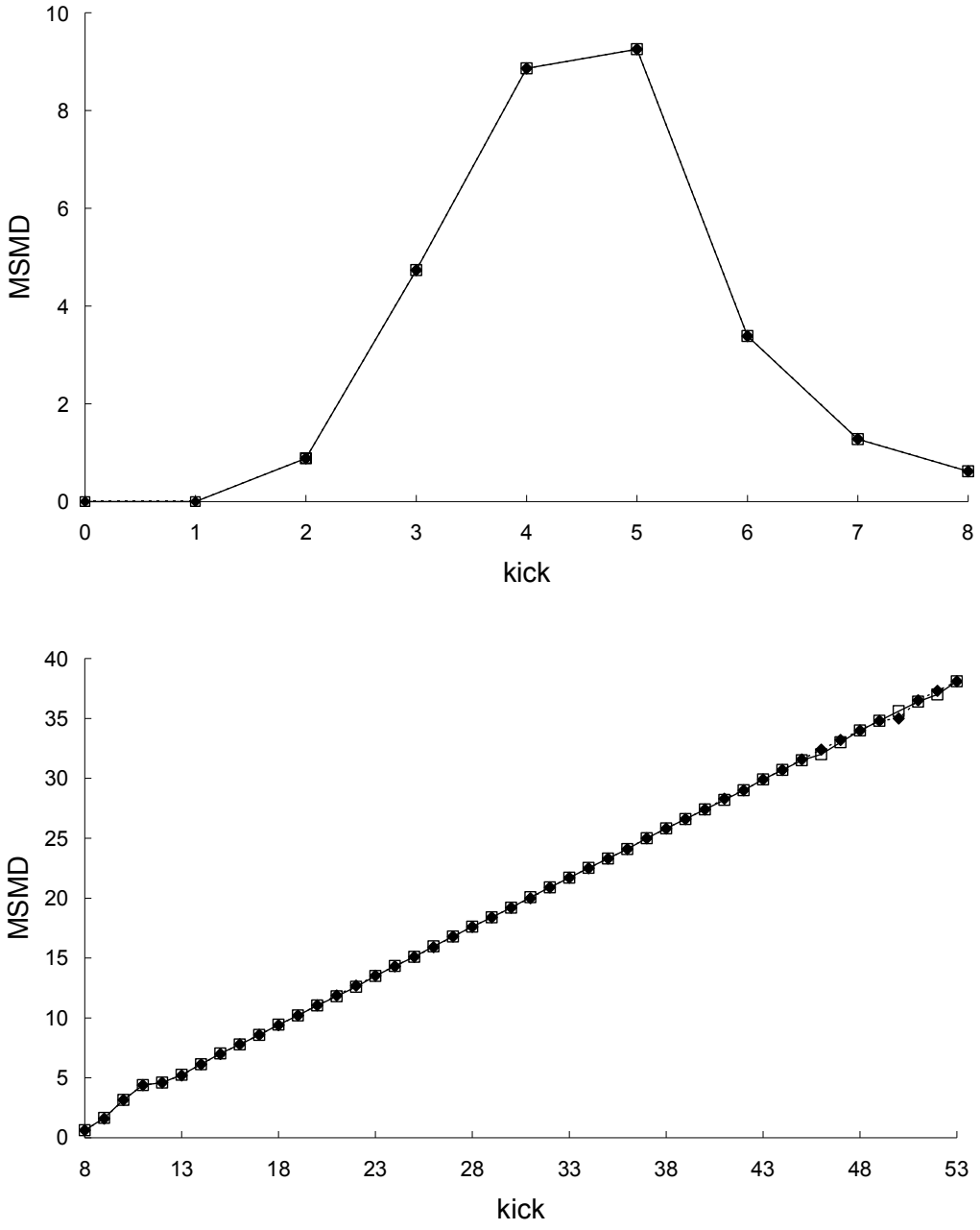

Figure 2.13. Newtonian (squares) and special-relativistic (diamonds) MSMD in the third example for the first 8 kicks (top plot) and from kick 8 to kick 53 (bottom plot).

which is approximately

$$\langle P_n \rangle^2 - 2\langle P_n \rangle \langle P_0 \rangle + \langle P_0 \rangle^2$$

since $<P_n P_0> \approx <P_n><P_0>$. Moreover, the mean trajectory ($<X_n>$, $<P_n>$) of the ensemble is well-approximated by the central trajectory (X_n, P_n), that is, the single trajectory with the same initial conditions as the mean trajectory: $X_0 = <X_0>$ and $P_0 = <P_0>$. Hence, the MSMD in each theory is approximately given by the square momentum displacement

$$(P_n - P_0)^2 = P_n^{\,2} - 2P_n P_0 + P_0^{\,2} \tag{2.16}$$

of the central trajectory, which is chaotic in the two examples, before the position probability density is delocalized – see Figs. 2.14 and 2.15. The initial fluctuations of the Newtonian and special-relativistic MSMD are therefore due to the fluctuations of the square momentum displacement of the corresponding chaotic central trajectory. Furthermore, the difference between the Newtonian and special-relativistic MSMD grows exponentially initially – see Figs. 2.16 and 2.17 – because the difference between the Newtonian and special-relativistic central-trajectory square momentum displacements grows exponentially initially. In Fig. 2.16 (Fig. 2.17), the exponential growth constant of the MSMD difference (measured from kick 2 to kick 12 (7)) is 1.49 (1.97), which is slightly smaller

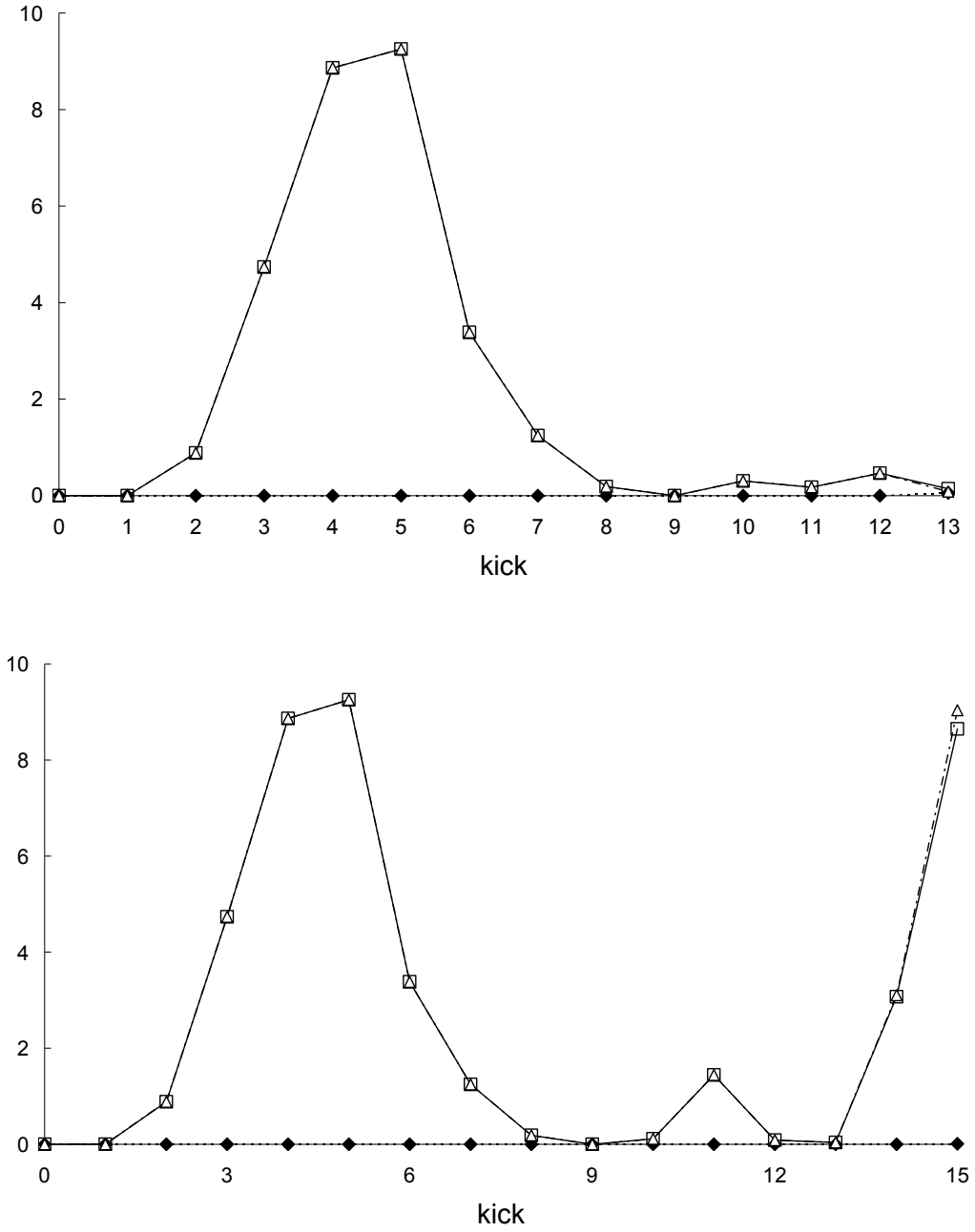

Figure 2.14. Newtonian (top plot) and special-relativistic (bottom plot) MSMD (squares), momentum variances (diamonds) and central-trajectory square momentum displacements (triangles) in the second example from initial until each ensemble is delocalized.

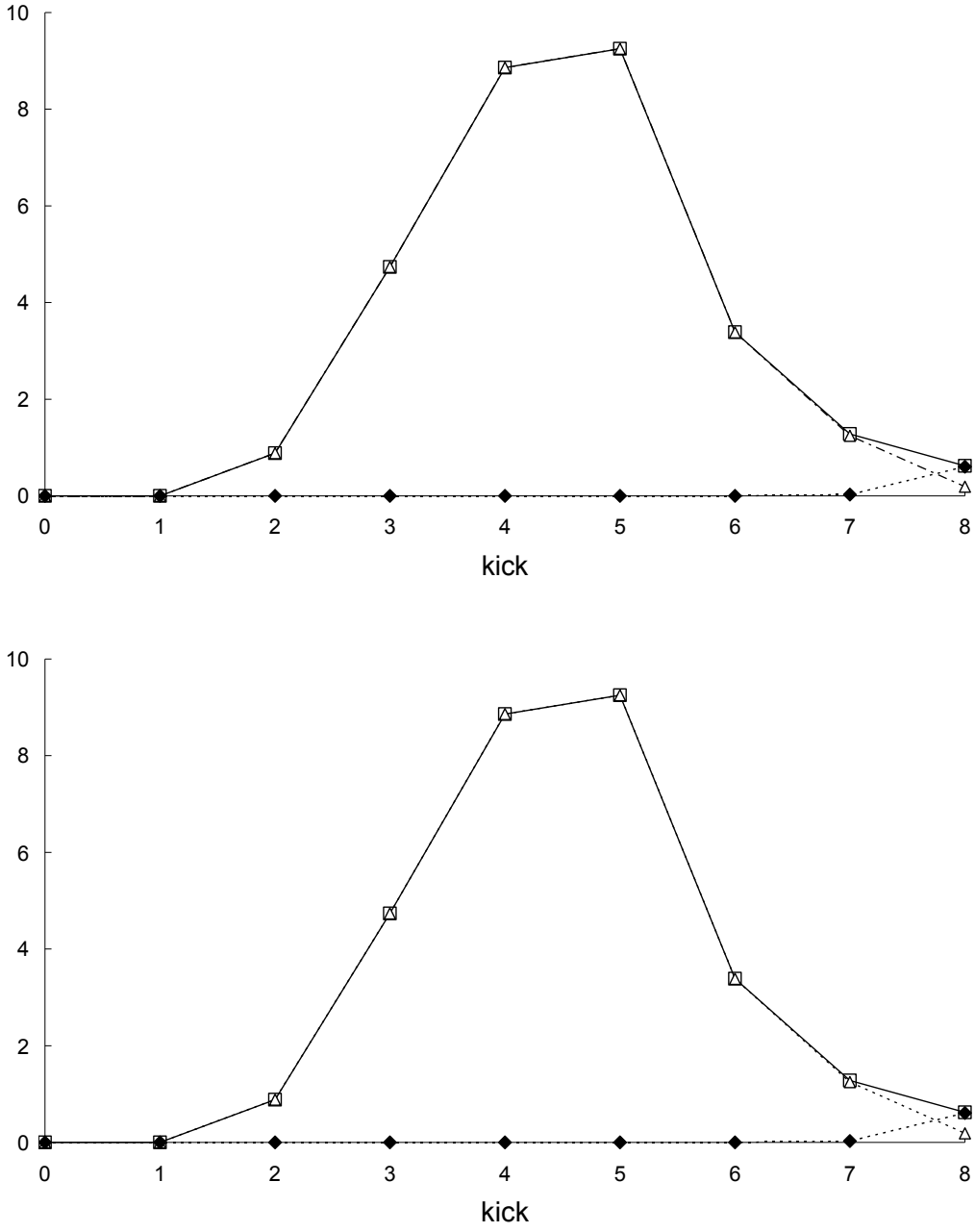

Figure 2.15. Newtonian (top plot) and special-relativistic (bottom plot) MSMD (squares), momentum variances (diamonds) and central-trajectory square momentum displacements (triangles) in the third example from initial until each ensemble is delocalized.

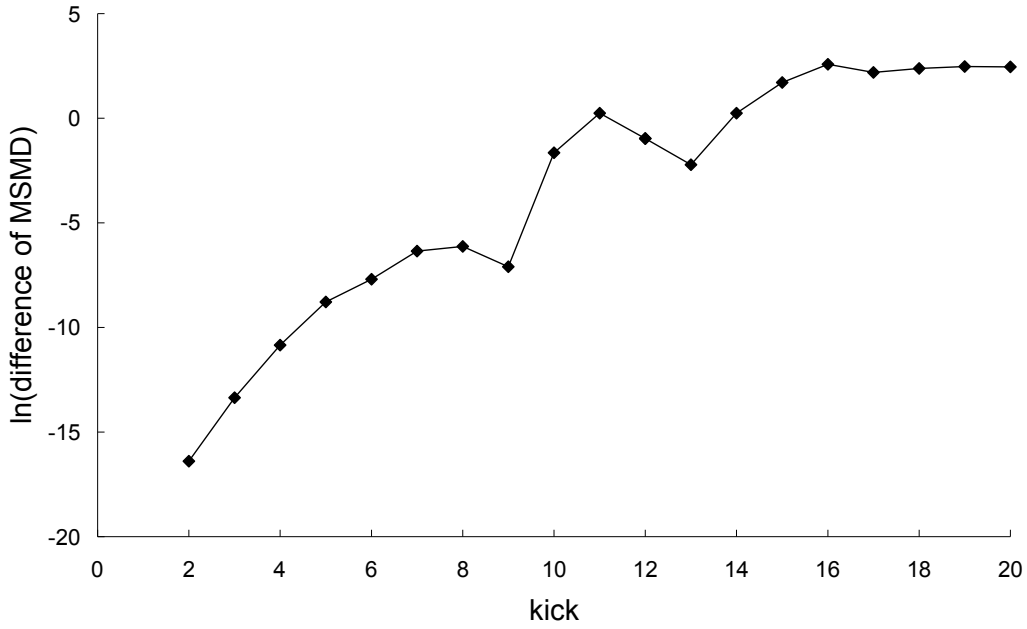

Figure 2.16. Difference between the Newtonian and special-relativistic MSMD in the second example.

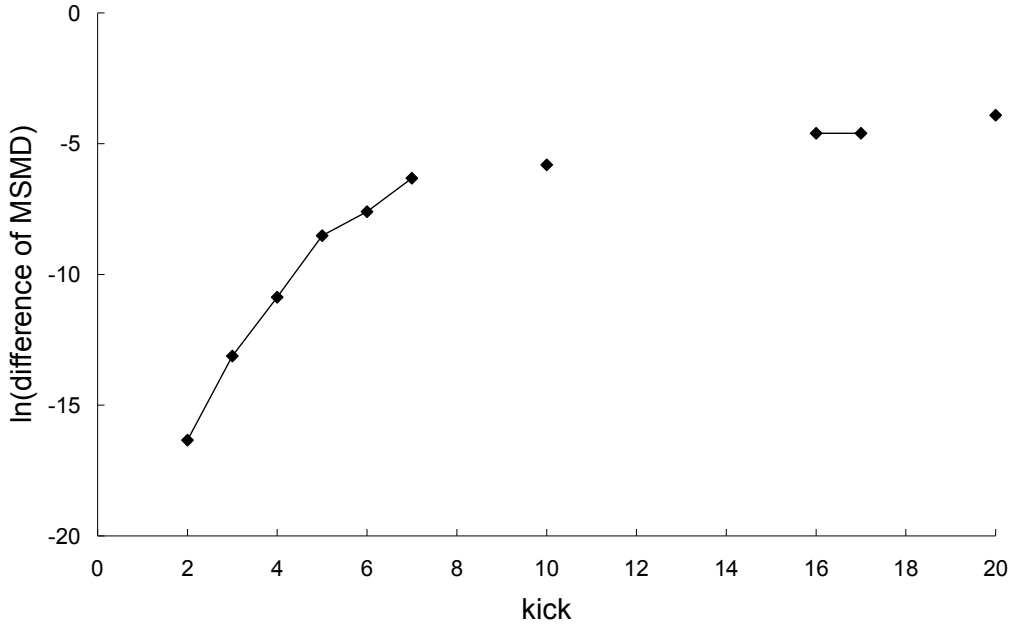

Figure 2.17. Difference between the Newtonian and special-relativistic MSMD in the third example. Data which cannot be resolved in accuracy is not plotted.

(greater) than the Lyapunov exponents of 1.6 for the Newtonian and special-relativistic central trajectories. In the second example, the breakdown of agreement between the Newtonian and special-relativistic MSMD at kick 10 before the delocalization of the position probability densities is therefore due to the breakdown of agreement between the Newtonian and special-relativistic central-trajectory square momentum displacements triggered by the breakdown of agreement between the Newtonian and special-relativistic central trajectories. In contrast, in the third example, there is no breakdown of agreement between the Newtonian and special-relativistic MSMD before the position probability densities are delocalized because the agreement between the Newtonian and special-relativistic central trajectories only breaks down at kick 10 *after* the position probability densities are both delocalized at kick 8.

Generally, in each theory, after the position probability density is delocalized, the behavior of the MSMD calculated using an initially Gaussian ensemble is similar to the behavior of the MSMD calculated using an initially semi-uniform ensemble for the same parameter K, which is either linear growth or power-law growth. The linear growth rates or power-law exponents of the former MSMD and latter MSMD are close. In the second and third examples where $K = 10.053$, the growth is linear (see Figs. 2.11, 2.12 and 2.13). In the second example,

although the Newtonian and special-relativistic MSMD both grow linearly at close rates after the delocalization of the position probability densities, they start at different values and therefore the two MSMD remain different from one another. On the other hand, in the third example, the two MSMD remain close after the delocalization of the position probability densities because they grow linearly at close rates from close values.

The second and third examples illustrate that, typically, the agreement between the MSMD predicted by the two theories breaks down if the initial Gaussian ensemble is well-localized (i.e., sufficiently localized) in phase space such that the Newtonian and special-relativistic position probability densities are delocalized *after* the breakdown of agreement between the Newtonian and special-relativistic central trajectories. The breakdown of agreement between the two MSMD occurs when the agreement between the two central trajectories breaks down and therefore is rapid if the two central trajectories are chaotic (as the second example shows) but very slow if the two central trajectories are non-chaotic (Lan, 2006).

Since the MSMD can be written as, see Eq. (2.10), the MSMD at kick (n-1) plus a sum of correlation functions, if the MSMD predicted by the two theories agree with each other for the first (n-1) kicks and disagree completely from kick n

onwards, the Newtonian predictions for the sum of correlation functions and some/all of the correlation functions in the sum should disagree completely with the special-relativistic predictions for n, n+1, …. For instance, in the second example, since the two predictions for the MSMD disagree completely from kick 10 onwards, the two predictions for the sum of correlation functions and some/all of the correlation functions in the sum should disagree completely for $n \geq 10$. For example, the Newtonian and special-relativistic predictions for the sum of correlation functions for $n = 10$ are 0.31 and 0.11 respectively. In addition, Fig. 2.18 shows, for example, that the Newtonian predictions for the correlation functions

$C_{9-i}(i) = \langle u_{9-i} u_9 \rangle$, where $i = 0,\ldots, 9$,

disagree completely with the special-relativistic predictions, except when $i = 5$ and 9.

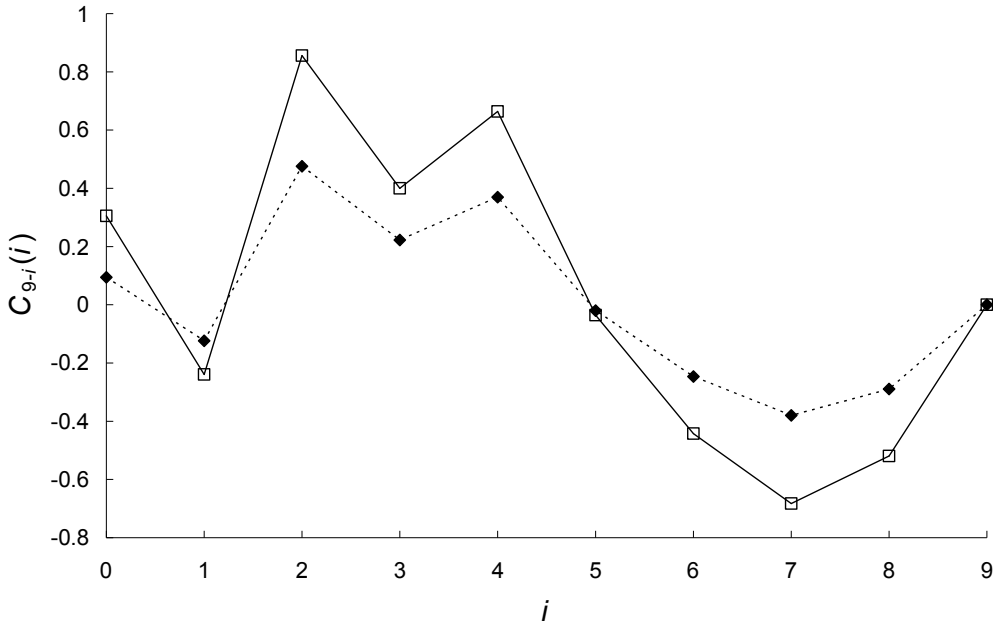

Figure 2.18. Comparison of Newtonian (squares) and special-relativistic (diamonds) correlation functions $C_{9-i}(i)$ versus kicks i for the second example.

Thesis Chapter Declaration

Monash University

Declaration for Thesis Chapter 3

Declaration by candidate

In the case of Chapter 3, the nature and extent of my contribution to the work was the following:

Nature of contribution	Extent of contribution (%)
Conceived and designed the experiments, performed the experiments, analyzed the data, contributed materials/analysis tools and wrote the manuscript.	70%

The following co-authors contributed to the work. Co-authors who are students at Monash University must also indicate the extent of their contribution in percentage terms:

Name	Nature of contribution	Extent of contribution (%) for student co-authors only
Dr. Lan Boon Leong	Supervisory role - Conceived and designed the experiments, analyzed the data, contributed materials/analysis tools and wrote the manuscript.	
Dr. Florentino Borondo	Conceptual input and wrote the manuscript.	

Candidate's Signature		**Date**

Declaration by co-authors
The undersigned hereby certify that:

(1) the above declaration correctly reflects the nature and extent of the candidate's contribution to this work, and the nature of the contribution of each of the co-authors.
(2) they meet the criteria for authorship in that they have participated in the conception, execution, or interpretation, of at least that part of the publication in their field of expertise;
(3) they take public responsibility for their part of the publication, except for the responsible author who accepts overall responsibility for the publication;
(4) there are no other authors of the publication according to these criteria;
(5) potential conflicts of interest have been disclosed to (a) granting bodies, (b) the editor or publisher of journals or other publications, and (c) the head of the responsible academic unit; and
(6) the original data are stored at the following location(s) and will be held for at least five years from the date indicated below:

Location(s)	School of Science, Sunway Campus

		Date
Signature 1		
Signature 2		

Chapter 3
Low-Speed Chaotic Dynamical System (II) – Scattering System

3.1 Introduction

In this chapter, I extend the comparison of the Newtonian and special-relativistic single-trajectory predictions for the low-speed model scattering system presented in (Lan and Borondo, 2011) to a comparison of statistical quantities which are calculated from the same parameters and initial ensemble of trajectories. In particular, I focus here on the position and momentum means, standard deviations and probability density functions, mean dwell time, and transmission and reflection coefficients. The dwell time is, for each trajectory in the ensemble, defined as $(t_{out} - t_{in})$ where t_{in} is the time when the particle first enters the scattering region and t_{out} is the time when the particle subsequently first exits the scattering region. The transmission coefficient (reflection coefficient) is defined as the ratio of the number of transmitted (reflected) particles to the total number of particles in the ensemble. A comparison of Newtonian and

special-relativistic statistical predictions has not yet been done for a low-speed scattering system.

The model scattering system I have chosen to study allows sufficiently-accurate calculation of the statistical quantities because the time-evolution of each trajectory in the ensemble is described by an exact analytical map in both the Newtonian and special-relativistic frameworks. Details of the model scattering system and calculations are given next (Sec. 3.2), followed by the presentation and discussion of the results (Sec. 3.3).

3.2 Calculation

The scattering system consists of a particle of rest mass m_0 moving in the one-dimensional potential well introduced by Beeker and Eckelt (1993):

$$V(x) = -\frac{V_0}{\beta}\left(1 + x^2\right)^{-\beta/2}, \tag{3.1}$$

which is periodically turned on only for an instant of time. The potential well is characterized by two parameters V_0 and β, where V_0/β determines the depth of the well and β determines its asymptotic behavior.

The Newtonian equations of motion for this periodically-delta-kicked scattering system are easily integrated exactly (Beeker and Eckelt, 1993) to yield

a mapping for the position x and momentum p from just before the nth kick to just before the (n+1)th kick:

$$p_{n+1} = p_n - V_0 T x_n \left(1 + x_n^2\right)^{-(\beta+2)/2}, \tag{3.2}$$

$$x_{n+1} = x_n + \frac{T}{m_0} p_{n+1}, \tag{3.3}$$

where T is the kicking period.

The corresponding special-relativistic equations of motion are also easily integrated exactly (Lan and Borondo, 2011) to produce a mapping for the position x and momentum p from just before the nth kick to just before the (n+1)th kick:

$$p_{n+1} = p_n - V_0 T x_n \left(1 + x_n^2\right)^{-(\beta+2)/2}, \tag{3.4}$$

$$x_{n+1} = x_n + \frac{T p_{n+1}}{m_0 \sqrt{1 + \left[p_{n+1}/(m_0 c)\right]^2}}. \tag{3.5}$$

For both theories, I consider an initially Gaussian ensemble of trajectories centered in the mean values $\langle x \rangle$ and $\langle p \rangle$, and with standard deviations σ_x and σ_p:

$$\frac{1}{2\pi\sigma_x\sigma_p} \exp\left[-\frac{\left(x - \langle x \rangle\right)^2}{2\sigma_x^2} - \frac{\left(p - \langle p \rangle\right)^2}{2\sigma_p^2}\right].$$

Each trajectory in the Newtonian (special-relativistic) ensemble is time-evolved using the map given by Eqs. (3.2) and (3.3) [Eqs. (3.4) and (3.5)]. For both theories, each statistical quantity is calculated by averaging over the ensemble of trajectories. First, the statistical quantity is calculated using 10^6 trajectories, where its accuracy is determined by comparing the 30-significant-figure calculation with

the quadruple-precision (35 significant figures) calculation. The statistical quantity is then recalculated using 10^7 trajectories where its accuracy is determined in the same manner. Finally, the accuracy of the statistical quantity is determined by comparing the 10^6-trajectories calculation with the 10^7-trajectories calculation. I used $m_0 = 1$, $T = 1$, and $c = 10^5$ in all of our calculations.

3.3 Results - Statistical predictions: Mean, standard deviation, probability distribution, mean dwell time, reflection and transmission coefficients

In this section I present and discuss four examples illustrating the general results. In all cases, the mean speed is low, representing only 0.001% of the speed of light.

In the first example, the parameters of the scattering potential well are taken as $V_0 = 8$ and $\beta = 4$. The corresponding potential profile is plotted in Fig. 3.1. For these parameters, the scattering is chaotic, i.e., the scattering function has intertwining regular and irregular intervals down to all scales, from both the Newtonian (Beeker and Eckelt, 1993) and special-relativistic (Lan and Borondo,

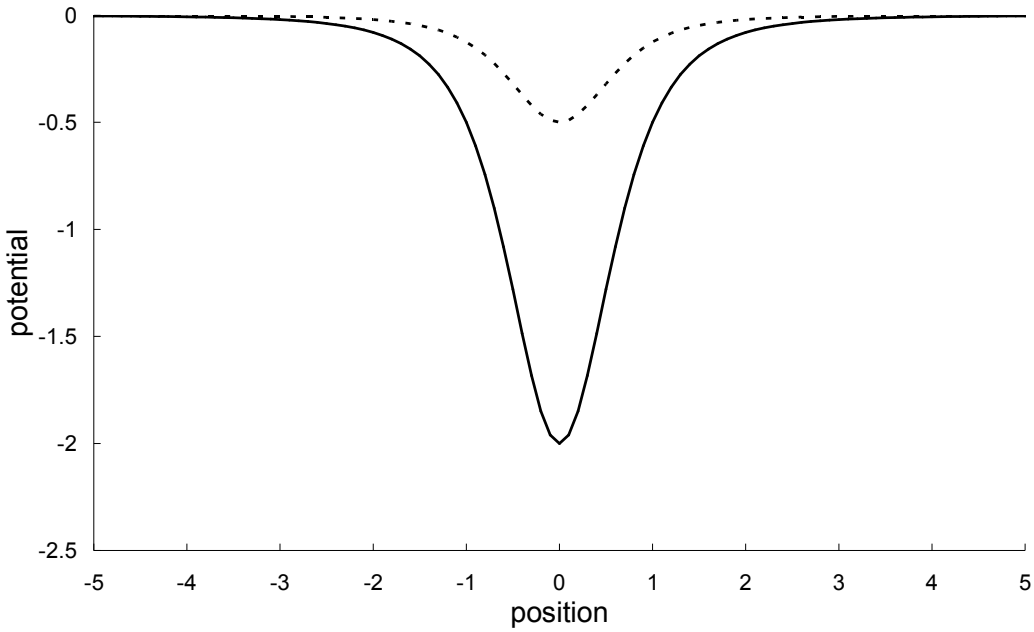

Figure 3.1. Scattering potential well for $V_0 = 8$ and $\beta = 4$ (solid line), and $V_0 = 2$ and $\beta = 4$ (dotted line).

2011) perspectives. The means and standard deviations of the initially Gaussian ensemble are taken as $\langle x \rangle = -20$, $\langle p \rangle = 1.2497$ and $\sigma_x = \sigma_p = 10^{-11}$. This initially localized ensemble is far from and to the left of the scattering region ranging from $x = -4$ to $x = 4$.

Figure 3.2 shows that the Newtonian mean trajectory, i.e., mean position and mean momentum, agrees with the special-relativistic mean trajectory for the first 35 kicks. The two mean trajectories are completely different, however, from kick 36 onwards. This breakdown of agreement can be understood as follows. The

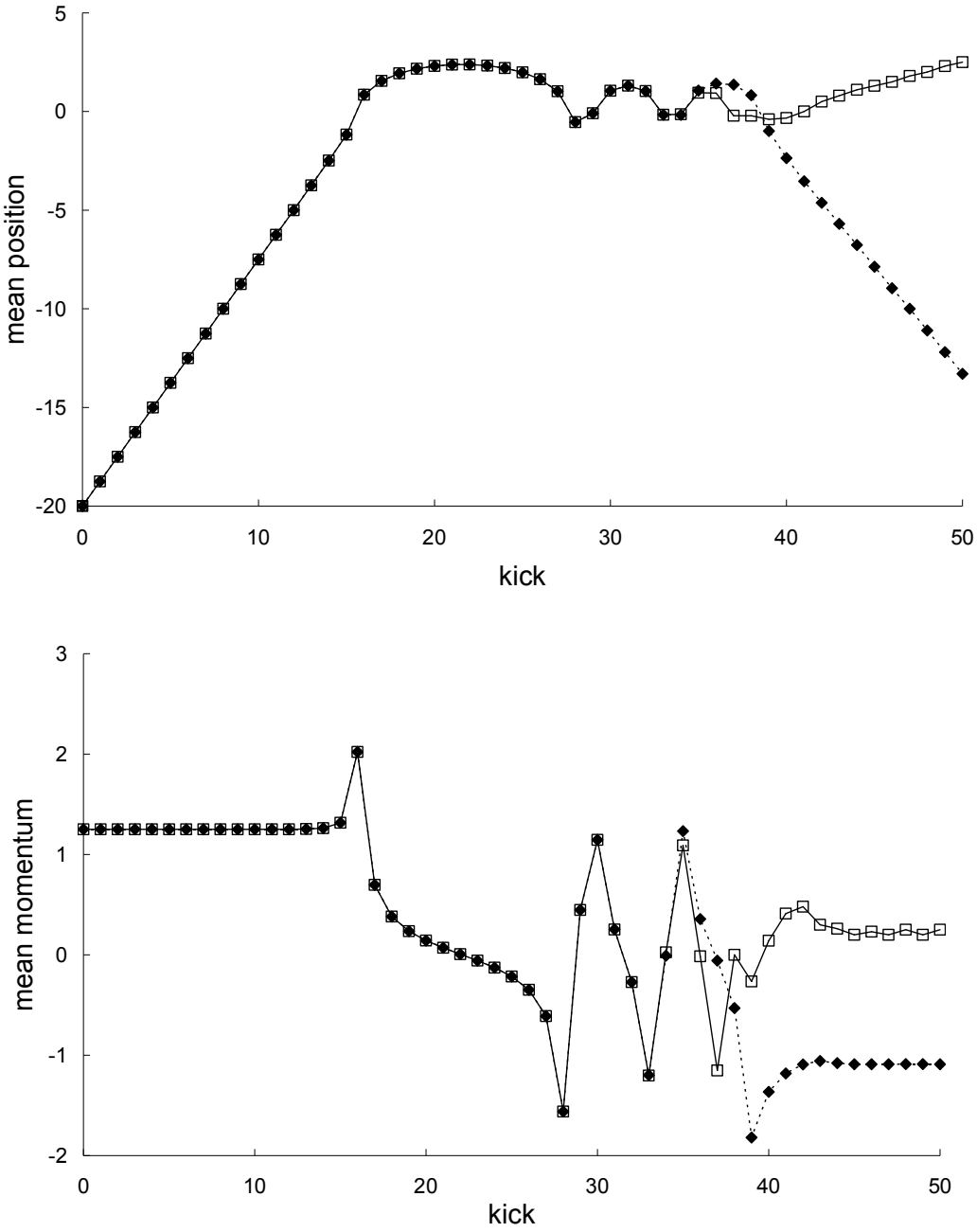

Figure 3.2. Newtonian (squares) and special-relativistic (diamonds) mean positions (top plot) and mean momentums (bottom plot) for the chaotic scattering case in the first example discussed in the text.

Newtonian (special-relativistic) mean trajectory is well-approximated by the Newtonian (special-relativistic) single trajectory with the same initial conditions until the Newtonian (special-relativistic) ensemble is delocalized in phase space at kick 38 (kick 39). Since the agreement between the Newtonian and special-relativistic single trajectories breaks down earlier, at kick 36, the agreement between the Newtonian and special-relativistic mean trajectories therefore also breaks down at the same kick. Furthermore, the breakdown of agreement between the Newtonian and special-relativistic mean trajectories is rapid because the difference between them grows exponentially in the scattering region, like the growth of the difference between the Newtonian and special-relativistic single trajectories shown previously in (Lan and Borondo, 2011).

Figure 3.3 shows that the agreement between the Newtonian and special-relativistic standard deviations also breaks down at kick 36. Fig. 3.4 shows that this rapid breakdown of agreement is due to the exponential growth of the difference between the Newtonian and special-relativistic standard deviations up to kick 38 while the ensembles are still in the scattering region.

The mean dwell time, transmission coefficient and reflection coefficient

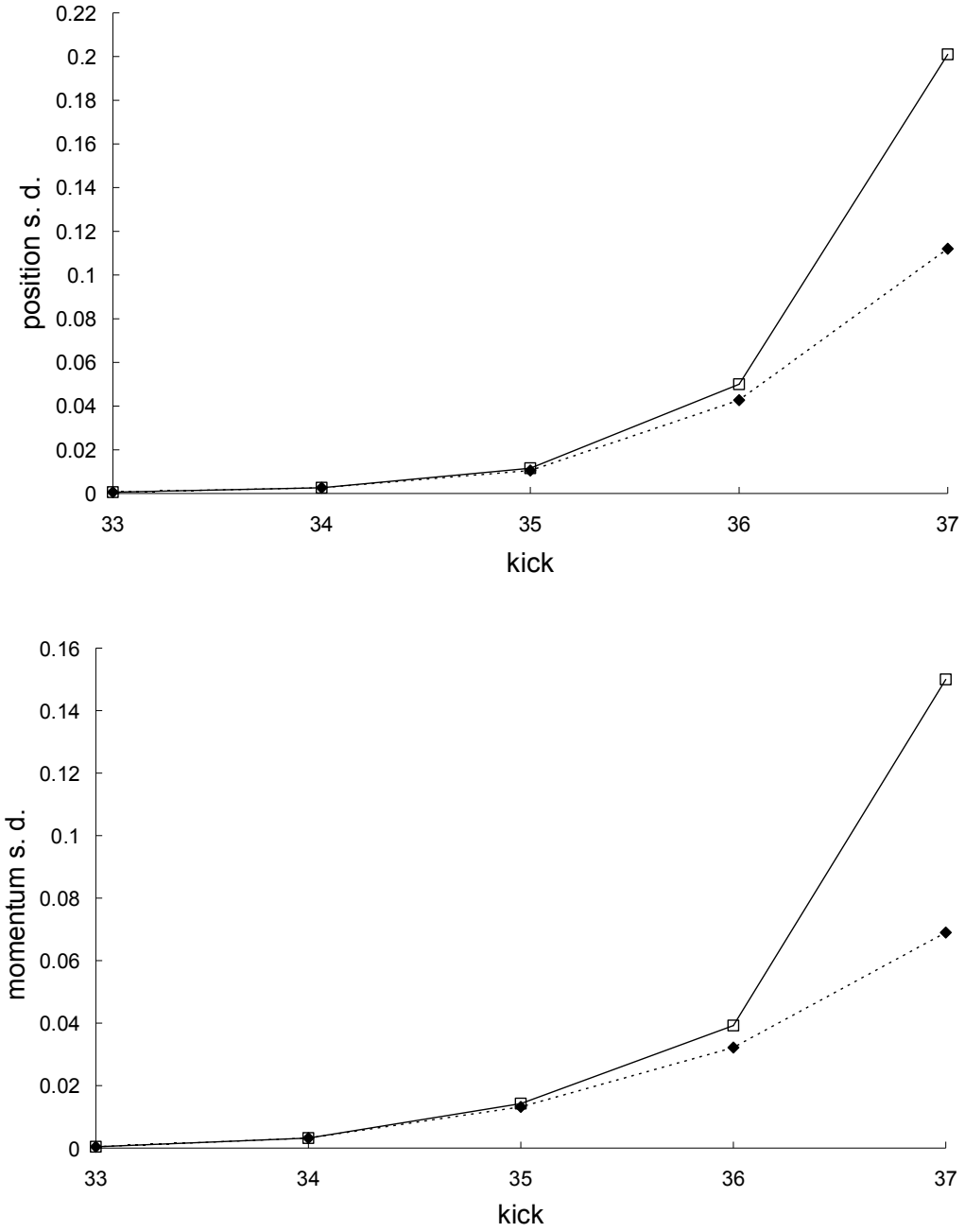

Figure 3.3. Newtonian (squares) and special-relativistic (diamonds) position standard deviations (top plot) and momentum standard deviations (bottom plot) for the chaotic scattering case in the first example. The Newtonian and special-relativistic standard deviations are not plotted before kick 33 because they are close to each other.

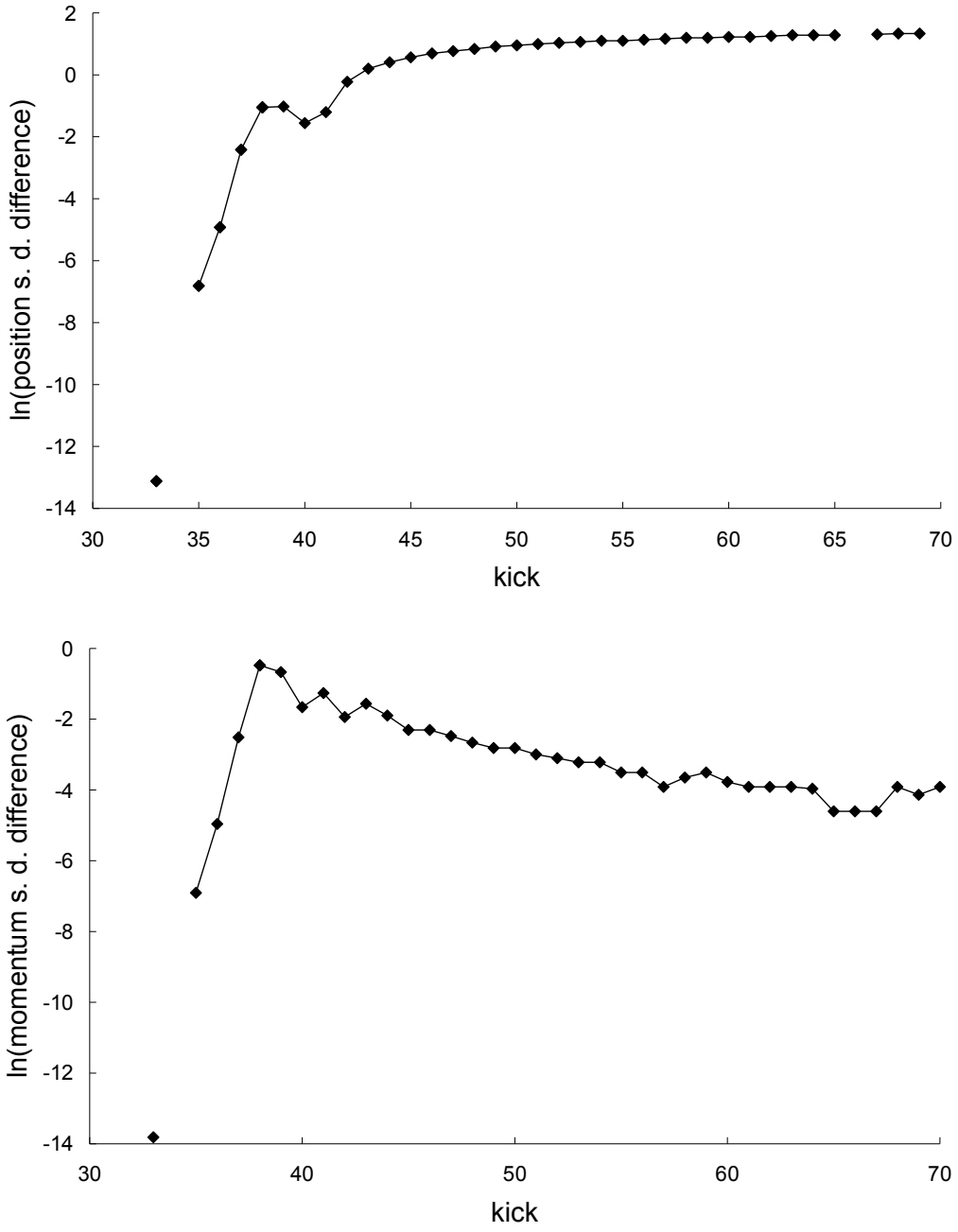

Figure 3.4. Difference between the Newtonian and special-relativistic standard deviations – for position (top plot), and momentum (bottom plot) – for the chaotic scattering case in the first example. The standard-deviation differences before kick 33 and at kick 34 are not shown because they cannot be resolved with the accuracy of our calculations. After the exponential growth, which ends at kick 38, the position-standard-deviation difference grows linearly from kick 50 onwards and the momentum-standard-deviation difference is essentially constant from kick 60 onwards.

predicted by the two theories are also, remarkably, very different. Indeed, the Newtonian mean dwell time is 32.9 kicks, while the corresponding special-relativistic value is only 30.3 kicks. Even more striking is the difference in the transmission coefficients, since the Newtonian value of 0.57 is more than two times the special-relativistic one of 0.24. Similarly, for the reflection coefficient, the special-relativistic value of 0.75 is about two times the Newtonian value of 0.42. Fig. 3.5 shows the different Newtonian and special-relativistic position

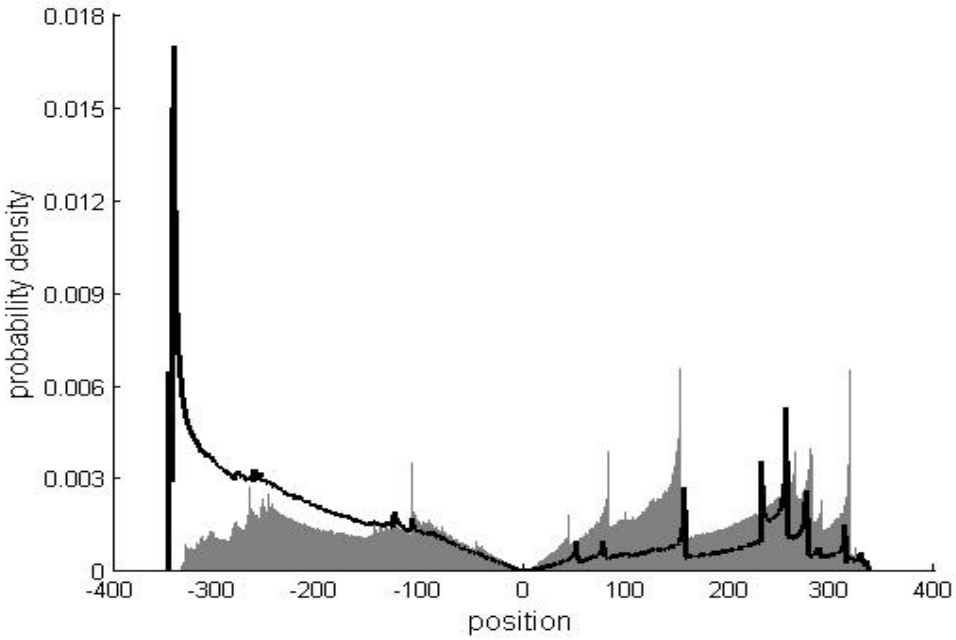

Figure 3.5. Newtonian (shaded grey) and special-relativistic (bold line) position probability densities for the chaotic scattering case in the first example at kick 160.

probability densities at kick 160 after the ensembles have exited the scattering region.

In the second example, the scattering is also chaotic. All the parameters are the same as in the first example except that a broader initial Gaussian ensemble, both in position and momentum with $\sigma_x = \sigma_p = 10^{-7}$, is used. In contrast to what happened in the previous example, there is no breakdown of agreement between the position and momentum means and standard deviations predicted by the two theories. In this example, when the Newtonian and special-relativistic ensembles delocalized in phase space at kick 32, the Newtonian and special-relativistic mean trajectories are still close to one another because the agreement between the Newtonian and special-relativistic single trajectories with the same initial conditions only breaks down sometime later at kick 36. The Newtonian and special-relativistic standard deviations at kick 32 are also still close to one another. Hence, since the Newtonian and special-relativistic delocalized phase-space distributions are close to one another at kick 32, the subsequent predictions of the means and standard deviations by the two theories continue to be close. Furthermore, the other statistical quantities predicted by the two theories are also close, in particular, they agree to at least 2 significant figures: the two theories predict 25 kicks for the mean dwell time, 0.39 for the transmission coefficient and

0.60 for the reflection coefficient.

These two examples of chaotic scattering illustrate that the statistical predictions of the two theories completely disagree if the initially Gaussian ensemble is well, i.e., sufficiently, localized in phase space, such that the Newtonian and special-relativistic ensembles delocalize *after* the agreement between the Newtonian and special-relativistic single trajectories, with the same initial conditions as the Newtonian and special-relativistic mean trajectories, breaks down.

In the third example, the parameters of the scattering potential well are taken to be $V_0 = 2$ and $\beta = 4$ – the corresponding potential profile has also been plotted in Fig. 3.1. For these values of the parameters, the scattering is non-chaotic, i.e., the scattering function varies regularly from both the Newtonian (Beeker and Eckelt, 1993) and special-relativistic (Lan and Borondo, 2011) perspectives. The means and standard deviations of the initially Gaussian ensemble are taken as $\langle x \rangle = -20$, $\langle p \rangle = 1.2497$ and $\sigma_x = \sigma_p = 10^{-4}$. This choice initially localize the ensemble far from and to the left of the scattering region, which is in the range $x = -3.5$ to $x = 3.5$. In this case, the transmission and reflection coefficients predicted by the two theories are the same, and equal to 1 and 0, respectively. Both the Newtonian and special-relativistic ensembles are still localized in phase space when they are

far away from the scattering region on the other side at $x \approx 20$ at kick 40. Fig. 3.6 shows that when the Newtonian and special-relativistic ensembles are far away from the scattering region on the other side, the Newtonian and special-relativistic mean trajectories are still close to one another – this is because they are well-approximated by the corresponding single trajectories (with the same initial conditions) which are still also close to one another. The Newtonian and special-relativistic standard deviations are also close to one another – see Fig. 3.7. The mean dwell times from the two theories are also the same: 6 kicks.

In the fourth and final example, the scattering is also non-chaotic. All the parameters are the same as in the third example except that the initial Gaussian ensemble is broader in both position and momentum with $\sigma_x = \sigma_p = 10^{-2}$. In contrast to the previous example, the Newtonian and special-relativistic ensembles are already delocalized in phase space at kick 17 in the scattering region. The two ensembles are still close to one another when they delocalize, which means that there is no subsequent breakdown of agreement between the means and the standard deviations predicted by the two theories for the position and momentum. Furthermore, the transmission and reflection coefficients predicted by the two theories are the same, 1 and 0, respectively. The two

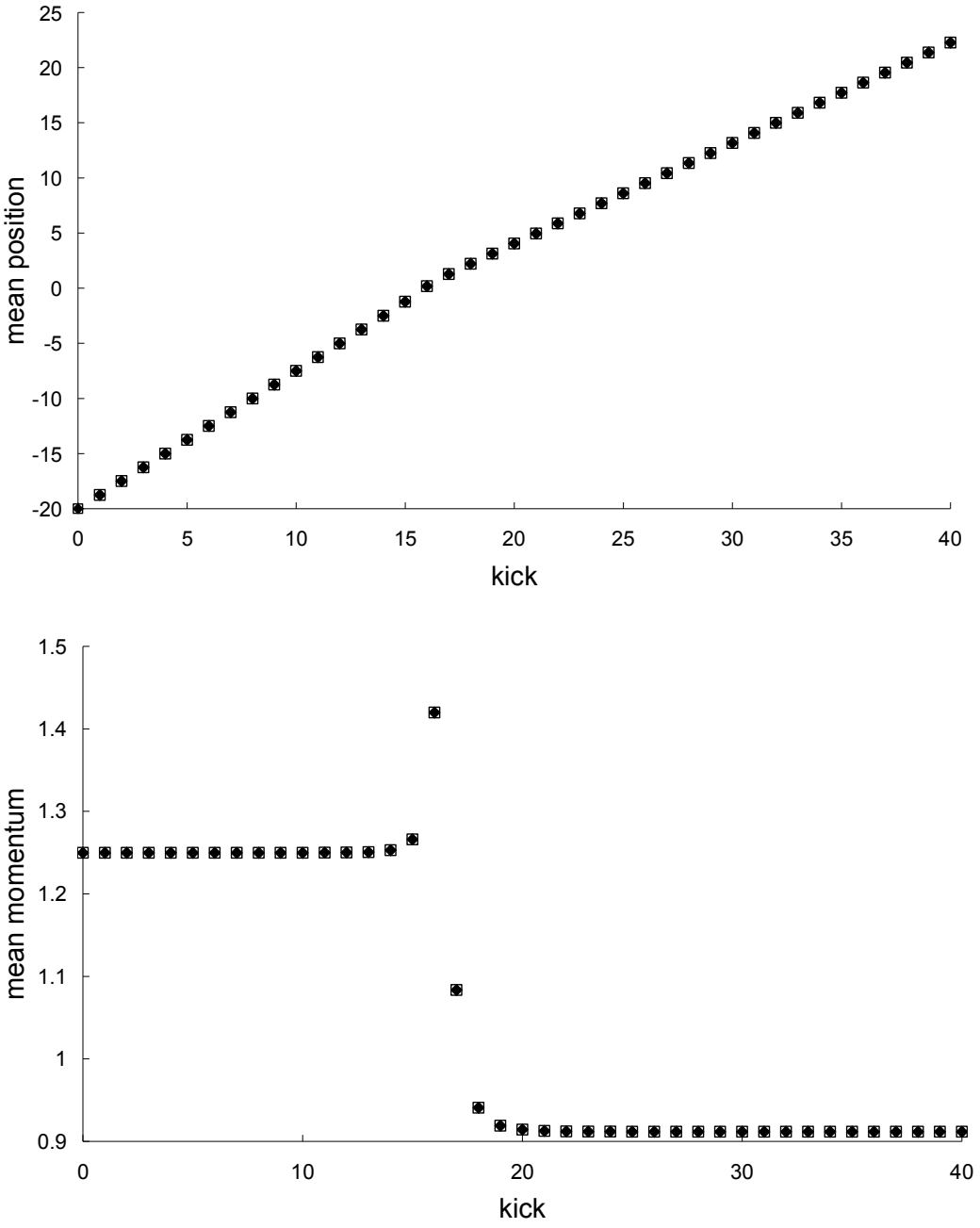

Figure 3.6. Newtonian (squares) and special-relativistic (diamonds) mean positions (top plot) and mean momentums (bottom plot) for the non-chaotic scattering case in the third example discussed in the text.

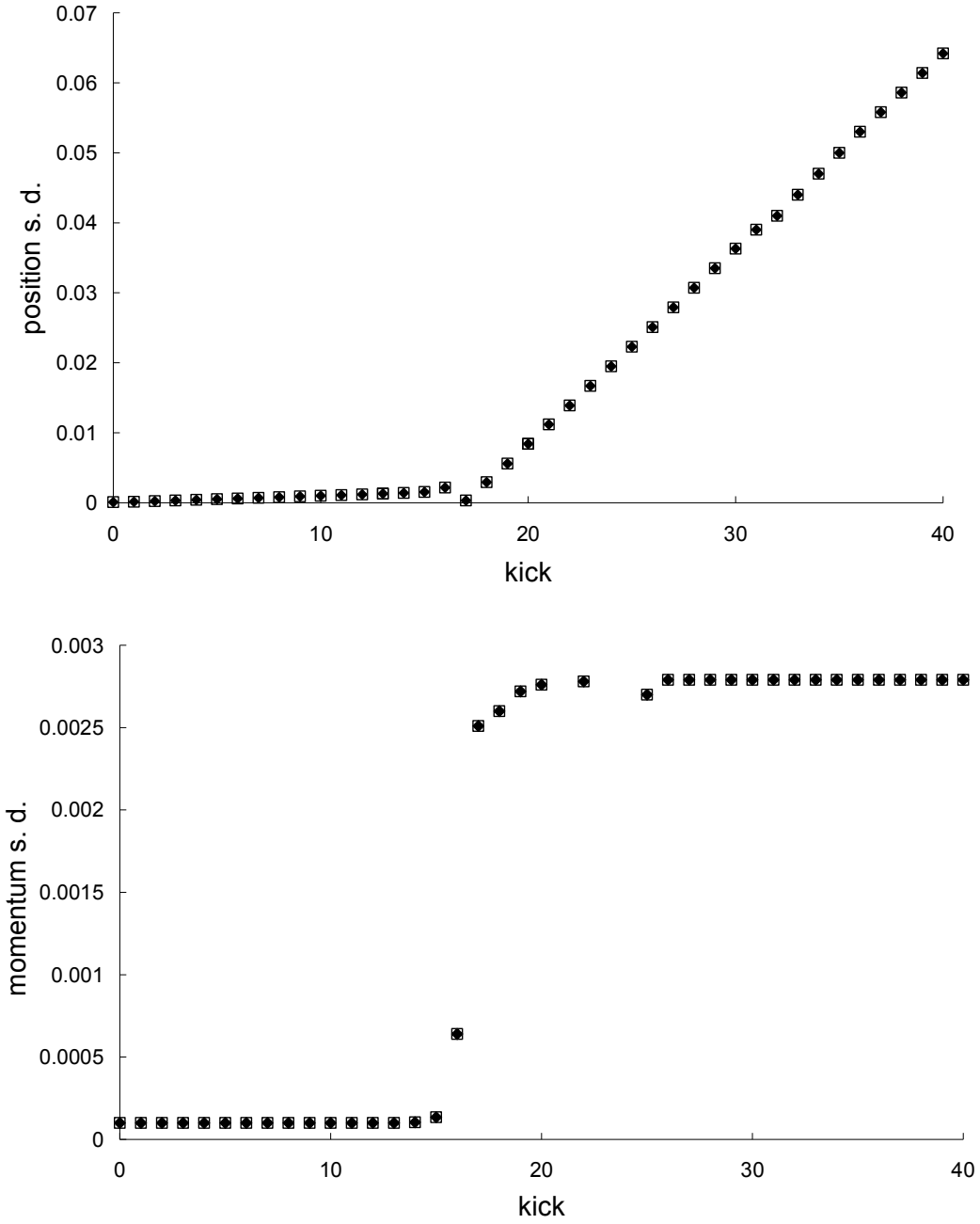

Figure 3.7. Newtonian (squares) and special-relativistic (diamonds) position standard deviations (top plot) and momentum standard deviations (bottom plot) for the non-chaotic scattering case in the third example.

predictions for the mean dwell time agree to at least 3 significant figures, they are both equal to 5.64 kicks.

The third and fourth examples above illustrate that if the scattering is non-chaotic, there is no breakdown of agreement between the statistical predictions of the two theories.

Thesis Chapter Declaration

Monash University

Declaration for Thesis Chapter 4

Declaration by candidate

In the case of Chapter 4, the nature and extent of my contribution to the work was the following:

Nature of contribution	Extent of contribution (%)
Conceived and designed the experiments, performed the experiments, analyzed the data, contributed materials/analysis tools and wrote the manuscript.	70%

The following co-authors contributed to the work. Co-authors who are students at Monash University must also indicate the extent of their contribution in percentage terms:

Name	Nature of contribution	Extent of contribution (%) for student co-authors only
Dr. Lan Boon Leong	Supervisory role - Conceived and designed the experiments, analyzed the data, contributed materials/analysis tools and wrote the manuscript.	

Candidate's Signature		**Date**

Declaration by co-authors
The undersigned hereby certify that:

(1) the above declaration correctly reflects the nature and extent of the candidate's contribution to this work, and the nature of the contribution of each of the co-authors.
(2) they meet the criteria for authorship in that they have participated in the conception, execution, or interpretation, of at least that part of the publication in their field of expertise;
(3) they take public responsibility for their part of the publication, except for the responsible author who accepts overall responsibility for the publication;
(4) there are no other authors of the publication according to these criteria;
(5) potential conflicts of interest have been disclosed to (a) granting bodies, (b) the editor or publisher of journals or other publications, and (c) the head of the responsible academic unit; and
(6) the original data are stored at the following location(s) and will be held for at least five years from the date indicated below:

Location(s)	School of Science, Sunway Campus

		Date
Signature		

Chapter 4

Low-Speed Weak-Gravity Chaotic Dynamical System - Bouncing Ball System

4.1 Introduction

In this chapter, I study a *low-speed weak-gravity* system – the bouncing ball system (Tufillaro *et al*., 1986; Tufillaro *et al*., 1992) – to ascertain if the Relationships #2 and #3 in Sec. 1.2 are correct by comparing the Newtonian and special-relativistic single-trajectory and statistical predictions (in particular, the means, standard deviations and probability distributions for the position and velocity) with the corresponding general-relativistic predictions. Here, the gravitational field of the earth is modeled as the field due to a uniform sphere. Moreover, both elastic and inelastic collisions between the ball and table are considered.

The Newtonian map for the bouncing ball system is known (Tufillaro *et al*., 1986; Tufillaro *et al*., 1992), however, the relativistic maps are unknown. To derive the general-relativistic map, I need to know the general-relativistic free fall motion of a particle – see the derivation in Sec. 4.2. The derivations of the

relativistic maps are given in Sec. 4.3. Details of the bouncing ball system, as well as the Newtonian and relativistic single-trajectory and statistical quantity calculations are given in Sec. 4.4, and the results are presented in Sec. 4.5.

4.2 Newtonian and relativistic free-fall motion

Here I consider the radial motion of a particle of mass m due to the gravitational field of a uniform sphere of mass M and radius R.

In the Newtonian framework, the change in gravitational potential energy of the particle from an initial position r_0 to a final position r is given by

$$\Delta U = U(r) - U(r_0) = -GMm\left[\frac{1}{r} - \frac{1}{r_0}\right]. \tag{4.1}$$

If the distance travelled by the particle is small compared to r_0, that is, $|r - r_0|/r_0 \ll 1$, then $1/r$ is essentially given by

$$\frac{1}{r} = \frac{1}{r_0}\left(1 + \frac{r - r_0}{r_0}\right)^{-1} \approx \frac{1}{r_0}\left(1 - \frac{r - r_0}{r_0}\right) = \frac{1}{r_0} - \frac{r - r_0}{r_0^2}, \tag{4.2}$$

since higher-order terms involving $(r - r_0)/r_0$ are negligible. If the particle is initially near the surface of the sphere, that is, $r_0 \approx R$, then

$$GM/r_0^2 \approx GM/R^2 = g. \tag{4.3}$$

Substituting Eqs. (4.2) and (4.3) into Eq. (4.1) reduces Eq. (4.1) to approximately

the change in gravitational potential energy of a particle in a uniform gravitational field

$$\Delta U \approx mgr - mgr_0. \tag{4.4}$$

The Newtonian position and velocity of the particle at time t are therefore given by the well-known equations:

$$r - r_0 = v_0(t - t_0) - \frac{1}{2}g(t - t_0)^2, \tag{4.5}$$

$$v = v_0 - g(t - t_0). \tag{4.6}$$

In the special-relativistic framework, if $|r - r_0|/r_0 \ll 1$ and $r_0 \approx R$, Eqs. (4.2) and (4.3) reduce the change in gravitational potential energy of the particle to

$$\Delta U = -\frac{GMm}{\sqrt{1-(v/c)^2}}\left[\frac{1}{r} - \frac{1}{r_0}\right] \approx \frac{mgr - mgr_0}{\sqrt{1-(v/c)^2}}. \tag{4.7}$$

Solution of the special-relativistic equation of motion with the force derived from the gravitational potential energy $U(r)$ in Eq. (4.7) yields (Srinivasa Rao, 1966; Lapidus, 1972a, 1972b)

$$r - r_0 = -(c^2/g)\ln\left\{\frac{1}{2}\left[\left(1 + \frac{v_0}{c}\right)e^{-g(t-t_0)/c} + \left(1 - \frac{v_0}{c}\right)e^{g(t-t_0)/c}\right]\right\}, \tag{4.8}$$

$$v = c\left[\frac{(1 + v_0/c)e^{-g(t-t_0)/c} - (1 - v_0/c)e^{g(t-t_0)/c}}{(1 + v_0/c)e^{-g(t-t_0)/c} + (1 - v_0/c)e^{g(t-t_0)/c}}\right] \tag{4.9}$$

for the position and velocity of the particle at time t.

In the general-relativistic framework, the gravitational field outside the uniform sphere is described by the Schwarzschild metric (Landau and Lifshitz,

1975) in terms of the Schwarzschild coordinates (ct, r, θ, ϕ)

$$ds^2 = c^2 d\tau^2 = \left(1 - \frac{r_s}{r}\right) c^2 dt^2 - \frac{dr^2}{\left(1 - \frac{r_s}{r}\right)} - r^2 \left(d\theta^2 + \sin^2 \theta d\phi^2\right), \tag{4.10}$$

where ds is the interval between neighboring events, τ is the proper time, and $r_s = 2GM/c^2$ is the Schwarzschild radius. For purely radial motion (Srinivasa Rao, 1966; Srinivasa Rao and Gopala Rao, 1974) along the line ϕ = constant in the equatorial plane $\theta = \pi/2$, the metric Eq. (4.10) is simplified, with $d\phi = d\theta = 0$, to

$$ds^2 = c^2 d\tau^2 = \left(1 - \frac{r_s}{r}\right) c^2 dt^2 - \frac{dr^2}{\left(1 - r_s / r\right)} \tag{4.11}$$

and the geodesic equations are reduced to

$$\frac{cd^2 t}{c^2 d\tau^2} + \left(\frac{r_s / r^2}{1 - r_s / r}\right) \frac{cdt}{cd\tau} \frac{dr}{cd\tau} = 0, \tag{4.12}$$

$$\frac{d^2 r}{c^2 d\tau^2} + \left(1 - \frac{r_s}{r}\right)\left(\frac{r_s}{2r^2}\right)\left(\frac{cdt}{cd\tau}\right)^2 - \left(1 - \frac{r_s}{r}\right)^{-1}\left(\frac{r_s}{2r^2}\right)\left(\frac{dr}{cd\tau}\right)^2 = 0. \tag{4.13}$$

The local velocity (Landau and Lifshitz, 1975; Zel'dovich and Novikov, 1996) of the particle, measured by a local observer who is at rest at a particular Schwarzschild radial coordinate and is next to the particle, is

$$v = \left(1 - \frac{r_s}{r}\right)^{-1} \frac{dr}{dt} = \left(1 - \frac{2GM}{c^2 r}\right)^{-1} \frac{dr}{dt}. \tag{4.14}$$

The integral of Eq. (4.12), which is given by

$$\frac{cdt}{cd\tau} = k\left(1 - \frac{r_s}{r}\right)^{-1}, \tag{4.15}$$

where k is a constant, and the integral of Eq. (4.13), which is given by Eq. (4.11),

together with the initial condition $v = v_0$ at $r = r_0$, lead to the following expression for dr/dt:

$$\left(\frac{dr}{dt}\right)^2 = \left(1-\frac{2GM}{c^2 r}\right)^2 \left(1-\frac{2GM}{c^2 r_0}\right)^{-1} \left[v_0^2\left(1-\frac{2GM}{c^2 r}\right) + 2GM\left(\frac{1}{r}-\frac{1}{r_0}\right)\right]. \quad (4.16)$$

If $|r - r_0|/r_0 \ll 1$ and $r_0 \approx R$, substituting Eqs. (4.2) and (4.3) into Eq. (4.16) and integrating it with initial condition $r = r_0$ at $t = t_0$ yields the general-relativistic position of the particle at time t

$$r - r_0 = -\frac{c^2}{2g}\left(1-\frac{2gr_0}{c^2}\right)\left\{1-\left\{\frac{1}{2}\left[\left(1+\frac{v_0}{c}\right)e^{-\frac{g(t-t_0)}{c}} + \left(1-\frac{v_0}{c}\right)e^{\frac{g(t-t_0)}{c}}\right]\right\}^{-2}\right\}. \quad (4.17)$$

In the limit of weak gravity ($2gr/c^2 \ll 1$ and $2gr_0/c^2 \ll 1$), Eq. (4.17) reduces to the special-relativistic Eq. (4.8). In the limit of weak gravity and low speed ($v/c \ll 1$, $v_0/c \ll 1$ and $g(t - t_0)/c \ll 1$), Eq. (4.17) reduces to the Newtonian Eq. (4.5).

Substituting Eqs. (4.14), (4.2), (4.3) and (4.17) sequentially into Eq. (4.16) yields the general-relativistic velocity of the particle at time t, which is the same as the special-relativistic Eq. (4.9). In the limit of low speed, Eq. (4.9) reduces to the Newtonian Eq. (4.6).

4.3 Derivation of the Special-Relativistic and General-Relativistic Maps

Following (Tufillaro *et al*., 1986; Tufillaro *et al*., 1992), the earth is assumed to be a uniform sphere of radius R. Furthermore, in between impacts with the table, the ball, which is initially close to the earth's surface ($r_0 \approx R$), undergoes free-fall motion along the radial direction where the distance it travels $|r - r_0|$ is assumed small compared to its initial position r_0 ($|r - r_0|/r_0 \ll 1$). The relativistic position and velocity of the ball between impacts (which are derived in Sec. 4.2) are needed in the derivations of the relativistic maps. In the derivations, it is convenient to transform the position r of the ball, which is measured relative to the center of the earth, to y: $y = r - R_{\mathrm{TLP}}$, where R_{TLP} is the distance from the center of the earth to the table's lowest position. The table's position $s(t) = A[\sin(\omega t + \theta_0) + 1]$ is measured relative to R_{TLP}.

In between the kth and (k+1)th impacts, the ball moves with initial velocity v_k and position y_k just after the kth impact. The ball's initial position y_k is the same as the table's position $A[\sin(\theta_k) + 1]$ just after the kth impact, where $\theta_k = \omega t_k + \theta_0$ is the table's phase and t_k is the time just after the kth impact. In the general-relativistic framework, the ball's position at time t after the kth impact is

[based on Eq. (4.17) in Sec. 4.2]

$$y - y_k = -\frac{c^2}{2g}\left\{1 - \frac{2g\left(R_{\mathrm{TLP}} + y_k\right)}{c^2}\right\}\left\{1 - \left\{\frac{1}{2}\left[\left(1 + \frac{v_k}{c}\right)e^{-\frac{g(t-t_k)}{c}} + \left(1 - \frac{v_k}{c}\right)e^{\frac{g(t-t_k)}{c}}\right]\right\}^{-2}\right\},$$

(4.18)

and the ball's velocity at time t after the kth impact is [based on Eq. (4.9) in Sec. 4.2]

$$v = c\left[\frac{\left(1 + v_k / c\right)e^{-g(t-t_k)/c} - \left(1 - v_k / c\right)e^{g(t-t_k)/c}}{\left(1 + v_k / c\right)e^{-g(t-t_k)/c} + \left(1 - v_k / c\right)e^{g(t-t_k)/c}}\right]. \tag{4.19}$$

Setting the difference between the ball's position $y(t)$ [Eq. (4.18)] and table's position $s(t) = A\left[\sin\left(\omega t + \theta_0\right) + 1\right]$ at the $(k+1)$th impact to zero yields the impact-phase map (the map is given in the next section).

If the collision between the ball and table is inelastic, $\bar{v}'_{k+1}$ and $\bar{v}_{k+1}$, which are respectively the ball's velocity just before and just after the $(k+1)$th impact in the *table's* reference frame, are related through

$$\bar{v}_{k+1} = -\alpha \bar{v}'_{k+1} \tag{4.20}$$

where α ($0 < \alpha < 1$) is the coefficient of restitution. $\alpha = 1$ if the collision is elastic. The ball's velocity just before and just after the $(k+1)$th impact in the *ground's* reference frame are respectively

$$v'_{k+1} = \frac{\bar{v}'_{k+1} + u_{k+1}}{1 + \dfrac{\bar{v}'_{k+1} u_{k+1}}{c^2}} \quad \text{and} \quad v_{k+1} = \frac{\bar{v}_{k+1} + u_{k+1}}{1 + \dfrac{\bar{v}_{k+1} u_{k+1}}{c^2}}, \tag{4.21}$$

where u_{k+1} is the table's velocity at the $(k+1)$th impact in the ground's reference

frame. Solving for $\bar{v}'_{k+1}$ and $\bar{v}_{k+1}$ from Eq. (4.21) and substituting into Eq. (4.20) yields the velocity map (the map is also given in the next section). The expression for v'_{k+1} is obtained by substituting $t = t_{k+1}$ into Eq. (4.19).

In the derivation of the special-relativistic map, Eq. (4.18) is replaced by the special-relativistic position of the ball between the *k*th and (*k*+1)th impacts based on the special-relativistic Eq. (4.8) in Sec. 4.2. In the derivation (Tufillaro *et al*., 1986; Tufillaro *et al*., 1992) of the Newtonian map, the Newtonian Eqs. (4.5) and (4.6) in Sec. 4.2 were utilized to obtain the position and velocity of the ball between the *k*th and (*k*+1)th impacts, and Eq. (4.21) is used without the terms involving c^2.

4.4 Calculation

The bouncing ball system (Tufillaro *et al*., 1986; Tufillaro *et al*., 1992) consists of a ball bouncing repeatedly on a table which is oscillating sinusoidally with amplitude A and frequency ω. The impact between the ball and the table is instantaneous, where the coefficient of restitution α ($0 \leq \alpha \leq 1$) measures the kinetic energy loss of the ball at each impact: the impact is elastic if $\alpha = 1$, inelastic if $\alpha < 1$. The table is not affected by the impact because the table's mass

is much larger than the ball's mass. In between impacts, the ball undergoes free-fall motion due to the gravitational field of the earth, which is assumed to be a uniform sphere.

In the Newtonian framework, the dynamics of the bouncing ball is described by the two-dimensional map derived by Tufillaro and co-workers (1986, 1992). Following (Tufillaro *et al*., 1986; Tufillaro *et al*., 1992), I derive the special-relativistic map and general-relativistic map in terms of the ball's velocity v and the table's phase θ just after each impact. The table's phase is given by ($\omega t + \theta_0$) modulus 2π. I will refer to the table's phase just after each impact as the impact phase. My derivations (see Secs. 4.2 and 4.3) of the relativistic maps for the bouncing ball follow the same steps as the derivation (Tufillaro *et al*., 1986; Tufillaro *et al*., 1992) of the Newtonian map.

In the Newtonian framework, the dynamics of the bouncing ball is (Tufillaro *et al*., 1986; Tufillaro *et al*., 1992) described by the impact-phase map

$$A\left[\sin\left(\theta_k\right)+1\right]+v_k\left[\frac{1}{\omega}\left(\theta_{k+1}-\theta_k\right)\right]-\frac{1}{2}g\left[\frac{1}{\omega}\left(\theta_{k+1}-\theta_k\right)\right]^2-A\left[\sin\left(\theta_{k+1}\right)+1\right]=0 \tag{4.22}$$

and the velocity map

$$v_{k+1}=\left(1+\alpha\right)\omega A\cos\left(\theta_{k+1}\right)-\alpha\left\{v_k-g\left[\frac{1}{\omega}\left(\theta_{k+1}-\theta_k\right)\right]\right\} \tag{4.23}$$

where $g=GM/R^2$, M and R are respectively the mass and radius of the earth,

and G is the gravitational constant.

In the special-relativistic framework, the impact-phase map is

$$A\left[\sin\left(\theta_k\right)+1\right]-\frac{c^2}{g}\ln\left\{\frac{1}{2}\left[\left(1+\beta_k\right)e^{-\frac{g}{c}\left(\frac{\theta_{k+1}-\theta_k}{\omega}\right)}+\left(1-\beta_k\right)e^{\frac{g}{c}\left(\frac{\theta_{k+1}-\theta_k}{\omega}\right)}\right]\right\} - A\left[\sin\left(\theta_{k+1}\right)+1\right]=0 \tag{4.24}$$

where $\beta_k=\frac{v_k}{c}$. The velocity map is

$$v_{k+1}=\frac{-c^2\alpha\left(\frac{v'_{k+1}-u_{k+1}}{c^2-v'_{k+1}u_{k+1}}\right)+u_{k+1}}{1-\alpha u_{k+1}\left(\frac{v'_{k+1}-u_{k+1}}{c^2-v'_{k+1}u_{k+1}}\right)} \tag{4.25}$$

where $u_{k+1}=A\omega\cos\left(\theta_{k+1}\right)$ is the table's velocity just after the (k+1)th impact, and

$$v'_{k+1}=c\left[\frac{\left(1+\beta_k\right)e^{-\frac{g}{c}\left(\frac{\theta_{k+1}-\theta_k}{\omega}\right)}-\left(1-\beta_k\right)e^{\frac{g}{c}\left(\frac{\theta_{k+1}-\theta_k}{\omega}\right)}}{\left(1+\beta_k\right)e^{-\frac{g}{c}\left(\frac{\theta_{k+1}-\theta_k}{\omega}\right)}+\left(1-\beta_k\right)e^{\frac{g}{c}\left(\frac{\theta_{k+1}-\theta_k}{\omega}\right)}}\right]$$

is the ball's velocity just before the (k+1)th impact.

In the general-relativistic framework, the impact-phase map is

$$A\left[\sin\left(\theta_k\right)+1\right]-A\left[\sin\left(\theta_{k+1}\right)+1\right] -\frac{c^2}{2g}\left\{1-\frac{2g\left[R_{\mathrm{TLP}}+A\left[\sin\left(\theta_k\right)+1\right]\right]}{c^2}\right\}\left\{1-\left\{\frac{1}{2}\left[\left(1+\beta_k\right)e^{\frac{g}{c}\left(\frac{\theta_{k+1}-\theta_k}{\omega}\right)}+\left(1-\beta_k\right)e^{\frac{g}{c}\left(\frac{\theta_{k+1}-\theta_k}{\omega}\right)}\right]\right\}^{-2}\right\}=0 \tag{4.26}$$

where the constant R_{TLP} is the distance between the table's lowest position and the

center of the earth. The velocity map is also given by Eq. (4.25).

The general-relativistic map [Eqs. (4.26) and (4.25)] is approximately the same as the special-relativistic map [Eqs. (4.24) and (4.25)] if gravity is *weak* [$2g(R_{\mathrm{TLP}} + y)/c^2 << 1$ and $2g(R_{\mathrm{TLP}} + y_0)/c^2 << 1$], where y is the ball's position relative to R_{TLP}. And the general-relativistic map is approximately the same as the Newtonian map [Eqs. (4.22) and (4.23)] if the ball's speed and table's speed are *low* [$v/c << 1$, $v_0/c << 1$, $g(t - t_0)/c << 1$ and $u/c << 1$] and gravity is *weak*. Furthermore, the special-relativistic map is approximately the same as the Newtonian map if the ball's speed and table's speed are *low*.

To time-evolve the Newtonian and relativistic trajectories, the impact-phase maps Eq. (4.22), Eq. (4.24) and Eq. (4.26), which are implicit algebraic equations for θ_{k+1}, must be solved numerically by finding the zero of the function on the left side of the equation given θ_k and v_k. I used Brent's method for this purpose. First, each trajectory is calculated in quadruple precision (35 significant figures) with a tolerance of 10^{-30} for the zeros. The trajectory is then recalculated in quadruple precision but using a smaller tolerance of 10^{-32} for the zeros. Finally, the accuracy of the trajectory is determined by the standard method (Lichtenberg and Lieberman, 1983) of comparing the less-accurate calculation (10^{-30}-tolerance) with the more-accurate calculation (10^{-32}-tolerance). For example, if the

Newtonian velocity is 7.123456789… from the 10^{-30}-tolerance calculation and 7.123456799… from the 10^{-32}-tolerance calculation, then it is accurate to 8 significant figures, i.e., 7.1234567. I used g = 981 cm/s^2, $c = 3\times10^{10}$ cm/s, and $R_{\mathrm{TLP}} = 6.4\times10^{8}$ cm (mean radius of the Earth).

The trajectory generated by each of the three maps can be chaotic. A trajectory is defined (Sprott, 2003) as chaotic if it exhibits sensitive dependence on initial conditions, that is, the distance between the trajectory and another initially-nearby trajectory from the same theory grows, on average, exponentially for a short time, where the exponential growth constant is not exactly equal to but close to the Lyapunov exponent which is a long-time asymptotic quantity. To determine if a trajectory is chaotic, I inspect the trajectory in phase space, check for sensitivity of the trajectory to initial conditions and calculate (Sprott, 2003) the largest Lyapunov exponent to see if it is positive.

As for the statistical quantities, they are calculated as follows. For each theory, the ensemble of trajectories is initially Gaussian distributed in position and velocity with means $\langle y_0 \rangle$ and $\langle v_0 \rangle$, and standard deviations σ_{y_0} and σ_{v_0}:

$$\rho(y,v,t=0) = \frac{1}{2\pi\sigma_{y_0}\sigma_{v_0}} \exp\left[-\frac{1}{2}\left[\left(\frac{y-\langle y_0\rangle}{\sigma_{y_0}}\right)^2 + \left(\frac{v-\langle v_0\rangle}{\sigma_{v_0}}\right)^2\right]\right]. \qquad (4.27)$$

Each trajectory in the Newtonian (relativistic) ensemble is time-evolved using the Newtonian (relativistic) impact-phase map and velocity map. For each theory, the

mean trajectory, i.e., mean position and mean velocity, just after each impact is calculated from the ensemble of trajectories. First, the mean trajectory is calculated using 10^6 trajectories in quadruple precision, where the accuracy of the 10^{-30}-tolerance calculation is determined by comparison with the 10^{-32}-tolerance calculation. The mean trajectory is then recalculated using 10^7 trajectories with the same accuracy determination. Finally, the accuracy of the mean trajectory is determined by comparing the 10^6-trajectories calculation with the 10^7-trajectories calculation. The position and velocity standard deviations and probability density functions are calculated in the same manner.

In the following results section, instead of reporting the impact phase θ, i.e., the table's phase just after each impact, I report the ball's position (which is also the table's position) $y = A[\sin(\theta) + 1]$ just after each impact, together with the ball's velocity v just after each impact, when comparing the predictions of the three theories.

4.5 Results

4.5.1 Single-trajectory predictions

Three examples are presented and discussed to illustrate the general results.

In all three examples, the ball's speed and table's speed remained *low* (about $10^{-10}c$), and gravity is *weak* ($2g(R_{TLP}+y)$ is about $10^{-9}c^2$).

In the first two examples, the system is dissipative with $\alpha = 0.5$. In both examples, the initial conditions are 0.02022 cm for the ball's position and 8.17001 cm/s for the ball's velocity. The table's frequency ($\omega/2\pi$) is 60 Hz, but the table's amplitude A is slightly different: 0.0102 cm in the first example, 0.012 cm in the second example.

In the first example, the Newtonian, special-relativistic and general-relativistic trajectories are all non-chaotic. Fig. 4.1 shows that the three trajectories are close to one another and they converge to period-one fixed-point attractors which are almost identical.

In the second example, the Newtonian, special-relativistic and general-relativistic trajectories, which are plotted in phase space in the top part of Figs. 4.2, 4.3 and 4.4 respectively, are all chaotic as evidenced by the sensitivity to initial conditions (shown in the bottom part of Figs. 4.2, 4.3 and 4.4 respectively) and positive largest Lyapunov exponent of 0.34 for each trajectory. Fig. 4.5 shows that the agreement between the special-relativistic trajectory and general-relativistic trajectory breaks down very quickly at impact 55, and the

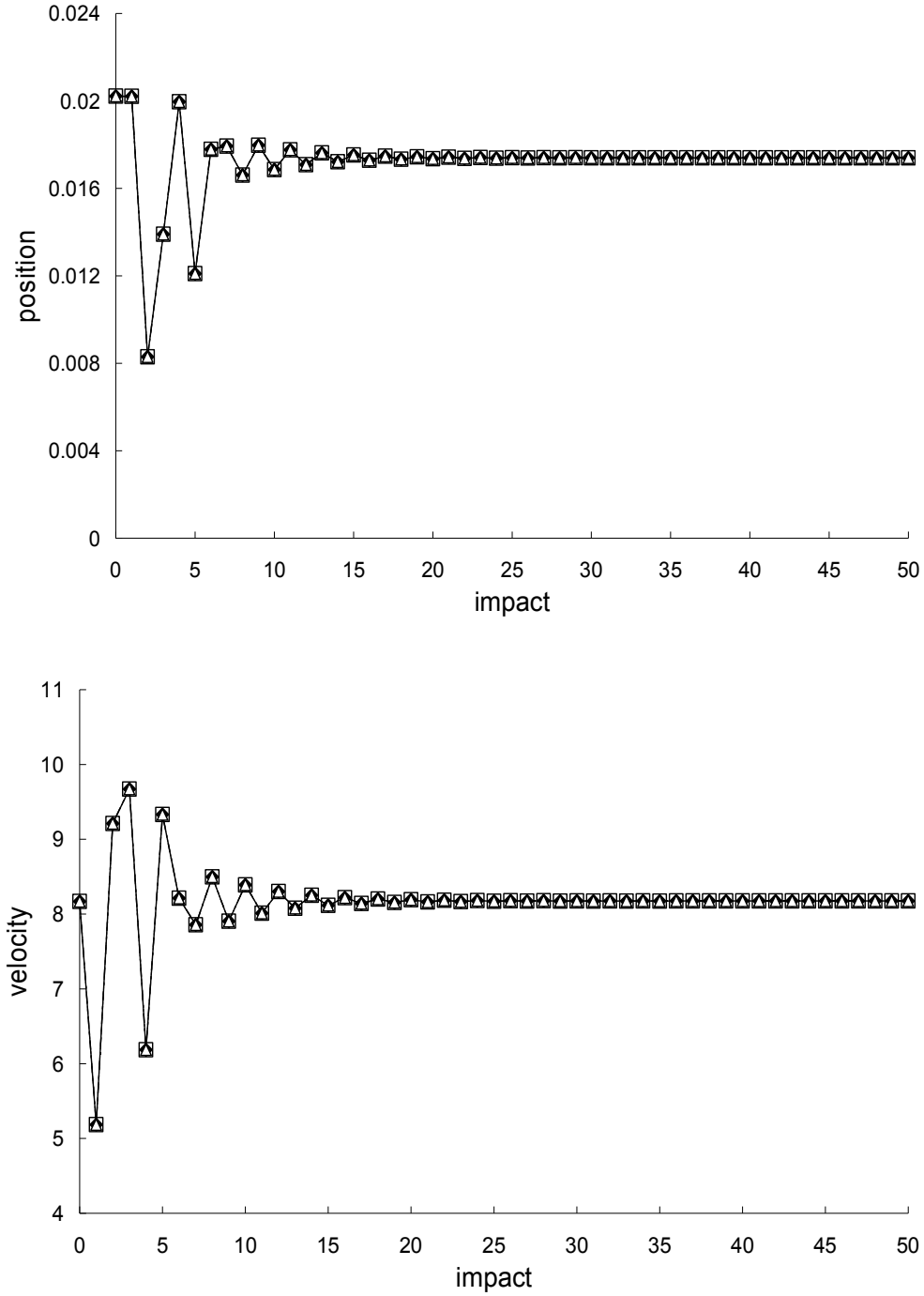

Figure 4.1. Comparison of the Newtonian (squares), special-relativistic (diamonds) and general-relativistic (triangles) positions (top plot) and velocities (bottom plot) for the non-chaotic first example.

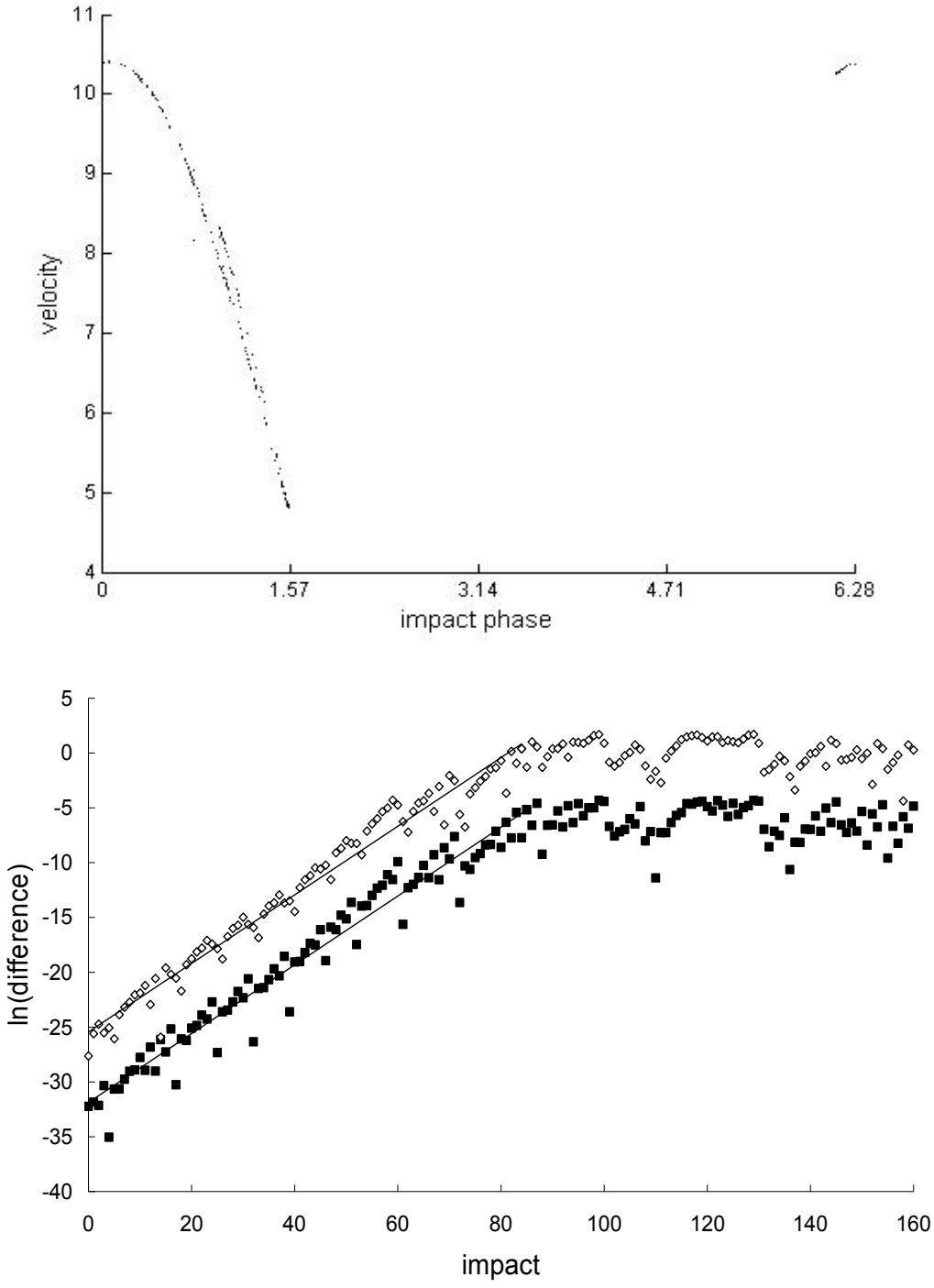

Figure 4.2. Top: Chaotic Newtonian phase-space trajectory, plotted for the first 210 impacts, from the second example. Bottom: Natural-log of the magnitude of the difference [position difference (squares), velocity difference (diamonds)] between the chaotic Newtonian trajectory and another Newtonian trajectory which differed initially by 10^{-14} in position and 10^{-12} in velocity. Straight-line fits up to impact 84 are also plotted.

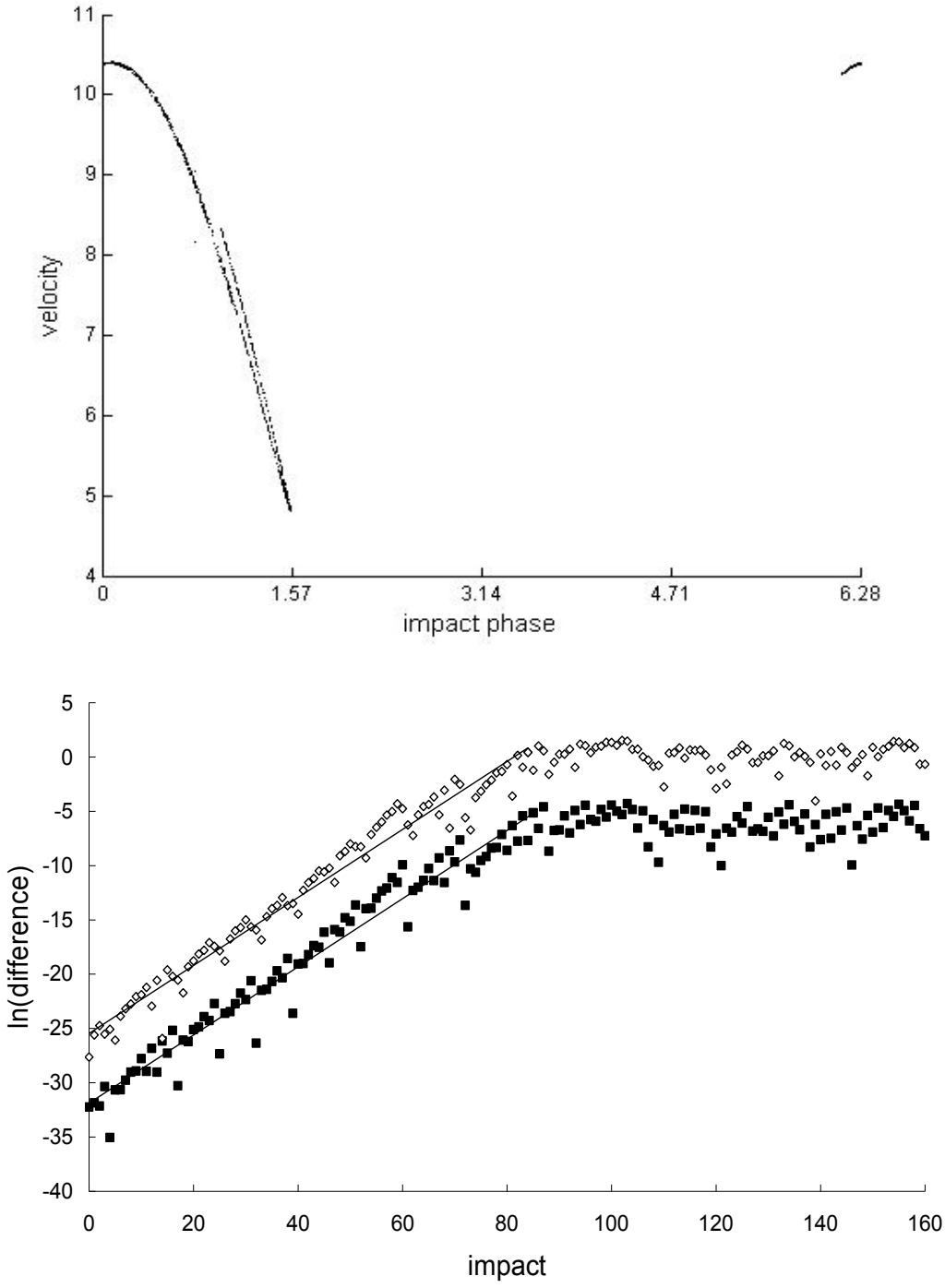

Figure 4.3. Top: Chaotic special-relativistic phase-space trajectory, plotted for the first 1000 impacts, from the second example. Bottom: Natural-log of the magnitude of the difference [position difference (squares), velocity difference (diamonds)] between the chaotic special-relativistic trajectory and another special-relativistic trajectory which differed initially by 10^{-14} in position and 10^{-12} in velocity. Straight-line fits up to impact 84 are also plotted.

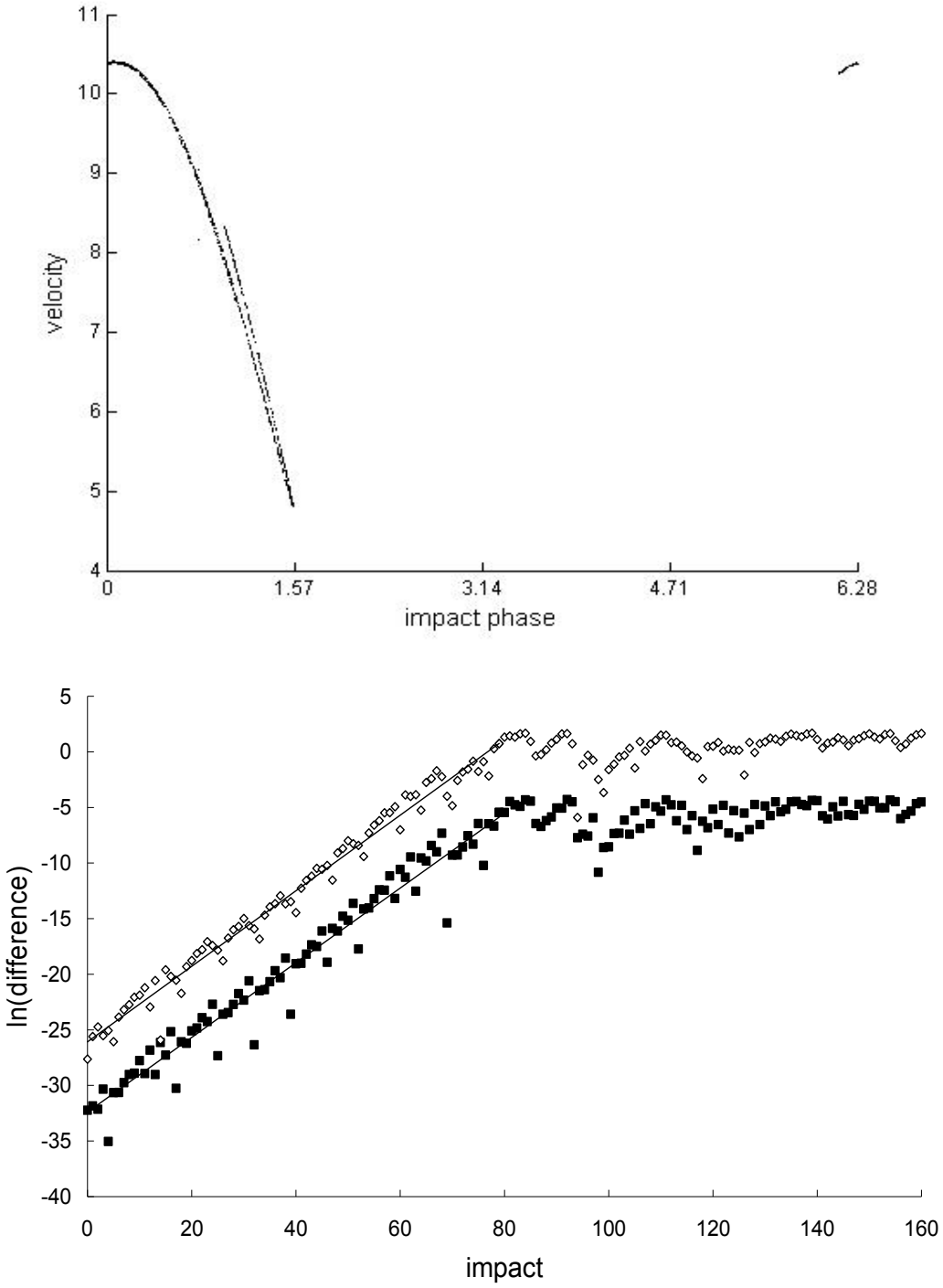

Figure 4.4. Top: Chaotic general-relativistic phase-space trajectory, plotted for the first 1000 impacts, from the second example. Bottom: Natural-log of the magnitude of the difference [position difference (squares), velocity difference (diamonds)] between the chaotic general-relativistic trajectory and another general-relativistic trajectory which differed initially by 10^{-14} in position and 10^{-12} in velocity. Straight-line fits up to impact 79 are also plotted.

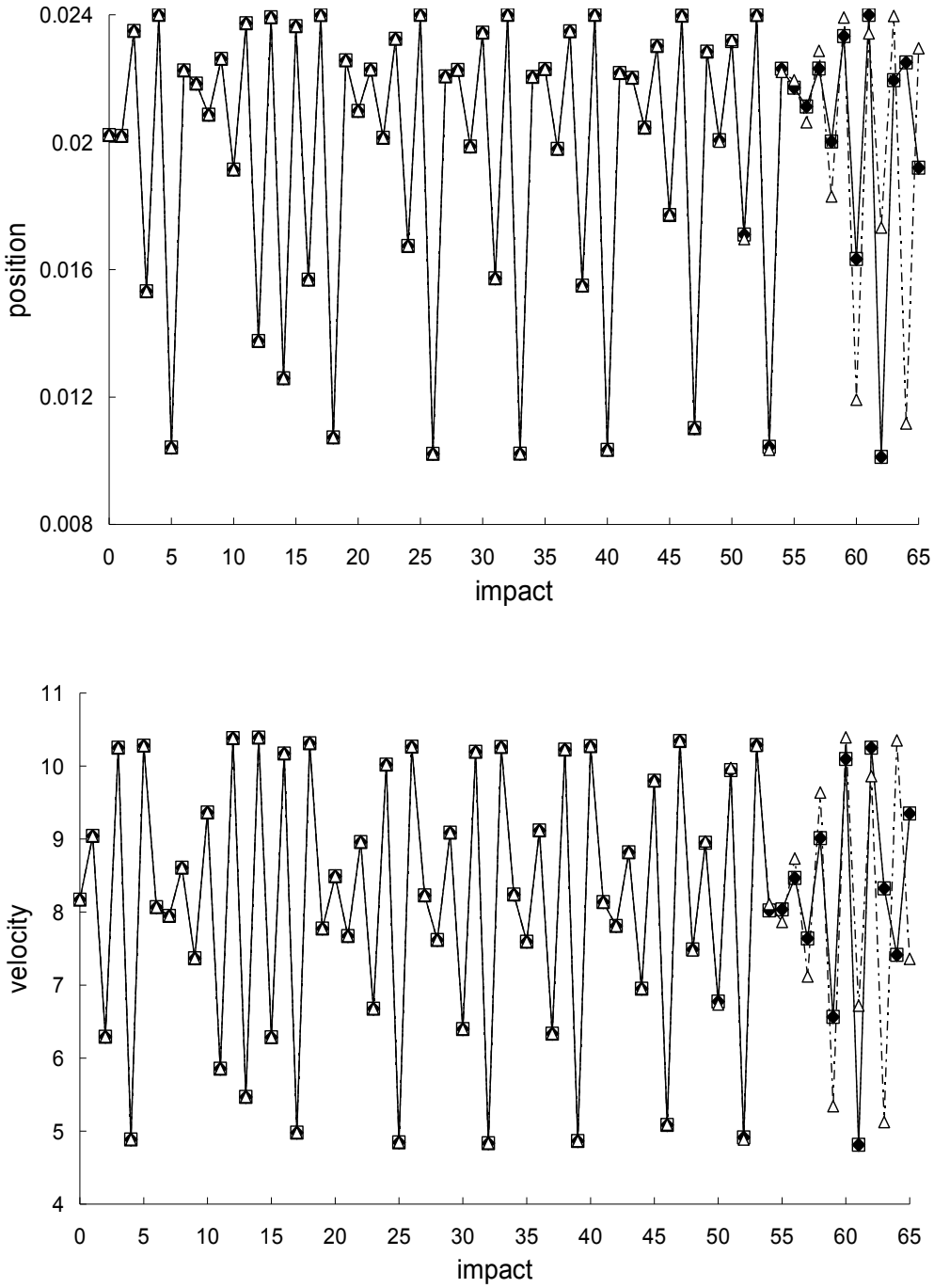

Figure 4.5. Comparison of the Newtonian (squares), special-relativistic (diamonds) and general-relativistic (triangles) positions (top plot) and velocities (bottom plot) for the chaotic second example.

agreement between the Newtonian trajectory and general-relativistic trajectory also breaks down at impact 55. The breakdown of agreement between the Newtonian and special-relativistic trajectories (not shown in Fig. 4.5) occurs later, at impact 95.

Figures 4.6 and 4.7 show, respectively, that the rapid breakdown of agreement between the special-relativistic and general-relativistic trajectories and between the Newtonian and general-relativistic trajectories are due to the, on average, exponential growth – that is, exponential growth with small fluctuations – of the magnitude of the difference between the two trajectories for at least the first 61 impacts:

$$\Delta y_n \approx \Delta y_1 e^{c_1 (n-1)} \tag{4.28}$$

$$\Delta v_n \approx \Delta v_1 e^{c_2 (n-1)} \tag{4.29}$$

where $n = 1,2,\ldots$. In both cases, the exponential growth constants for the position difference in Eq. (4.28) and velocity difference in Eq. (4.29) are close to each other: $c_1 \approx 0.360$ and $c_2 \approx 0.363$. This exponential growth constant of about 0.36 is close to (i) the exponential growth constant for the magnitude of the difference (plotted in Figs. 4.2, 4.3 and 4.4) between the chaotic trajectory and another initially-nearby trajectory from the same theory – the growth constants are 0.31,

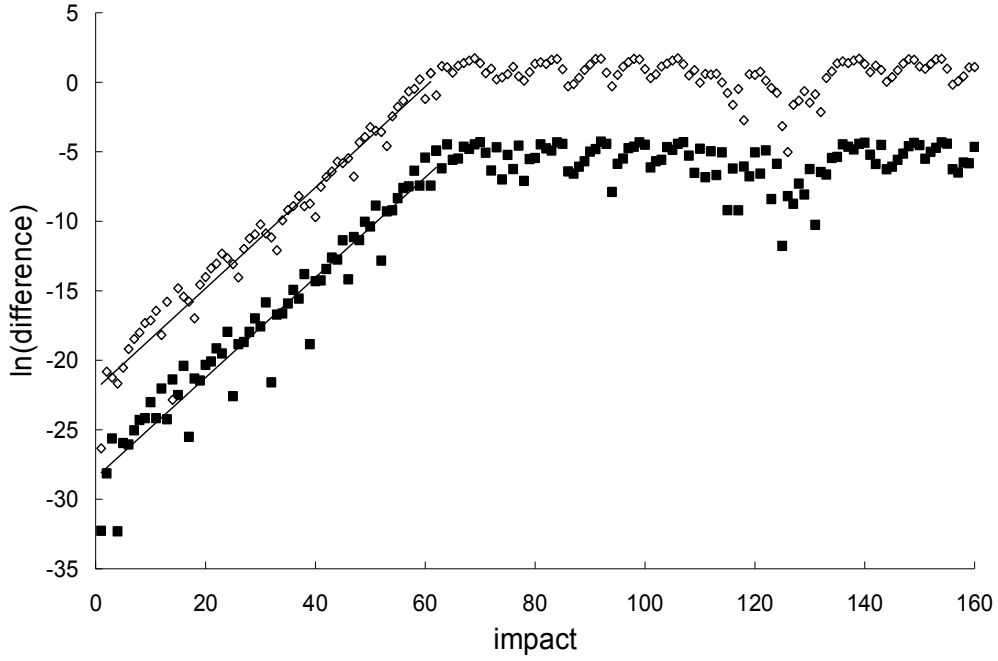

Figure 4.6. Natural-log of the magnitude of the difference between the special-relativistic and general-relativistic positions (squares) and velocities (diamonds) for the chaotic second example. Straight-line fits up to impact 61 are also plotted.

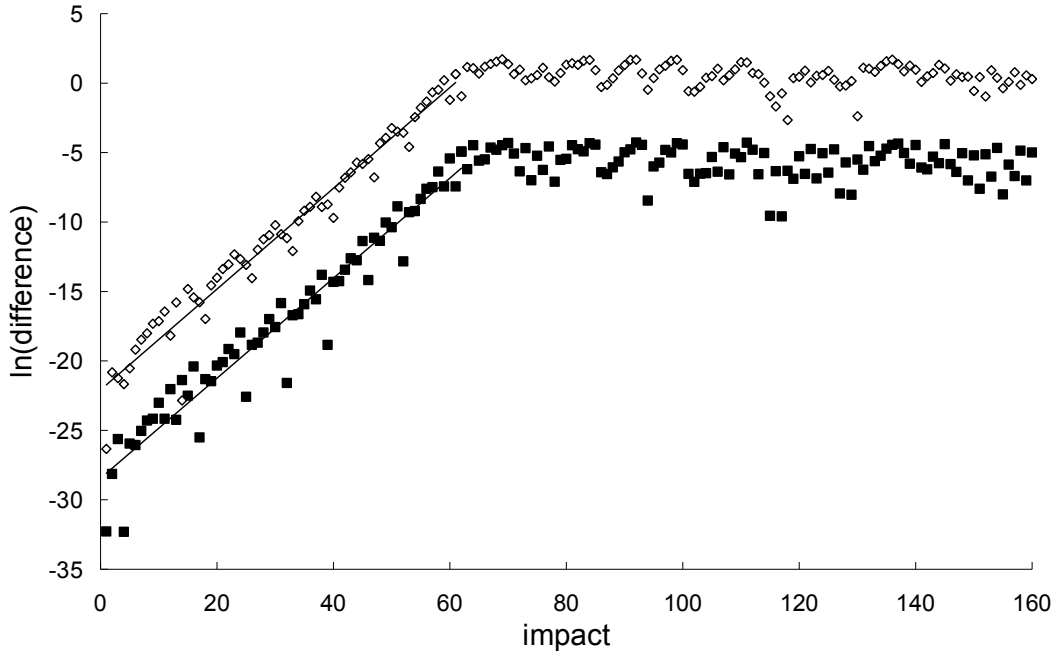

Figure 4.7. Natural-log of the magnitude of the difference between the Newtonian and general-relativistic positions (squares) and velocities (diamonds) for the chaotic second example. Straight-line fits up to impact 61 are also plotted.

0.31 and 0.34, respectively, for the Newtonian, special-relativistic and general-relativistic case, where the two nearby trajectories differed initially by 10^{-14} in position and 10^{-12} in velocity, and (ii) the largest Lyapunov exponent of 0.34 for the Newtonian, special-relativistic and general- relativistic chaotic trajectories. I note that the magnitude of the difference between the Newtonian and special-relativistic trajectories also grows exponentially on average, consistent with the results in (Lan, 2006, 2009a; Lan and Cheng, 2010; Lan and Borondo, 2011) for low-speed systems, with growth constants $c_1 \approx 0.319$ and $c_2 \approx 0.320$.

In the non-dissipative case, where $\alpha = 1$, the agreement between the special-relativistic and Newtonian chaotic trajectories with the general-relativistic chaotic trajectory also breaks down exponentially fast. The agreement also breaks down for non-chaotic trajectories but it takes a much longer time to occur because the difference between the trajectories only grows linearly. Fig. 4.8 illustrates this linear growth for the difference between the Newtonian and general-relativistic quasiperiodic trajectories (the trajectories are plotted in phase space in Fig. 4.9) – in this third example, the table's frequency and amplitude are 60 Hz and 0.005 cm, and the ball's initial position and velocity are 0.00991 cm and 8.17001 cm/s. The

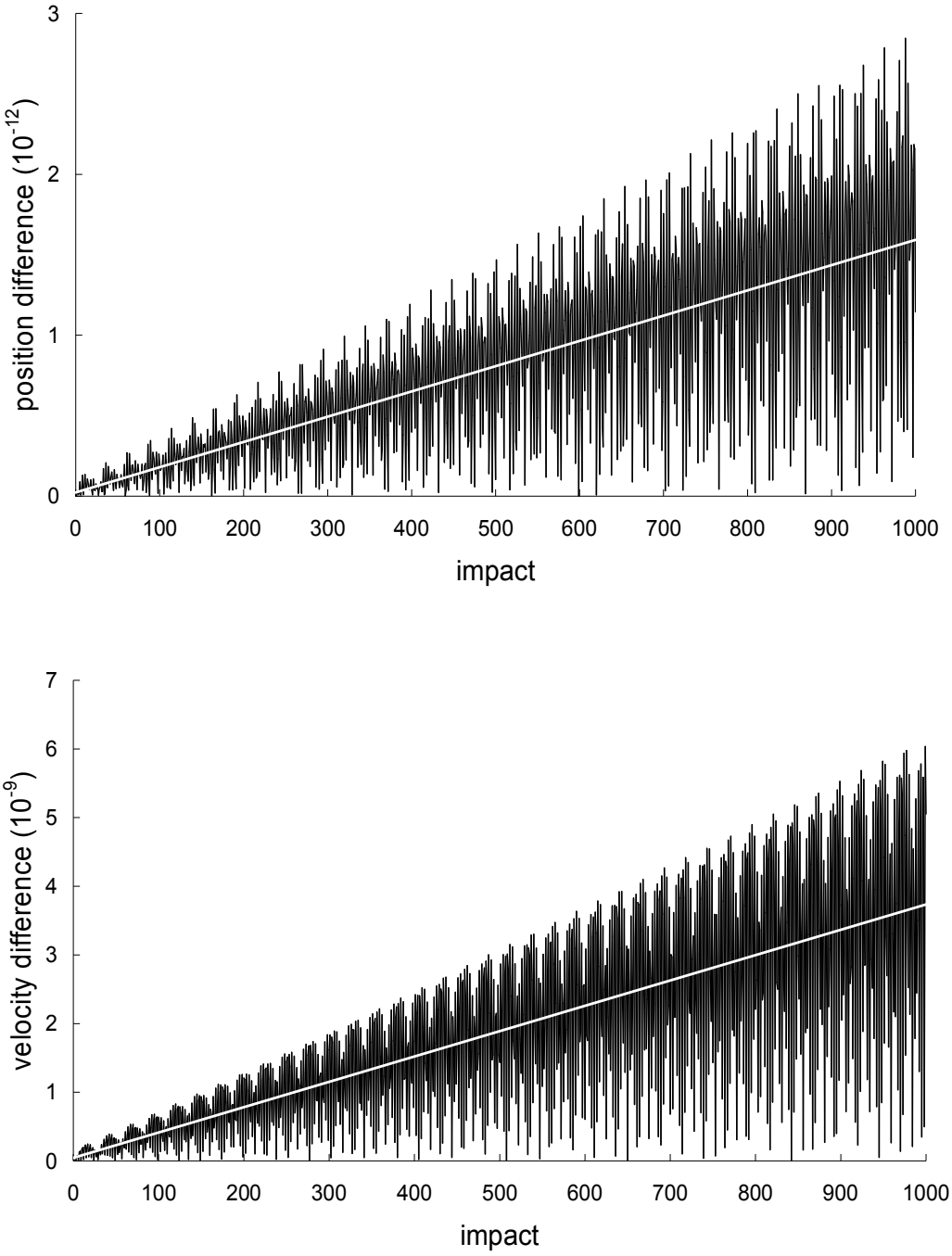

Figure 4.8. Magnitude of the difference between the Newtonian and general-relativistic positions (top plot) and velocities (bottom plot) for the non-chaotic third example. Straight-line fits are also plotted.

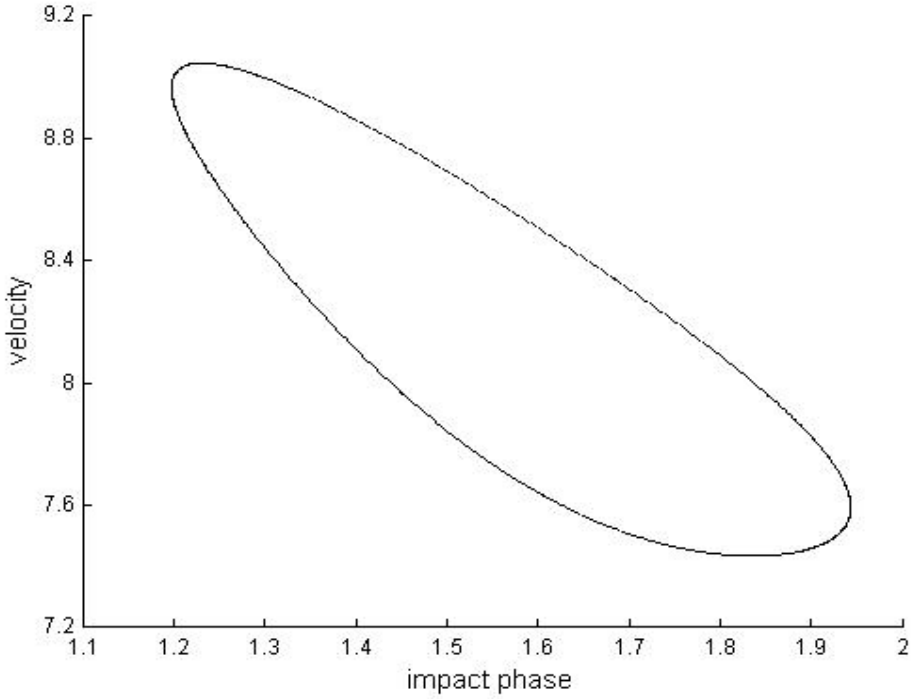

Figure 4.9. Quasiperiodic Newtonian, special-relativistic and general-relativistic phase-space trajectories, plotted for the first 1000 impacts, from the non-chaotic third example. The three trajectories are still close to one another at impact 1000 and thus they are indistinguishable in the plot.

linear growth rates of the magnitude of the position difference and velocity difference are 2×10^{-15} cm and 4×10^{-12} cm/s, respectively, per impact. It would thus require 2.5×10^{10} (!) impacts for the magnitude of the velocity difference to grow to 0.1 cm/s. Similar linear growth rates were found for the difference between the special-relativistic and general-relativistic quasiperiodic trajectories in this example (the special-relativistic trajectory is also plotted in Fig. 4.9).

In general, the breakdown of agreement between the special-relativistic and

general-relativistic trajectories for *weak gravity*, and between the Newtonian and general-relativistic trajectories for *low speed* and *weak gravity* can be further understood as follows.

Firstly, rewriting the general-relativistic impact-phase map [Eq. (4.26)] and taking the natural logarithm on both sides yield

$$\begin{aligned}&\ln\left\{1-\left\{1-\frac{2g\left[R_{\mathrm{TLP}}+A\left[\sin\left(\theta_k\right)+1\right]\right]}{c^2}\right\}^{-1}\left\{\frac{2gA\left[\sin\left(\theta_k\right)-\sin\left(\theta_{k+1}\right)\right]}{c^2}\right\}\right\}\\&=-2\ln\left\{\frac{1}{2}\left[\left(1+\beta_k\right)e^{-\frac{g}{c}\left(\frac{\theta_{k+1}-\theta_k}{\omega}\right)}+\left(1-\beta_k\right)e^{\frac{g}{c}\left(\frac{\theta_{k+1}-\theta_k}{\omega}\right)}\right]\right\}\end{aligned}. \tag{4.30}$$

For *weak* gravity, we have $2g\{R_{TLP}+A[\sin(\theta_k)+1]\}/c^2<<1$ and this implies that the factor $\{1-2g[R_{TLP}+A[\sin(\theta_k)+1]]/c^2\}^{-1}$ in the logarithmic function on the left of Eq. (4.30) is approximately 1. Furthermore, for *weak* gravity, we have $2g\{R_{TLP}+A[\sin(\theta_{k+1})+1]\}/c^2<<1$, therefore we can use the expansion $\ln(1+x)=x-x^2/2$ for the logarithmic function on the left of Eq. (4.30) since $|x|<<1$. Consequently, Eq. (4.30) becomes

$$\begin{aligned}&A\left[\sin\left(\theta_k\right)+1\right]-\frac{c^2}{g}\ln\left\{\frac{1}{2}\left[\left(1+\beta_k\right)e^{-\frac{g}{c}\left(\frac{\theta_{k+1}-\theta_k}{\omega}\right)}+\left(1-\beta_k\right)e^{\frac{g}{c}\left(\frac{\theta_{k+1}-\theta_k}{\omega}\right)}\right]\right\}-A\left[\sin\left(\theta_{k+1}\right)+1\right]\\&+\frac{g}{c^2}\left\{A\left[\sin\left(\theta_k\right)+1\right]-A\left[\sin\left(\theta_{k+1}\right)+1\right]\right\}^2=0\end{aligned}. \tag{4.31}$$

The approximate general-relativistic impact-phase map given by Eq. (4.31) differs from the special-relativistic impact-phase map [Eq. (4.24)] by the last term which

involves $1/c^2$. The general-relativistic velocity map is exactly the same as the special-relativistic velocity map [Eq. (4.25)]. The breakdown of agreement between the special-relativistic and general-relativistic trajectories is thus essentially due to the small $1/c^2$ term in Eq. (4.31).

Secondly, for *weak* gravity, the factor $\{1 - 2g[R_{TLP} + A[\sin(\theta_k) + 1]]/c^2\}$ in the general-relativistic impact-phase map [Eq. (4.26)] is approximately 1. Additionally, for *low* speed, we have $g(\theta_{k+1} - \theta_k)/(c\omega) << 1$, therefore we can use the expansion $e^x = 1 + x + x^2/2$ for the exponential functions in the term with exponent -2 in Eq. (4.26) since $|x| << 1$. Furthermore, for *low* speed, we have $v_k/c << 1$, and hence we can expand the resulting $(1 + x)^{-2}$ term as $1 - 2x + 3x^2$ since $|x| << 1$. For *low* speed and *weak* gravity, Eq. (4.26) is thus approximately

$$\begin{aligned} &A[\sin(\theta_k)+1]+v_k\left(\frac{\theta_{k+1}-\theta_k}{\omega}\right)-\frac{g}{2}\left(\frac{\theta_{k+1}-\theta_k}{\omega}\right)^2-A[\sin(\theta_{k+1})+1] \\ &+\frac{3g}{2c^2}\left(\frac{\theta_{k+1}-\theta_k}{\omega}\right)^2\left[v_k-\frac{g}{2}\left(\frac{\theta_{k+1}-\theta_k}{\omega}\right)\right]^2=0 \end{aligned} . \tag{4.32}$$

Moreover, for *low* speed, $v'_{k+1}/c << 1$ and $u_{k+1}/c << 1$, and so the general-relativistic velocity map, which is exactly the same as the special-relativistic velocity map [Eq. (4.25)], is approximately

$$v_{k+1} = (1+\alpha)u_{k+1} - \alpha v'_{k+1} . \tag{4.33}$$

Furthermore, for *low* speed, we can use the expansion $e^x = 1 + x + x^2/2$ for the exponential functions in v'_{k+1} (the expression for v'_{k+1} is given after Eq. 4.25)

since $|x|<<1$, and then expand the resulting $(1 + x)^{-1}$ term as $(1 - x)$ since $|x|<<1$. Substituting the resulting approximate expression for v'_{k+1} and $u_{k+1} = A\omega\cos(\theta_{k+1})$ into Eq. (4.33) yields

$$v_{k+1} = (1+\alpha)A\omega\cos(\theta_{k+1}) - \alpha\left[v_k - g\left(\frac{\theta_{k+1}-\theta_k}{\omega}\right)\right] - \frac{\alpha g}{c^2}\left(\frac{\theta_{k+1}-\theta_k}{\omega}\right)\left[v_k^2 - v_k g\left(\frac{\theta_{k+1}-\theta_k}{\omega}\right) + \frac{g^2}{2}\left(\frac{\theta_{k+1}-\theta_k}{\omega}\right)^2\right], \quad (4.34)$$

where terms involving $1/c^4$ are omitted since they are very small. The approximate general-relativistic velocity map given by Eq. (4.34) differs from the Newtonian velocity map [Eq. (4.23)] by the last term which involves $1/c^2$. Similarly, the approximate general-relativistic impact-phase map given by Eq. (4.32) differs from the Newtonian impact-phase map [Eq. (4.22)] by the last term which involves $1/c^2$. The breakdown of agreement between the Newtonian and general-relativistic trajectories is therefore essentially due to the small $1/c^2$ term in Eq. (4.32) and Eq. (4.34).

4.5.2 Statistical predictions : Mean, standard deviation and probability distribution

In this section, I will present four examples to illustrate the general results. In the numerical calculations, I also used $g = 981$ cm/s^2, $c = 3\times10^{10}$ cm/s, and R_{TLP} =

6.4×10^8 cm (mean radius of the Earth). For all examples, the mean velocities of the ball and table remain low at about $10^{-10}c$, i.e., about 10^{-8} percent of the speed of light c, and the gravitational field is weak, about $10^{-9}c^2$.

In the first three examples, the system is dissipative with $\alpha = 0.5$. In the first example, the ensemble in each theory is initially Gaussian distributed with means $\langle y_0 \rangle = 0.02022$ cm and $\langle v_0 \rangle = 8.17001$ cm/s, and standard deviations $\sigma_{y_0} = 10^{-6}$ cm and $\sigma_{v_0} = 10^{-6}$ cm/s. The amplitude A and frequency $\omega/2\pi$ of the table's oscillation are, respectively, 0.0102 cm and 60 Hz. For the choice of parameters and initial conditions in this example, the trajectories in the ensembles are non-chaotic. Fig. 4.10 shows that the mean trajectories (mean positions and mean velocities) predicted by the three theories agree with each other and converge to mean values which are almost identical. Similarly, there is no breakdown of agreement between the position and velocity standard deviations predicted by the three theories (see Fig. 4.11). This result is also true when initial Gaussian ensembles with smaller widths – for example, the position and velocity standard deviations are of the order 10^{-10} or 10^{-13} – are used in the numerical calculations.

In the second example, all the parameters and initial conditions are the same as the first example except that the table's amplitude is 0.012 cm and the position

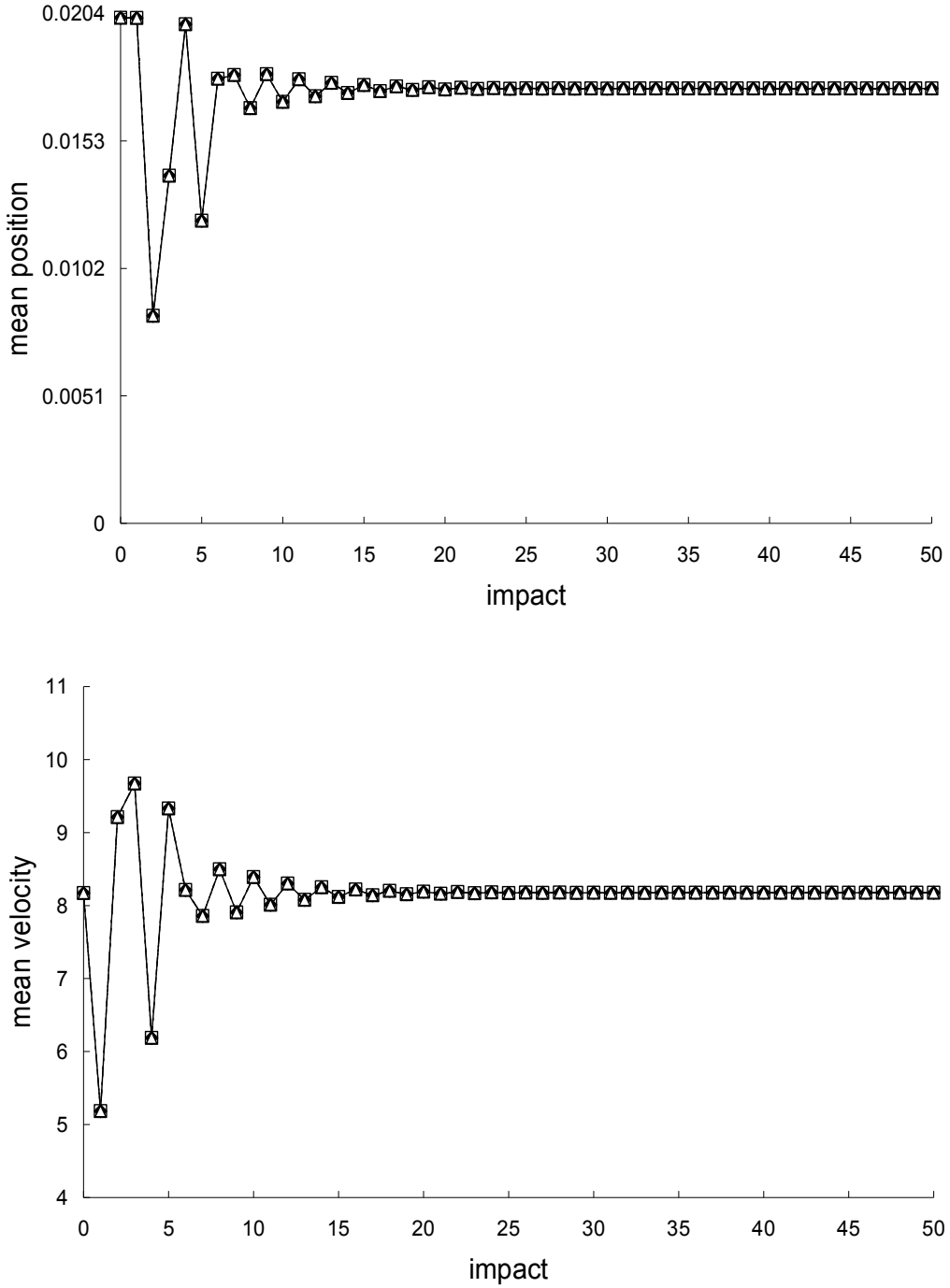

Figure 4.10. Newtonian (squares), special-relativistic (diamonds) and general-relativistic (triangles) mean positions (top plot) and mean velocities (bottom plot) for the non-chaotic first example.

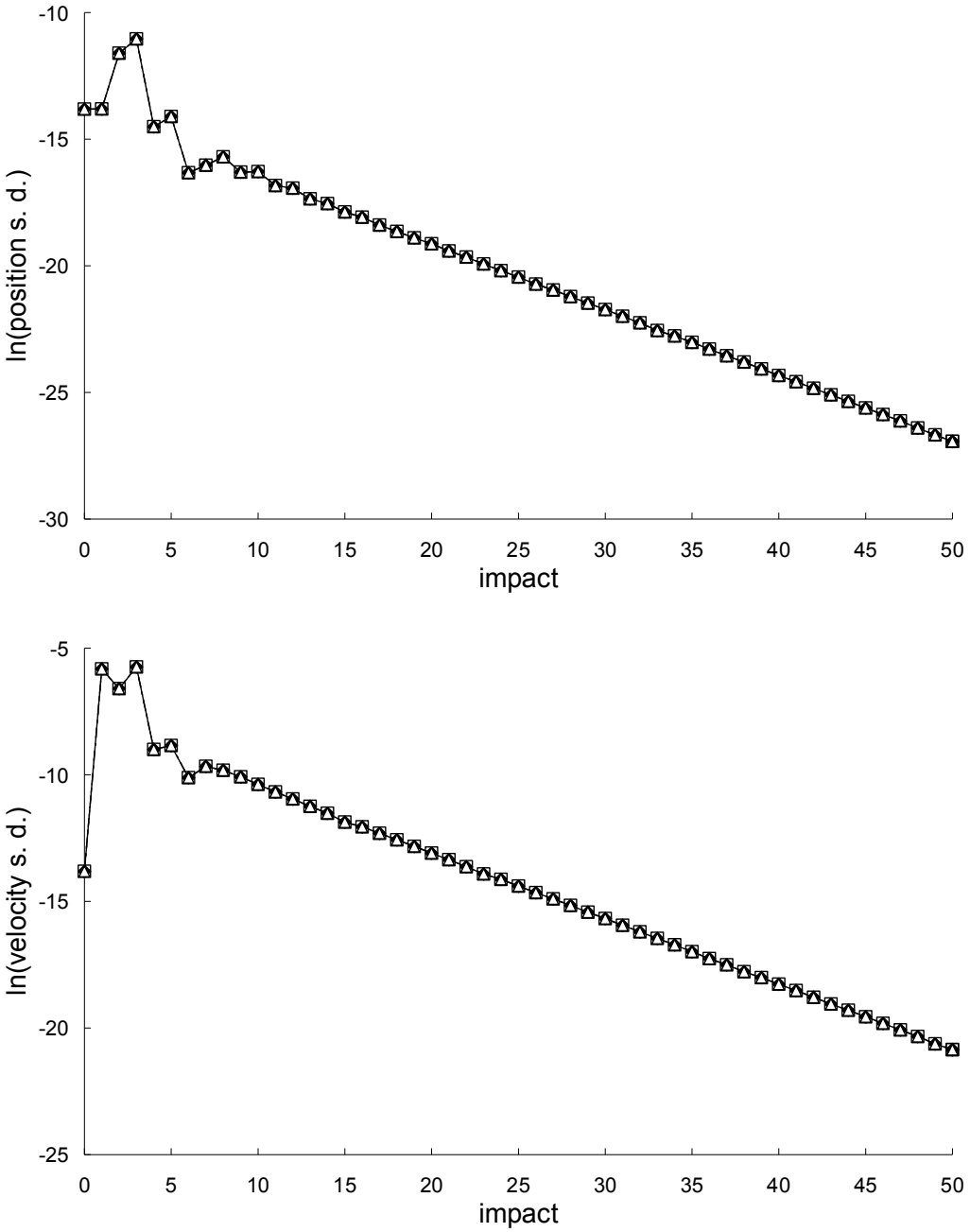

Figure 4.11. Natural-log of the Newtonian (squares), special-relativistic (diamonds) and general-relativistic (triangles) position standard deviations (top plot) and velocity standard deviations (bottom plot) for the non-chaotic first example.

and velocity standard deviations of the initial Gaussian ensemble are 10^{-13} cm and 10^{-13} cm/s respectively. In this example, the trajectories in the ensembles are chaotic. Fig. 4.12 shows that the Newtonian, special-relativistic and general-relativistic mean trajectories are close to each other for the first 54 impacts. However, the Newtonian and special-relativistic mean trajectories disagree completely with the general-relativistic mean trajectory from impact 55 onwards. The breakdown of agreements can be understood as follows. In each theory, the mean trajectory is well-approximated by the central trajectory, that is, the single trajectory with the same initial conditions as the mean trajectory, until the velocity probability density is delocalized which triggers the delocalization of the position probability density. The Newtonian, special-relativistic and general-relativistic velocity probability densities are delocalized at, respectively, impact 70, 70 and 67 – see Figs. 4.13, 4.14 and 4.15 respectively. In each theory, before the delocalization, the position and velocity standard deviations grow, on average, exponentially with grow constants close to the largest Lyapunov exponent of 0.34 for the central trajectory. The agreement between the special-relativistic (Newtonian) and general-relativistic central trajectories breaks down at impact 55, and, therefore, the agreement between the special-relativistic

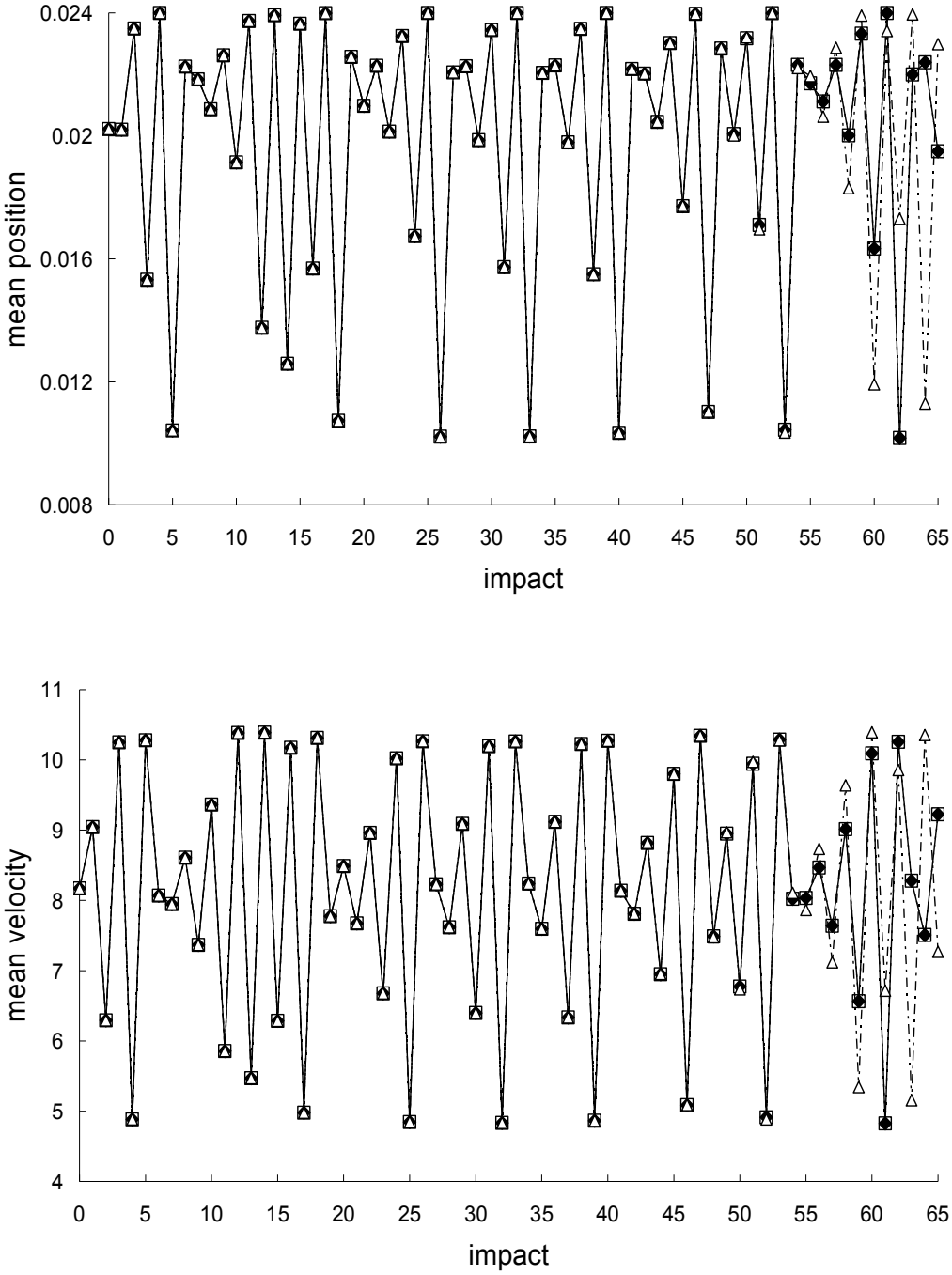

Figure 4.12. Newtonian (squares), special-relativistic (diamonds) and general-relativistic (triangles) mean positions (top plot) and mean velocities (bottom plot) for the chaotic second example.

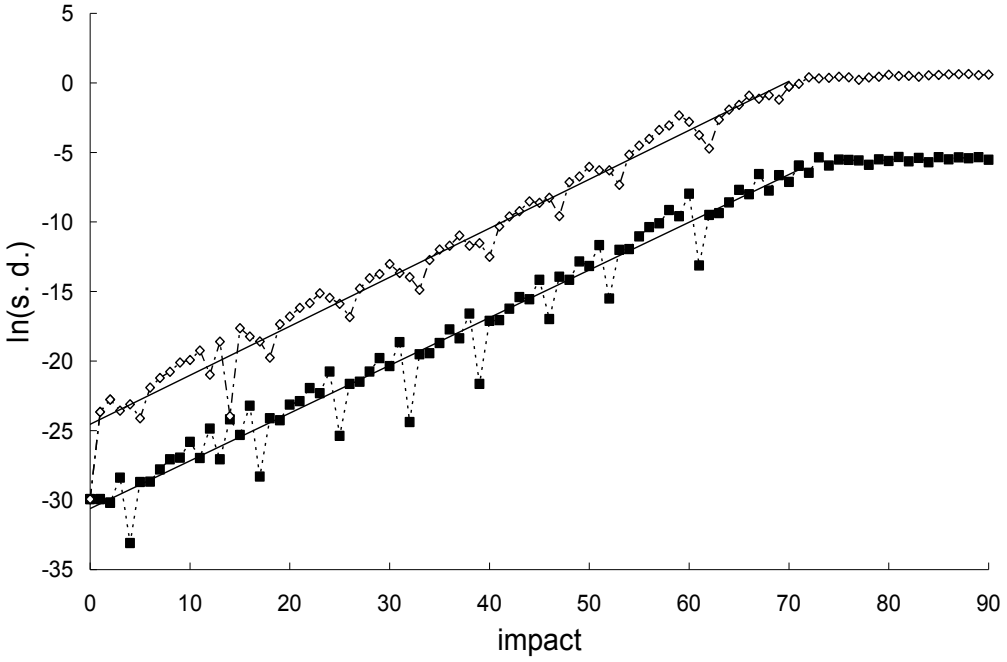

Figure 4.13. Natural-log of the Newtonian position standard deviations (squares) and velocity standard deviations (diamonds) for the chaotic second example. Straight-line fits up to impact 70 are also plotted.

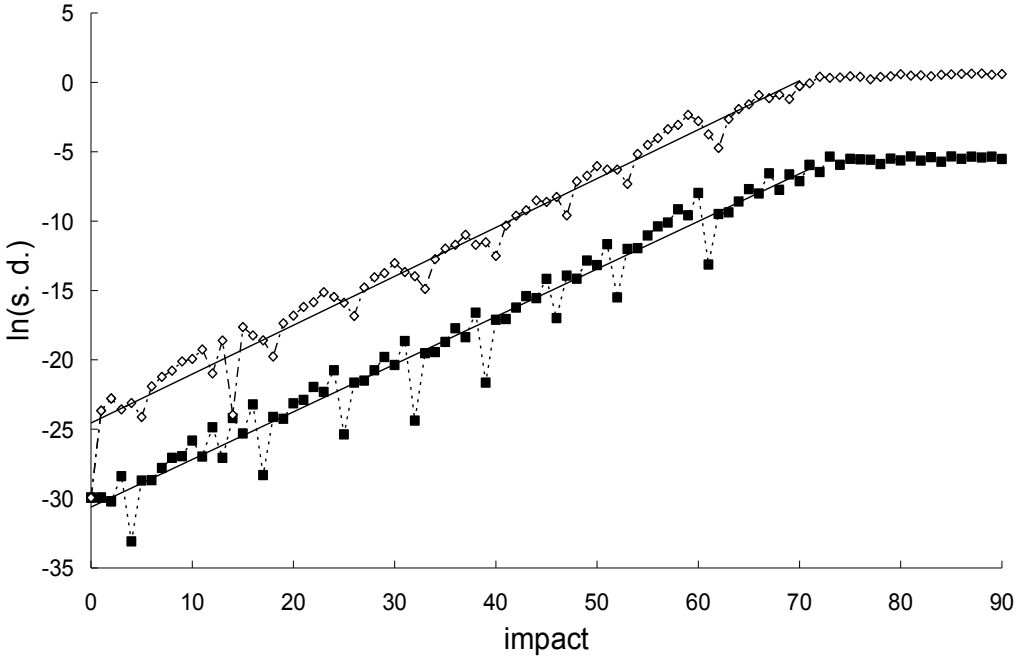

Figure 4.14. Natural-log of the special-relativistic position standard deviations (squares) and velocity standard deviations (diamonds) for the chaotic second example. Straight-line fits up to impact 70 are also plotted.

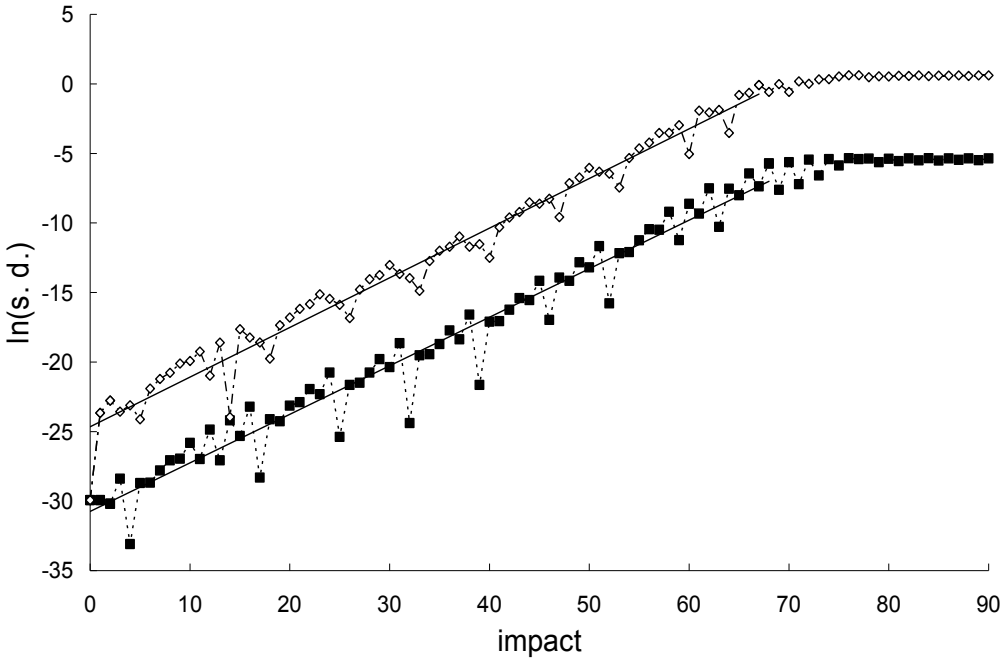

Figure 4.15. Natural-log of the general-relativistic position standard deviations (squares) and velocity standard deviations (diamonds) for the chaotic second example. Straight-line fits up to impact 67 are also plotted.

(Newtonian) and general-relativistic mean trajectories also breaks down at impact 55. Moreover, Fig. 4.16 (Fig. 4.17) shows that the difference between the special-relativistic (Newtonian) and general-relativistic mean trajectories grows, on average, exponentially, at least up to impact 61 because the difference between the special-relativistic (Newtonian) and general-relativistic central trajectories grows exponentially on average. All of the exponential growth constants of the mean-trajectory differences are also close to the largest Lyapunov exponent of

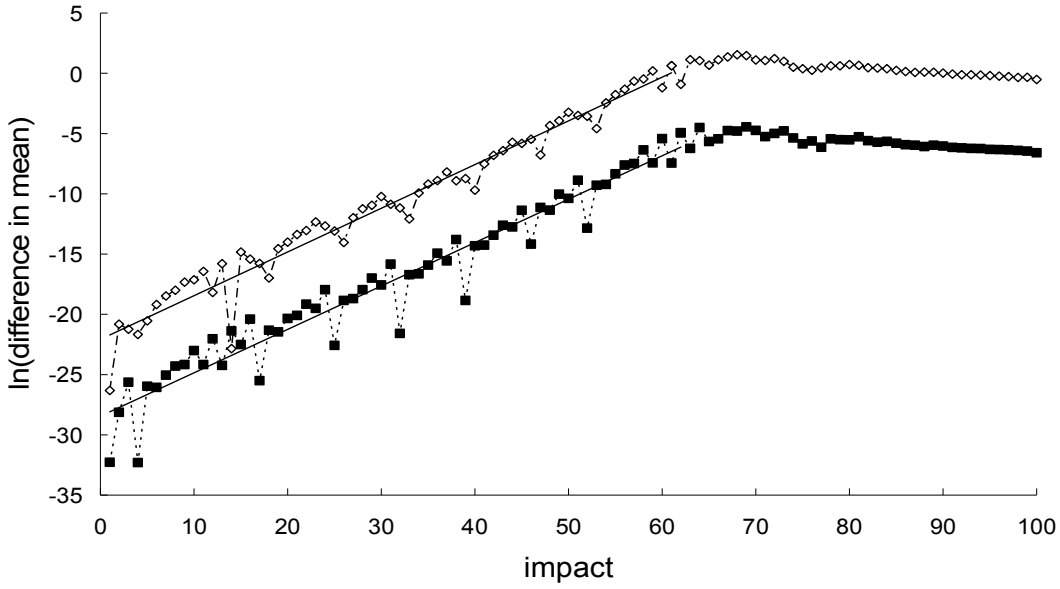

Figure 4.16. Natural-log of the magnitude of the difference between the special-relativistic and general-relativistic mean positions (squares) and mean velocities (diamonds) for the chaotic second example. Straight-line fits up to impact 61 are also plotted.

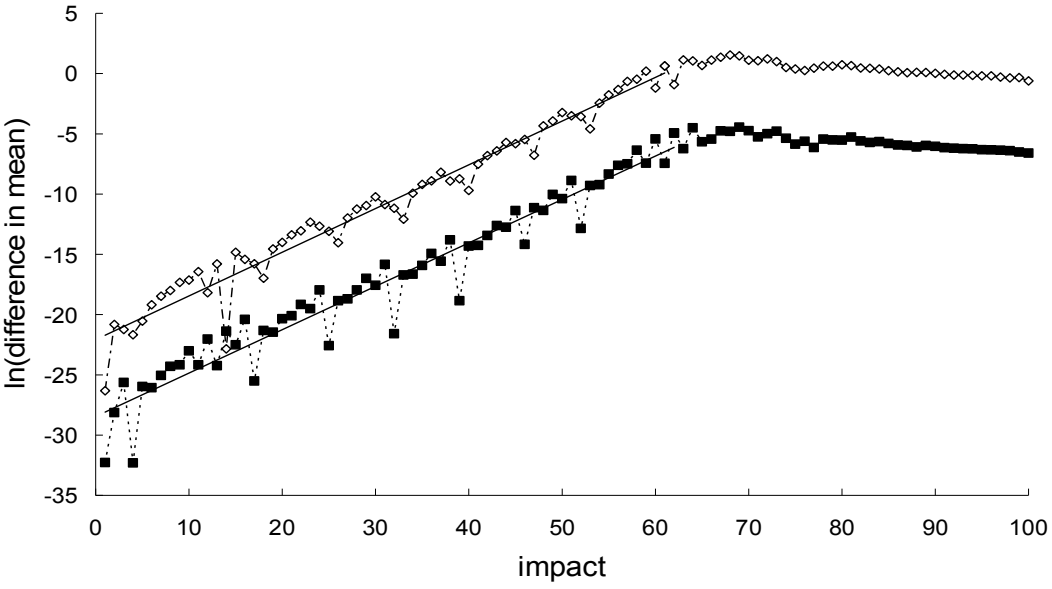

Figure 4.17. Natural-log of the magnitude of the difference between the Newtonian and general-relativistic mean positions (squares) and mean velocities (diamonds) for the chaotic second example. Straight-line fits up to impact 61 are also plotted.

0.34 for the central trajectory in each theory. The exponential growth of difference between the central trajectories caused the rapid breakdown of agreement between the mean trajectories.

Furthermore, Fig. 4.18 shows that the Newtonian and special-relativistic standard deviations disagree completely with the general-relativistic standard deviations from impact 52 onwards. The rapid breakdown of agreement between the special-relativistic (Newtonian) and general-relativistic standard deviations is due to the, on average, exponential growth of the difference between the special-relativistic (Newtonian) and general-relativistic standard deviations at least up to impact 61, see Fig. 4.19 (Fig. 4.20). In both figures, the exponential growth constants of the position and velocity standard-deviation differences are, respectively, 0.74 and 0.72, which are measured from impact 32 to impact 61 (the standard-deviation differences before impact 32 cannot be resolved with the accuracy I have for the standard deviations). These exponential growth constants are about two times the largest Lyapunov exponent of 0.34 for the central trajectory in each theory. Fig. 4.21 (Fig. 4.22) shows the different special-relativistic (Newtonian) and general-relativistic probability densities at impact 55.

In the second example, similar rapid breakdown of agreement occur between

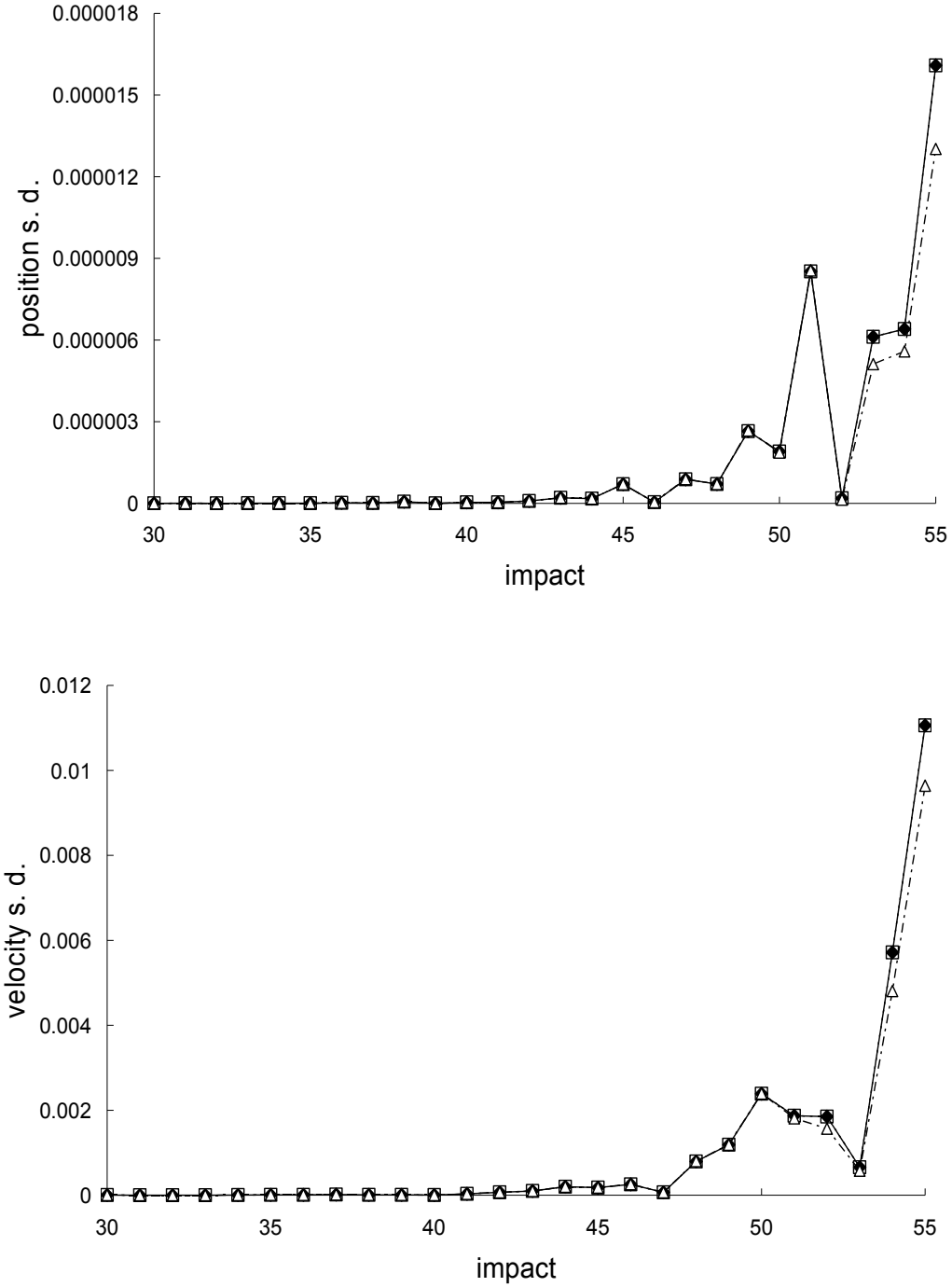

Figure 4.18. Newtonian (squares), special-relativistic (diamonds) and general-relativistic (triangles) position standard deviations (top plot) and velocity standard deviations (bottom plot) for the chaotic second example. The Newtonian and relativistic standard deviations before impact 30 are not plotted because they are still close to each other.

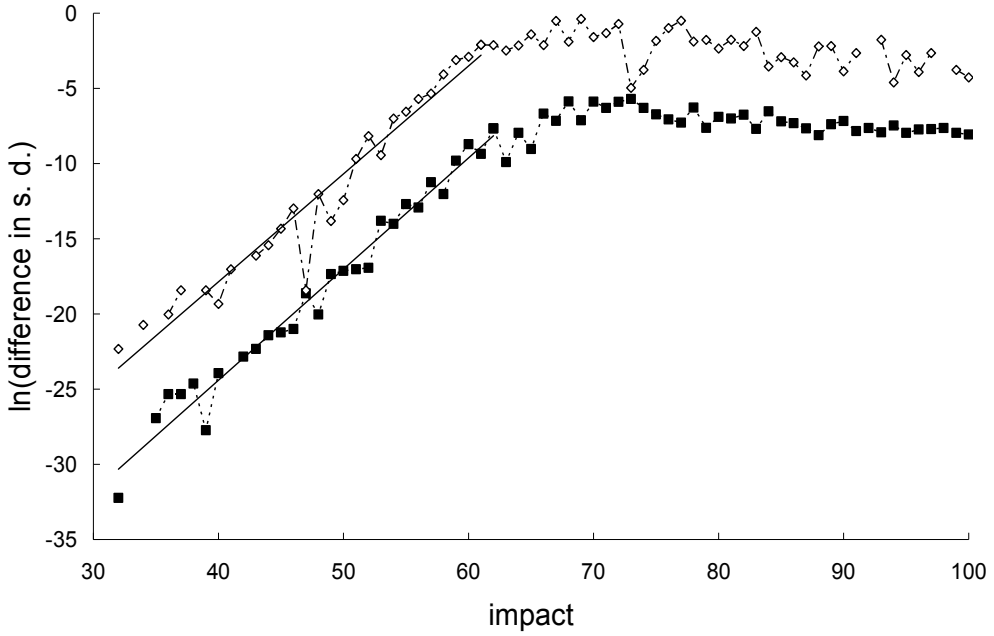

Figure 4.19. Natural-log of the absolute value of the difference between the special-relativistic and general-relativistic position standard deviations (squares) and velocity standard deviations (diamonds) for the chaotic second example. Straight-line fits up to impact 61 are also plotted. The standard-deviation differences before impact 32 cannot be resolved with the accuracy I have for the special-relativistic and general-relativistic standard deviations.

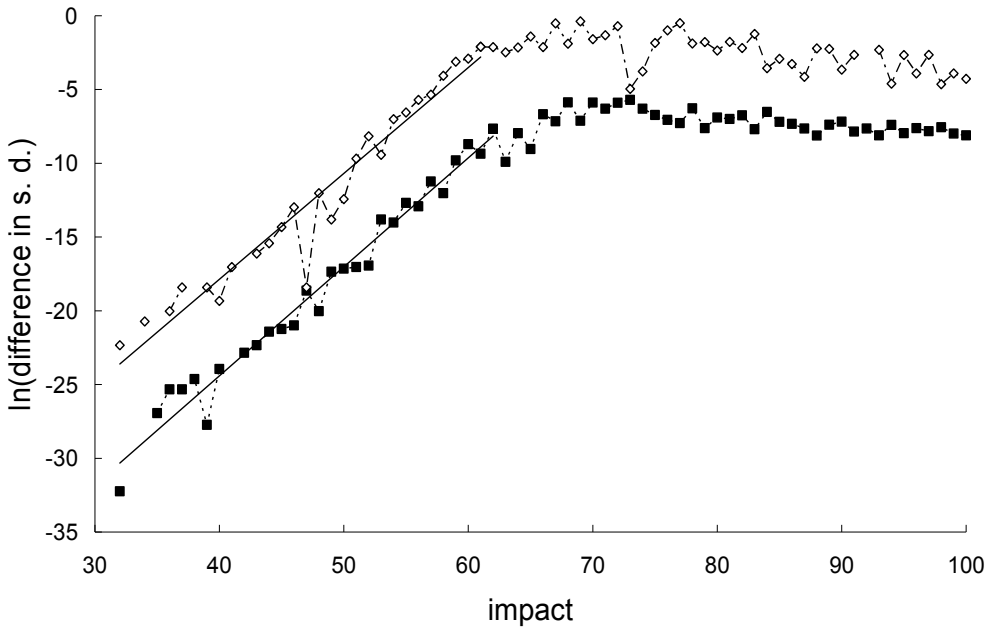

Figure 4.20. Natural-log of the absolute value of the difference between the Newtonian and general-relativistic position standard deviations (squares) and velocity standard deviations (diamonds) for the chaotic second example. Straight-line fits up to impact 61 are also plotted. The standard-deviation differences before impact 32 cannot be resolved with the accuracy I have for the Newtonian and general-relativistic standard deviations.

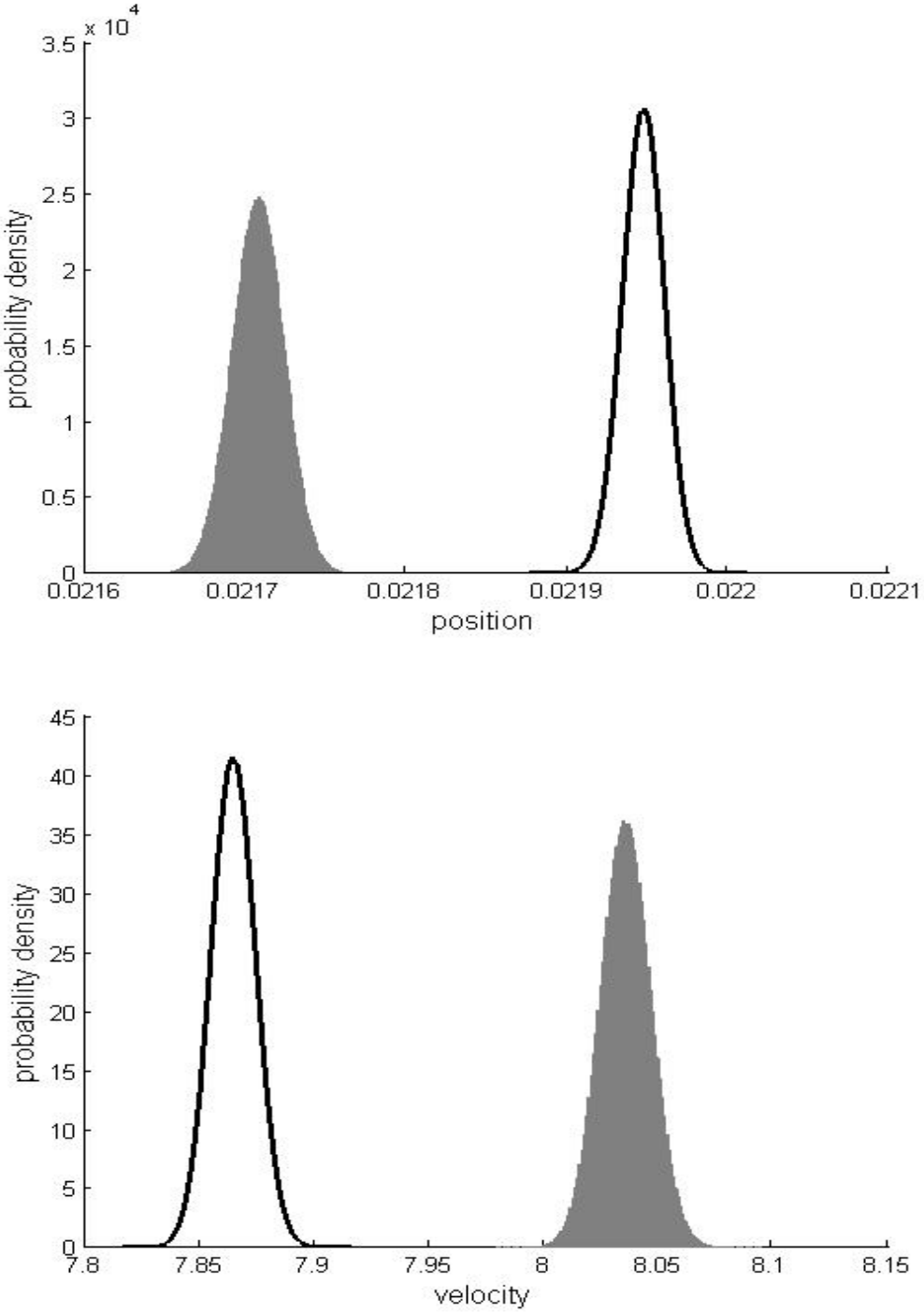

Figure 4.21. Special-relativistic (shaded grey) and general-relativistic (bold line) position probability densities (top plot) and velocity probability densities (bottom plot) for the chaotic second example at impact 55.

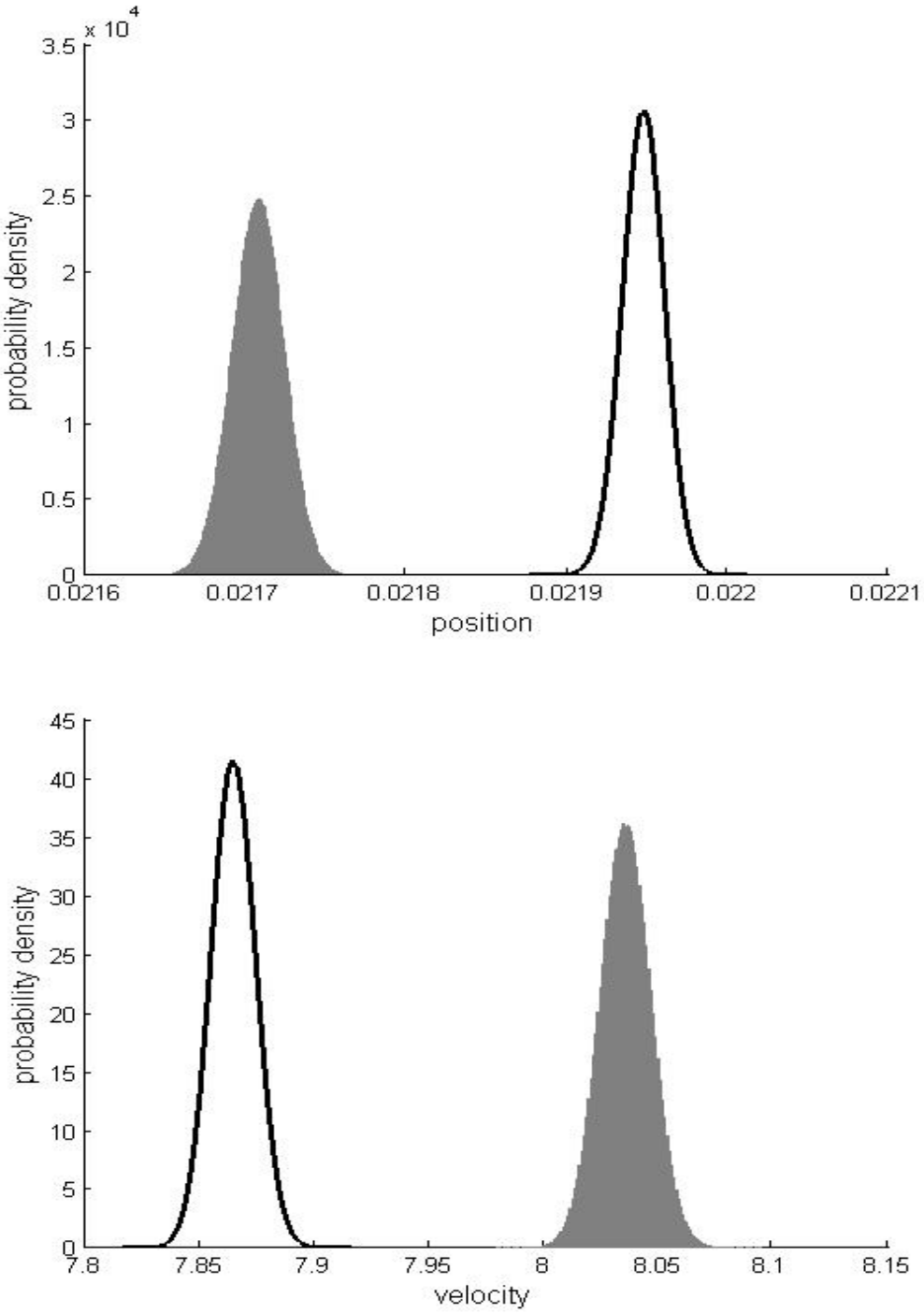

Figure 4.22. Newtonian (shaded grey) and general-relativistic (bold line) position probability densities (top plot) and velocity probability densities (bottom plot) for the chaotic second example at impact 55.

the Newtonian and special-relativistic mean trajectories and standard deviations. However, in order to see the breakdown of agreements, the initial Gaussian ensemble must be smaller in width, on the order of 10^{-17}.

In the third example, all the parameters and initial conditions are the same as in the second example, except that the position and velocity standard deviations of the initial Gaussian ensemble are larger, i.e., 10^{-10} cm and 10^{-10} cm/s respectively. The trajectories in the ensembles are also chaotic. However, in contrast to the second example, there is no breakdown of agreement between the special-relativistic (Newtonian) and general-relativistic mean trajectories and standard deviations. In this example, when the special-relativistic (Newtonian) and general-relativistic phase-space distributions are both delocalized at impact 49 (the delocalization occurs first for the velocity at impact 48 followed by the position delocalization at the next impact), the special-relativistic (Newtonian) and general-relativistic mean trajectories are still close to each other, because, recall from the second example, the agreement between the special-relativistic (Newtonian) and general-relativistic central trajectories only breaks down later at impact 55. Similarly, at impact 49, the special-relativistic (Newtonian) and general-relativistic standard deviations are also still close to one another. The special-relativistic (Newtonian) and general-relativistic means and standard

deviations therefore remain close to each other at subsequent impacts since the special-relativistic (Newtonian) and general-relativistic delocalized phase-space distributions at impact 49 are close to each other.

Recall, in the chaotic second example (with *smaller* initial standard deviations), the special-relativistic (Newtonian) and general-relativistic velocity probability densities delocalize *after* the agreement between the special-relativistic (Newtonian) and general-relativistic central trajectories breaks down. However, in the chaotic third example (with *larger* initial standard deviations), the special-relativistic (Newtonian) and general-relativistic velocity probability densities delocalize *before* the agreement between the special-relativistic (Newtonian) and general-relativistic central trajectories breaks down. The chaotic second and third examples therefore show that in order for the special-relativistic (Newtonian) and general-relativistic statistical predictions to break down, the initial Gaussian ensemble must be sufficiently well-localized, that is, the standard deviations must be sufficiently small such that the special-relativistic (Newtonian) and general-relativistic velocity probability densities delocalize *after* the agreement between the special-relativistic (Newtonian) and general-relativistic central trajectories breaks down.

If the system is conservative (α = 1), the agreement between the

special-relativistic (Newtonian) and general-relativistic predictions for the means and standard deviations can break down in both the chaotic and non-chaotic case. For the breakdown of agreement to occur, the initial Gaussian ensemble must be sufficiently well-localized such that the velocity probability densities delocalize *after* the agreement between central trajectories breaks down. In the chaotic case, the breakdown of agreement is rapid because the difference between the central trajectories grows exponentially, like the dissipative chaotic second example. But in the non-chaotic case, the breakdown of agreement takes a very long time to occur because the difference between the central trajectories only grows linearly - the fourth example illustrate this result, where the table is oscillating with amplitude 0.005 cm and frequency 60 Hz, and the means and standard deviations of the initial Gaussian ensemble are: $\langle y_0 \rangle$ = 0.00991 cm, $\langle v_0 \rangle$ = 8.17001 cm/s, σ_{y_0} = 10^{-6}, σ_{v_0} = 10^{-6} cm/s. In this example, the mean trajectories predicted by the three theories are still very close to one another at impact 500 – the three mean positions and mean velocities still agree to 6 and 6 significant figures respectively. Furthermore, at the same kick, the standard deviations predicted by the three theories are also very close to each other – the standard deviations still agree to 3 and 2 significant figures, respectively, for position and velocity.

Chapter 5
Summary and Discussion

First, the Newtonian and special-relativistic statistical predictions for the mean, the standard deviation and the probability density function of the position and momentum, as well as the mean square momentum displacement were compared for the periodically-delta-kicked particle at *low speed* in Chapter 2. Contrary to expectation, I found that the statistical predictions, which were calculated from the same parameters and initial Gaussian ensemble of trajectories, do not always agree if the initial ensemble is sufficiently well-localized in phase space. Moreover, the breakdown of agreement is very fast if the trajectories in the ensemble are chaotic, but very slow if the trajectories in the ensemble are non-chaotic.

Furthermore, I also compared the statistical dynamical quantities – position and momentum means, standard deviations and probability density functions, and the mean dwell time, and transmission and reflection coefficients – calculated from an initially Gaussian ensemble of trajectories using NM and SRM for a *low-speed* scattering system in Chapter 3. I also found that the statistical predictions made by the two theories do not always agree as conventionally

expected. In particular, the predictions are radically different if the scattering is chaotic and the initial ensemble is well localized in phase space. There is no breakdown of agreement between the two predictions if the scattering is non-chaotic.

Finally, I showed, contrary to expectation, in Chapter 4 that the single-trajectory and statistical dynamical quantities (in particular, the mean, standard deviation and probability density function for position and velocity) predicted by GRM for a *low-speed weak-gravity* bouncing ball system are not always well-approximated by the corresponding quantities predicted by SRM and NM for the same parameters and initial conditions. If the system is dissipative, the breakdown of agreement occurs for chaotic trajectories only. If the system is non-dissipative, the breakdown of agreement occurs for chaotic trajectories and non-chaotic trajectories. The agreement breaks down slowly in the non-chaotic case but rapidly in the chaotic case**.**

My finding raises three important fundamental questions in physics: When the

i. Newtonian and special-relativistic statistical predictions are completely different for a low-speed system,

ii. special-relativistic and general-relativistic single-trajectory and statistical

predictions are completely different for a weak-gravity system,

iii. Newtonian and general-relativistic single-trajectory and statistical predictions are completely different for a low-speed weak-gravity system,

which of the two predictions is empirically correct? Since special relativity and general relativity continue to be successfully tested (see (Ball, 2004; Pospelov and Romalis, 2004; Cho, 2005) and (Stairs, 2003; Will, 2005, 2006) for reviews of the experimental tests) in recent times, we expect the general-relativistic (special-relativistic) predictions to be empirically-correct for weak-gravity and low-speed weak-gravity (low-speed) systems. This implies that (i) special-relativistic mechanics must generally be used, instead of Newtonian mechanics, to correctly study the dynamics of a low-speed system, (ii) general-relativistic mechanics must generally be used, instead of special-relativistic mechanics, to correctly study the dynamics of a weak-gravity system, and (iii) general-relativistic mechanics must generally be used, instead of Newtonian mechanics, to correctly study the dynamics of a low-speed weak-gravity system. These paradigm shifts could potentially lead to new understanding and discoveries in these dynamical systems.

References

Afanasiev, V. V., R. Z. Sagdeev, and G. M. Zaslavsky, 1991, "Chaotic jets with multifractal space-time random walk," Chaos **1,** 143-159.

Altmann, E. G., and H. Kantz, 2008, "Anomalous transport in Hamiltonian systems," in *Anomalous transport: Foundations and applications*, edited by R. Klages, G. Radons, and I. M. Sokolov (Wiley-VCH, Weinheim), pp. 269-292.

Ashkenazy, Y., and L. P. Horwitz, 2000, "The effect of radiation on the stochastic web," Discrete Dyn. Nature Soc. **4,** 283-292.

Ball, P., 2004, "Back to the future," Nature **427**, 482-484.

Beeker, A., and P. Eckelt, 1993, "Scaling and decay in periodically driven scattering systems," Chaos **3,** 487-494.

Casati, G., B. V. Chirikov, F. M. Izraelev, and J. Ford, 1979, "Stochastic behavior of a quantum pendulum under a periodic perturbation," in *Stochastic behavior in classical and quantum Hamiltonian systems*, edited by G. Casati, and J. Ford, Lecture Notes in Physics Vol. 93 (Springer-Verlag, Berlin), pp. 334–352.

Chaĭkovsky, D. K., and G. M. Zaslavsky, 1991, "Channeling and percolation in two-dimensional chaotic dynamics," Chaos **1,** 463-472.

Chernikov, A. A., B. A. Petrovichev, A. V. Rogal'sky, R. Z. Sagdeev, and G. M. Zaslavsky, 1990, "Anomalous transport of streamlines due to their chaos and their spatial topology," Phys. Lett. A **144,** 127-133.

Chernikov, A. A., T. Tél, G. Vattay, and G. M. Zaslavsky, 1989, "Chaos in the relativistic generalization of the standard map," Phys. Rev. A **40,** 4072-4076.

Chirikov, B. V., 1979, "A universal instability of many-dimensional oscillator systems," Phys. Rep. **52,** 263-379.

Cho, A., 2005, "Special relativity reconsidered," Science **307,** 866-868.

Ciubotariu, C., L. Bădeliță, and V. Stancu, 2002, "Chaos in dissipative relativistic standard maps," Chaos, Solitons and Fractals **13,** 1253-1267.

Corben, H. C., and P. Stehle, 1994, *Classical mechanics*, *2nd ed*. (Dover Publications, New York).

Davies, P., 1992, Ed., *The new physics* (Cambridge University Press, Cambridge).

Desloge, E. A., 1990, "Relativistic motion of a free particle in a uniform gravitational field," International Journal of Theoretical Physics **29,** 193-208.

Einstein, A., 1961, *Relativity: the special and the general theory* (Three Rivers

Press, New York).

Erkal, C., 2000, "The simple pendulum: a relativistic revisit," Eur. J. Phys. **21,** 377-384.

Ford, J., and G. Mantica, 1992, "Does quantum mechanics obey the correspondence principle? Is it complete?," Am. J. Phys. **60,** 1086-1098.

Fox, R. F., and T. C. Elston, 1994, "Chaos and the quantum-classical correspondence in the kicked pendulum," Phys. Rev. E **49,** 3683-3696.

Hartle, J. B., 2003, *Gravity: An introduction to Einstein's general relativity* (Addison-Wesley, San Francisco).

Horwitz, L. P., and Y. Ashkenazy, 2000, "Chaos and maps in relativistic dynamical systems," Discrete Dyn. Nature Soc. **4,** 77-86.

Ishizaki, R., T. Horita, T. Kobayashi, and H. Mori, 1991, "Anomalous diffusion due to accelerator modes in the standard map," Prog. Theor. Phys. **85,** 1013-1022.

Ishizaki, R., T. Horita, and H. Mori, 1993, "Anomalous diffusion and mixing of chaotic orbits in Hamiltonian dynamical systems," Prog. Theor. Phys. **89,** 947-963.

Ishizaki, R., and H. Mori, 1997, "Anomalous diffusion induced by external force in the standard map," Prog. Theor. Phys. **97,** 201-211.

Ishizaki, R., and H. Mori, 1998, "Anomalous diffusion induced by external force in the standard map. II," Prog. Theor. Phys. **100,** 1131-1144.

Karimabadi, H., and V. Angelopoulos, 1989, "Arnol'd diffusion in two dimensions," Phys. Rev. Lett. **62,** 2342-2345.

Karney, C. F. F., 1983, "Long-time correlations in the stochastic regime," Physica D **8,** 360-380.

Lan, B. L., 1994, "Wave-packet initial motion, spreading, and energy in the periodically kicked pendulum," Phys. Rev. E **50,** 764-769.

Lan, B. L., 2006, "Comparison of the Newtonian and relativistic predicted trajectories for a low-speed periodically delta-kicked system," Chaos **16,** 033107.

Lan, B. L., 2007, "Disagreement between Newtonian and relativistic trajectories at low speed: another example," in *Proceedings of the 14th NPA conference*, Storrs, CT, USA, Vol. 4, pp. 116-117.

Lan, B. L., 2008, "Disagreement between Newtonian and relativistic trajectories at low speed," in *Proceedings of the Chaos2008 Conference*, Crete, Greece.

Lan, B. L., 2009a, "Disagreement between Newtonian and relativistic trajectories for a low-speed kicked dissipative system," in *Topics on chaotic systems: selected papers from Chaos 2008 international conference*, edited by C. H.

Skiadas, I. Dimotikalis, and C. Skiadas (World Scientific, Singapore), pp. 199-203.

Lan, B. L., 2009b, "Implications of the disagreement between Newtonian and relativistic low-speed trajectories," Chaos, Solitons and Fractals **42,** 534-537.

Lan, B. L., and F. Borondo, 2011, "Newtonian and special-relativistic predictions for the trajectories of a low-speed scattering system," Phys. Rev. E **83,** 036201.

Lan, B. L., and H. Y. Cheng, 2010, "Newtonian and special-relativistic predictions for the trajectory of a slow-moving dissipative dynamical system," Commun. Nonlinear Sci. Numer. Simulat. **15,** 2497-2503.

Landau, L. D., and E. M. Lifshitz, 1975, *The classical theory of fields* (Pergamon Press, Oxford).

Lapidus, I. R., 1972a, "Motion of a relativistic particle acted upon by a constant force and a uniform gravitational field," Am. J. Phys. **40,** 984-988.

Lapidus, I. R., 1972b, "The falling body problem in general relativity," Am. J. Phys. **40,** 1509-1510.

Lebœuf, P., 1998, "Normal and anomalous diffusion in a deterministic area-preserving map," Physica D **116,** 8-20.

Lichtenberg, A. J., and M. A. Lieberman, 1983, *Regular and stochastic motion* (Springer, New York).

Longcope, D. W., and R. N. Sudan, 1987, "Arnol'd diffusion in 1½ dimensions," Phys. Rev. Lett. **59,** 1500-1503.

Matrasulov, D. U., 1999, "Diffusive ionization of a relativistic hydrogenlike atom," Phys. Rev. A **60,** 700-703.

Matrasulov, D. U., G. M. Milibaeva, U. R. Salomov, and B. Sundaram, 2005, "Relativistic kicked rotor," Phys. Rev. E **72,** 016213.

McComb, W. D., 1999, *Dynamics and relativity* (Oxford University Press, Oxford).

Nomura, Y., Y. H. Ichikawa, and W. Horton, 1992, "Nonlinear dynamics of the relativistic standard map," Phys. Rev. A **45,** 1103-1115.

Pospelov, M., and M. Romalis, 2004, "Lorentz invariance on trial," Physics Today **57**, 40-46.

Sprott, J. C., 2003, *Chaos and time-series analysis* (Oxford University Press, Oxford).

Srinivasa Rao, K. N., 1966, "The motion of a falling particle in a Schwarzschild field," Ann. Inst. Henri Poincaré, Sect. A **5,** 227-233.

Srinivasa Rao, K. N., and A. V. Gopala Rao, 1974, "Falling body in the theories of

gravitation," J. Phys. A **7,** 485-488.

Stairs, I. H., 2003, "Testing general relativity with pulsar timing," Living Rev. Relativity **6,** 5. http://www.livingreviews.org/lrr-2003-5.

Tufillaro, N. B., T. Abbott, and J. Reilly, 1992, *An experimental approach to nonlinear dynamics and chaos* (Addison-Wesley, Redwood city, California).

Tufillaro, N. B., T. M. Mello, Y. M. Choi, and A. M. Albano, 1986, "Period doubling boundaries of a bouncing ball," J. Phys. (Paris) **47,** 1477-1482.

Will, C. M., 2005, "Was Einstein right? Testing relativity at the centenary," in *100 years of relativity. Space-time structure: Einstein and beyond*, edited by A. Ashtekar (World Scientific, Singapore), pp. 205-227.

Will, C. M., 2006, "The confrontation between general relativity and experiment," Living Rev. Relativity **9,** 3. http://www.livingreviews.org/lrr-2006-3.

Zaslavsky, G. M., 2002, "Chaos, fractional kinetics, and anomalous transport," Phys. Rep. **371,** 461-580.

Zaslavsky, G. M., M. Edelman, and B. A. Niyazov, 1997, "Self-similarity, renormalization, and phase space nonuniformity of Hamiltonian chaotic dynamics," Chaos **7,**159-181.

Zel'dovich, Ya. B., and I. D. Novikov, 1996, *Stars and relativity* (Dover Publications, New York).

Zheng, Y., and D. H. Kobe, 2006, "Anomalous momentum diffusion in the classical kicked rotor," Chaos, Solitons and Fractals **28**, 395-402.

Appendix - Publication list and reprints

Journal Publication

1. Shiuan-Ni Liang and Boon Leong Lan, *Newtonian versus general-relativistic prediction for the trajectory of a bouncing ball system*, Results in Physics 1, 36-39, 2011.

2. Shiuan-Ni Liang and Boon Leong Lan, *Comparison of Newtonian and Special-Relativistic Trajectories with the General-Relativistic Trajectory for a Low-Speed Weak-Gravity System*, PLoS ONE 7(4): e34720, 2012. (The reprint is attached)

3. Shiuan-Ni Liang and Boon Leong Lan, *Statistical Predictions for the Dynamics of a Low-Speed System: Newtonian versus Special-Relativistic Mechanics*, PLoS ONE 7(5): e36430, 2012. (The reprint is attached)

4. Shiuan-Ni Liang and Boon Leong Lan, *Newtonian versus special-relativistic statistical predictions for the dynamics of a low-speed scattering system*, PLoS ONE (submitted).

Conference Proceedings

1. Shiuan-Ni Liang and Boon Leong Lan, *Newtonian And Special Relativistic Predictions For The Trajectory Of A Bouncing Ball*, AIP Conf. Proc. 1250, 277-280 (2010).

2. Shiuan-Ni Liang, Kenneth Mapanga and Boon Leong Lan, *Mean Trajectory Predictions For A Low-Speed Dynamical System: Newton Versus Einstein*, AIP Conf. Proc. 1328, 95-97 (2011).

Selected Paper for Book Publication

1. Shiuan-Ni Liang and Boon Leong Lan, *Dynamics of a bouncing ball*, Chaotic Systems: Theory and Applications, Selected Papers from the 2nd Chaotic Modeling and Simulation International Conference (CHAOS2009), Eds. C. H. Skiadas and I. Dimotikalis, World Scientific, 165-169, 2010.

OPEN ACCESS Freely available online

PLoS one

Comparison of Newtonian and Special-Relativistic Trajectories with the General-Relativistic Trajectory for a Low-Speed Weak-Gravity System

Shiuan-Ni Liang, Boon Leong Lan*

School of Science, Monash University, Bandar Sunway, Selangor, Malaysia

Abstract

We show, contrary to expectation, that the trajectory predicted by general-relativistic mechanics for a *low-speed weak-gravity* system is not always well-approximated by the trajectories predicted by special-relativistic and Newtonian mechanics for the same parameters and initial conditions. If the system is dissipative, the breakdown of agreement occurs for chaotic trajectories only. If the system is non-dissipative, the breakdown of agreement occurs for chaotic trajectories and non-chaotic trajectories. The agreement breaks down slowly for non-chaotic trajectories but rapidly for chaotic trajectories. When the predictions are different, general-relativistic mechanics must therefore be used, instead of special-relativistic mechanics (Newtonian mechanics), to correctly study the dynamics of a weak-gravity system (a low-speed weak-gravity system).

Citation: Liang S-N, Lan BL (2012) Comparison of Newtonian and Special-Relativistic Trajectories with the General-Relativistic Trajectory for a Low-Speed Weak-Gravity System. PLoS ONE 7(4): e34720. doi:10.1371/journal.pone.0034720

Editor: Gerardo Adesso, University of Nottingham, United Kingdom

Received September 1, 2011; **Accepted** March 8, 2012; **Published** April 19, 2012

Funding: This work was funded by a Fundamental Research Grant Scheme FRGS/2/2010/ST/MUSM/02/1. The funders had no role in study design, data collection and analysis, decision to publish, or preparation of the manuscript.

Competing Interests: The authors have declared that no competing interests exist.

* E-mail: lan.boon.leong@monash.edu

Introduction

For dynamical systems where gravity does not play a dynamical role, it is expected (see, for example, [1–3]) that, if the speed of the system is *low* (i.e., much less than the speed of light c), the dynamics predicted by special-relativistic mechanics is always well-approximated by the prediction of Newtonian mechanics for the same parameters and initial conditions. However, in a recent study on a model Hamiltonian system [4], we found, contrary to expectation, that the Newtonian trajectory does not remain close to the special-relativistic trajectory although the particle speed is low – the two trajectories eventually become completely different regardless of whether the trajectories are chaotic or non-chaotic. But the agreement between the Newtonian and special-relativistic trajectories breaks down much faster – exponentially fast – in the chaotic case compared to the non-chaotic case. Similar rapid breakdown of agreement was also found in a model dissipative system [5,6] and a model scattering system [7] in the chaotic case but no breakdown of agreement was found in the non-chaotic case. The loss of agreement means [6–8] that special-relativistic mechanics must be used, instead of the standard practice of using Newtonian mechanics, to correctly study the dynamics of a low-speed system.

For dynamical systems where gravity does play a dynamical role but gravity is *weak* (i.e., gravitational potential $\ll c^2$ [9]), it is expected (see, for example, [3,10,11]) that the dynamical prediction of general-relativistic mechanics is always well-approximated by the prediction of special-relativistic mechanics for the same parameters and initial conditions. Furthermore, if gravity is *weak* and the speed of the system is *low*, the dynamical prediction of general-relativistic mechanics is expected (see, for example, [3,10–13]) to be always well-approximated by the Newtonian prediction for the same parameters and initial conditions. In this paper, we study a *low-speed weak-gravity* system – the bouncing ball system [14,15] – to ascertain if these expectations are correct by comparing the Newtonian and special-relativistic trajectories with the general-relativistic trajectory. In a recent paper [16], only the Newtonian and general-relativistic trajectories were compared, with the assumption that, in between impacts with the table, the ball free falls in an exact uniform gravitational field. Here, the gravitational field of the earth is instead modeled as the field due to a uniform sphere – this leads to a different general-relativistic description of the free-fall motion and consequently of the bouncing ball dynamics. Moreover, in the previous paper [16], only inelastic collision between the ball and table was considered; here, both elastic and inelastic collisions are considered. Details of the bouncing ball system and the Newtonian and relativistic trajectory calculations are given next. This is followed by the results and discussion, and concluding remarks on their significance.

Methods

The bouncing ball system [14,15] consists of a ball bouncing repeatedly on a table which is oscillating sinusoidally with amplitude A and frequency ω. The impact between the ball and the table is instantaneous, where the coefficient of restitution α ($0 \leq \alpha \leq 1$) measures the kinetic energy loss of the ball at each impact: the impact is elastic if $\alpha = 1$, inelastic if $\alpha < 1$. The table is not affected by the impact because the table's mass is much larger than the ball's mass. In between impacts, the ball undergoes free-

fall motion due to the gravitational field of the earth, which is assumed to be a uniform sphere.

In the Newtonian framework, the dynamics of the bouncing ball is described by the two-dimensional map derived by Tufillaro and co-workers [14,15]. Following [14,15], we derive the special-relativistic map and general-relativistic map in terms of the ball's velocity v and the table's phase θ just after each impact. The table's phase is given by $(\omega t+\theta_0)$ modulus 2π. We will refer to the table's phase just after each impact as the impact phase. Our derivations (see Text S1 and S2) of the relativistic maps for the bouncing ball follow the same steps as the derivation [14,15] of the Newtonian map.

In the Newtonian framework, the dynamics of the bouncing ball is [14,15] described by the impact-phase map

$$A[\sin(\theta_k)+1]+v_k\left[\frac{1}{\omega}(\theta_{k+1}-\theta_k)\right]-\frac{1}{2}g\left[\frac{1}{\omega}(\theta_{k+1}-\theta_k)\right]^2- A[\sin(\theta_{k+1})+1]=0 \quad (1)$$

and the velocity map

$$v_{k+1}=(1+\alpha)\omega A\cos(\theta_{k+1})-\alpha\left\{v_k-g\left[\frac{1}{\omega}(\theta_{k+1}-\theta_k)\right]\right\} \quad (2)$$

where $g=GM/R^2$, M and R are respectively the mass and radius of the earth, and G is the gravitational constant.

In the special-relativistic framework, the impact-phase map is

$$A[\sin(\theta_k)+1]-\frac{c^2}{g}\ln\left\{\frac{1}{2}\left[(1+\beta_k)e^{-\frac{g}{c}\left(\frac{\theta_{k+1}-\theta_k}{\omega}\right)}+(1-\beta_k)e^{\frac{g}{c}\left(\frac{\theta_{k+1}-\theta_k}{\omega}\right)}\right]\right\} - A[\sin(\theta_{k+1})+1]=0 \quad (3)$$

where $\beta_k=\frac{v_k}{c}$. The velocity map is

$$v_{k+1}=\frac{-c^2\alpha\left(\frac{v'_{k+1}-u_{k+1}}{c^2-v'_{k+1}u_{k+1}}\right)+u_{k+1}}{1-\alpha u_{k+1}\left(\frac{v'_{k+1}-u_{k+1}}{c^2-v'_{k+1}u_{k+1}}\right)} \quad (4)$$

where $u_{k+1}=A\omega\cos(\theta_{k+1})$ is the table's velocity just after the $(k+1)$th impact, and

$$v'_{k+1}=c\left[\frac{(1+\beta_k)e^{-\frac{g}{c}\left(\frac{\theta_{k+1}-\theta_k}{\omega}\right)}-(1-\beta_k)e^{\frac{g}{c}\left(\frac{\theta_{k+1}-\theta_k}{\omega}\right)}}{(1+\beta_k)e^{-\frac{g}{c}\left(\frac{\theta_{k+1}-\theta_k}{\omega}\right)}+(1-\beta_k)e^{\frac{g}{c}\left(\frac{\theta_{k+1}-\theta_k}{\omega}\right)}}\right]$$

is the ball's velocity just before the $(k+1)$th impact.

In the general-relativistic framework, the impact-phase map is

$$A[\sin(\theta_k)+1]-A[\sin(\theta_{k+1})+1] -\frac{c^2}{2g}\left\{1-\frac{2g[R_{\rm TLP}+A[\sin(\theta_k)+1]]}{c^2}\right\} \left\{1-\left\{\frac{1}{2}\left[(1+\beta_k)e^{-\frac{g}{c}\left(\frac{\theta_{k+1}-\theta_k}{\omega}\right)}+(1-\beta_k)e^{\frac{g}{c}\left(\frac{\theta_{k+1}-\theta_k}{\omega}\right)}\right]\right\}^{-2}\right\}=0 \quad (5)$$

where the constant $R_{\rm TLP}$ is the distance between the table's lowest position and the center of the earth. The velocity map is also given by Eq. (4).

The general-relativistic map [Eqs. (5) and (4)] is approximately the same as the special-relativistic map [Eqs. (3) and (4)] if gravity is *weak* [$2g(R_{\rm TLP}+y)/c^2\ll 1$ and $2g(R_{\rm TLP}+y_0)/c^2\ll 1$], where y is the ball's position relative to $R_{\rm TLP}$. And the general-relativistic map is approximately the same as the Newtonian map [Eqs. (1) and (2)] if the ball's speed and table's speed are *low* [$v/c\ll 1$, $v_0/c\ll 1$, $g(t-t_0)/c\ll 1$ and $u/c\ll 1$] and gravity is *weak*. Furthermore, the special-relativistic map is approximately the same as the Newtonian map if the ball's speed and table's speed are *low*.

To time-evolve the Newtonian and relativistic trajectories, the impact-phase maps Eq. (1), Eq. (3) and Eq. (5), which are implicit algebraic equations for θ_{k+1}, must be solved numerically by finding the zero of the function on the left side of the equation given θ_k and v_k. We used Brent's method for this purpose. First, each trajectory is calculated in quadruple precision (35 significant figures) with a tolerance of 10^{-30} for the zeros. The trajectory is then recalculated in quadruple precision but using a smaller tolerance of 10^{-32} for the zeros. Finally, the accuracy of the trajectory is determined by the standard method [17] of comparing the less-accurate calculation (10^{-30}-tolerance) with the more-accurate calculation (10^{-32}-tolerance). For example, if the Newtonian velocity is 7.123456789… from the 10^{-30}-tolerance calculation and 7.123456799… from the 10^{-32}-tolerance calculation, then it is accurate to 8 significant figures, i.e., 7.1234567. We used $g=981$ cm/s^2, $c=3\times10^{10}$ cm/s, and $R_{\rm TLP}=6.4\times10^8$ cm (mean radius of the Earth).

The trajectory generated by each of the three maps can be chaotic. A trajectory is defined [18] as chaotic if it exhibits sensitive dependence on initial conditions, that is, the distance between the trajectory and another initially-nearby trajectory from the same theory grows, on average, exponentially for a short time, where the exponential growth constant is not exactly equal to but close to the Lyapunov exponent which is a long-time asymptotic quantity. To determine if a trajectory is chaotic, we inspect the trajectory in phase space, check for sensitivity of the trajectory to initial conditions and calculate [18] the largest Lyapunov exponent to see if it is positive.

In the following results section, instead of reporting the impact phase θ, i.e., the table's phase just after each impact, we report the ball's position (which is also the table's position) $y=A[\sin(\theta)+1]$ just after each impact, together with the ball's velocity v just after each impact, when comparing the predictions of the three theories.

Results

Three examples are presented and discussed to illustrate the general results. In all three examples, the ball's speed and table's speed remained *low* (about $10^{-10}c$), and gravity is *weak* ($2g(R_{\rm TLP}+y)$ is about $10^{-9}c^2$).

In the first two examples, the system is dissipative with $\alpha=0.5$. In both examples, the initial conditions are 0.02022 cm for the ball's position and 8.17001 cm/s for the ball's velocity. The table's frequency $(\omega/2\pi)$ is 60 Hz, but the table's amplitude A is slightly different: 0.0102 cm in the first example, 0.012 cm in the second example.

In the first example, the Newtonian, special-relativistic and general-relativistic trajectories are all non-chaotic. Fig. 1 shows that the three trajectories are close to one another and they converge to period-one fixed-point attractors which are almost identical.

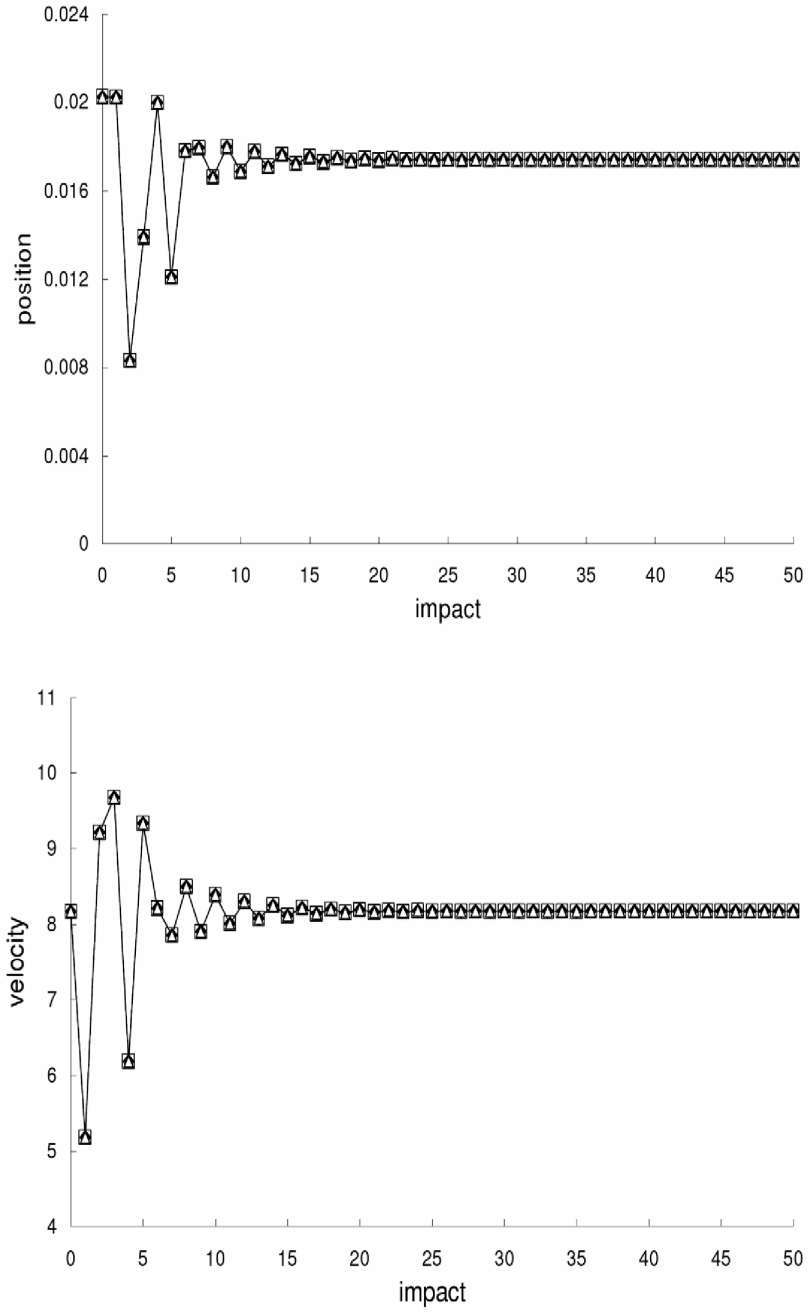

Figure 1. Comparison of trajectories for the first example. Comparison of the Newtonian (squares), special-relativistic (diamonds) and general-relativistic (triangles) positions (top plot) and velocities (bottom plot) for the non-chaotic first example.
doi:10.1371/journal.pone.0034720.g001

In the second example, the Newtonian, special-relativistic and general-relativistic trajectories, which are plotted in phase space in the top part of Figs. 2, 3 and 4 respectively, are all chaotic as evidenced by the sensitivity to initial conditions (shown in the bottom part of Figs. 2, 3 and 4 respectively) and positive largest Lyapunov exponent of 0.34 for each trajectory. Fig. 5 shows that the agreement between the special-relativistic trajectory and general-relativistic trajectory breaks down very quickly at impact 55, and the agreement between the Newtonian trajectory and general-relativistic trajectory also breaks down at impact 55. The breakdown of agreement between the Newtonian and special-relativistic trajectories (not shown in Fig. 5) occurs later, at impact 95.

Figs. 6 and 7 show, respectively, that the rapid breakdown of agreement between the special-relativistic and general-relativistic trajectories and between the Newtonian and general-relativistic trajectories are due to the, on average, exponential growth – that is, exponential growth with small fluctuations – of the magnitude

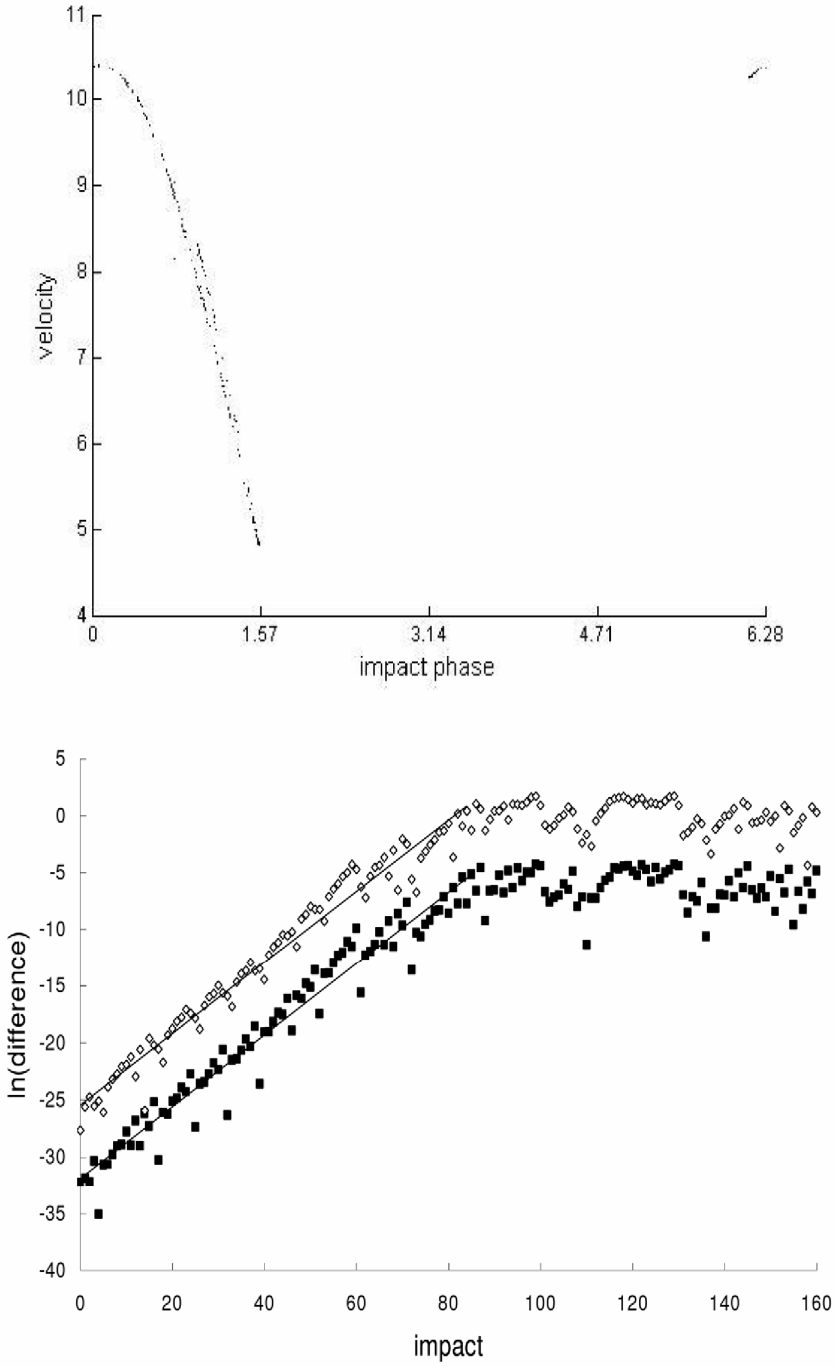

Figure 2. Newtonian trajectory for the second example. Top: Chaotic Newtonian phase-space trajectory, plotted for the first 210 impacts, from the second example. Bottom: Natural-log of the magnitude of the difference [position difference (squares), velocity difference (diamonds)] between the chaotic Newtonian trajectory and another Newtonian trajectory which differed initially by 10^{-14} in position and 10^{-12} in velocity. Straight-line fits up to impact 84 are also plotted.
doi:10.1371/journal.pone.0034720.g002

of the difference between the two trajectories for at least the first 61 impacts:

$$\Delta y_n \approx \Delta y_1 e^{c_1(n-1)} \tag{6}$$

$$\Delta v_n \approx \Delta v_1 e^{c_2(n-1)} \tag{7}$$

where $n = 1,2,\ldots$. In both cases, the exponential growth constants for the position difference in Eq. (6) and velocity difference in Eq.

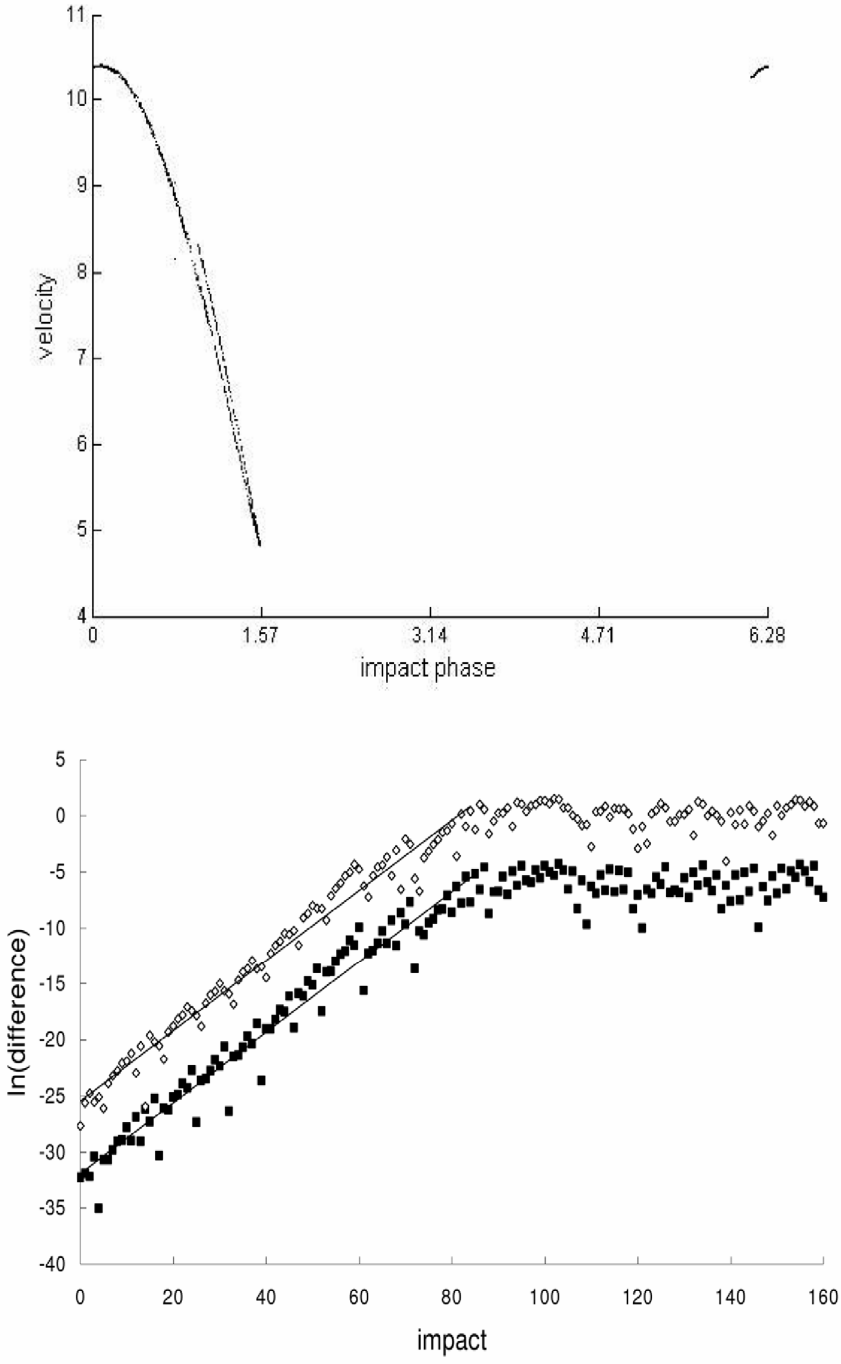

Figure 3. Special-relativistic trajectory for the second example. Top: Chaotic special-relativistic phase-space trajectory, plotted for the first 1000 impacts, from the second example. Bottom: Natural-log of the magnitude of the difference [position difference (squares), velocity difference (diamonds)] between the chaotic special-relativistic trajectory and another special-relativistic trajectory which differed initially by 10^{-14} in position and 10^{-12} in velocity. Straight-line fits up to impact 84 are also plotted.
doi:10.1371/journal.pone.0034720.g003

(7) are close to each other: $c_1 \approx 0.360$ and $c_2 \approx 0.363$. This exponential growth constant of about 0.36 is close to (i) the exponential growth constant for the magnitude of the difference (plotted in Figs. 2, 3 and 4) between the chaotic trajectory and another initially-nearby trajectory from the same theory – the growth constants are 0.31, 0.31 and 0.34, respectively, for the Newtonian, special-relativistic and general-relativistic case, where the two nearby trajectories differed initially by 10^{-14} in position and 10^{-12} in velocity, and (ii) the largest Lyapunov exponent of 0.34 for the Newtonian, special-relativistic and general- relativistic chaotic trajectories. We note that the magnitude of the difference between the Newtonian and special-relativistic trajectories also

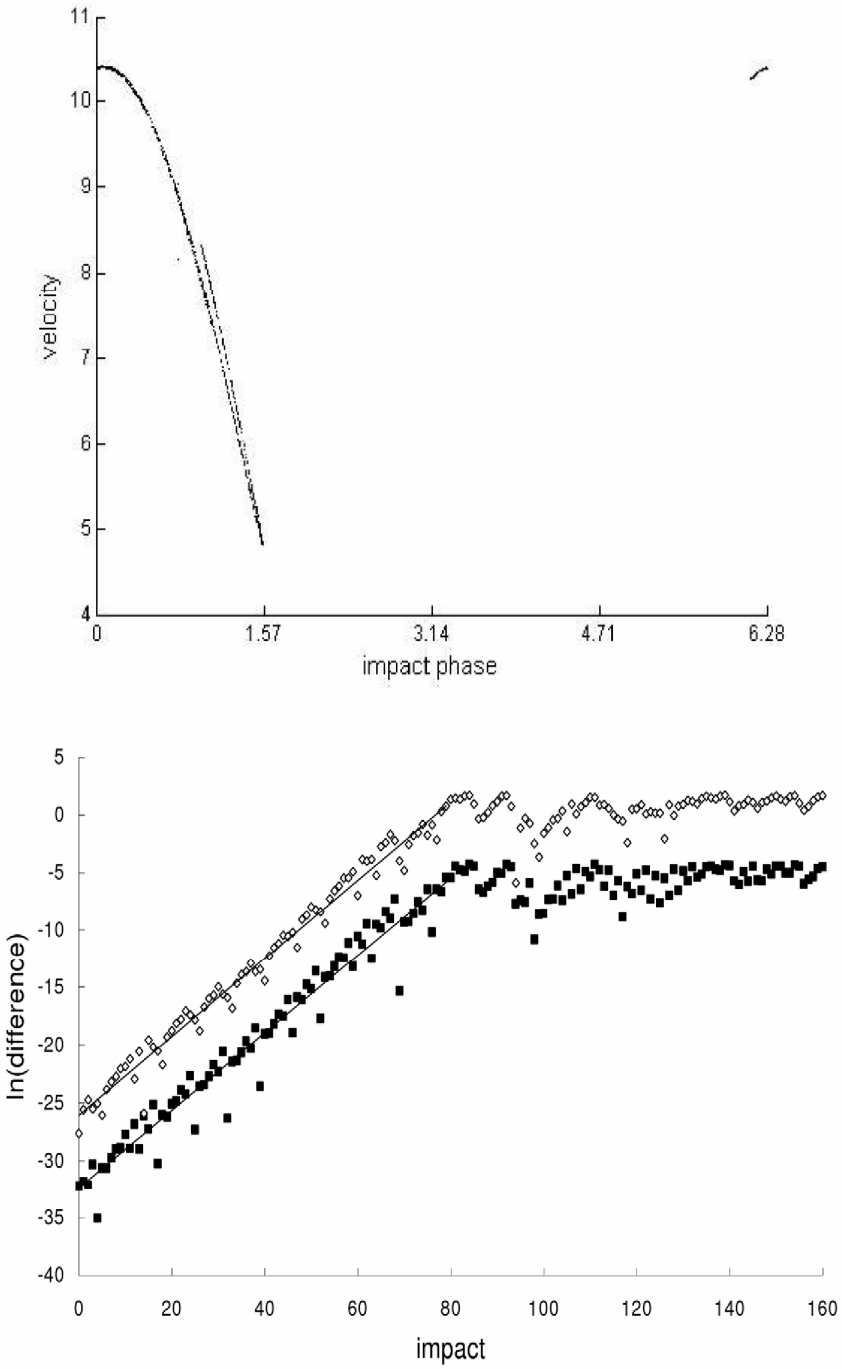

Figure 4. General-relativistic trajectory for the second example. Top: Chaotic general-relativistic phase-space trajectory, plotted for the first 1000 impacts, from the second example. Bottom: Natural-log of the magnitude of the difference [position difference (squares), velocity difference (diamonds)] between the chaotic general-relativistic trajectory and another general-relativistic trajectory which differed initially by 10^{-14} in position and 10^{-12} in velocity. Straight-line fits up to impact 79 are also plotted.
doi:10.1371/journal.pone.0034720.g004

grows exponentially on average, consistent with the results in [4–7] for low-speed systems, with growth constants $c_1 \approx 0.319$ and $c_2 \approx 0.320$.

In the non-dissipative case, where $\alpha = 1$, the agreement between the special-relativistic and Newtonian chaotic trajectories with the general-relativistic chaotic trajectory also breaks down exponentially fast. The agreement also breaks down for non-chaotic trajectories but it takes a much longer time to occur because the difference between the trajectories only grows linearly. Fig. 8 illustrates this linear growth for the difference between the Newtonian and general-relativistic quasiperiodic trajectories (the trajectories are plotted in phase space in Fig. 9) – in this third

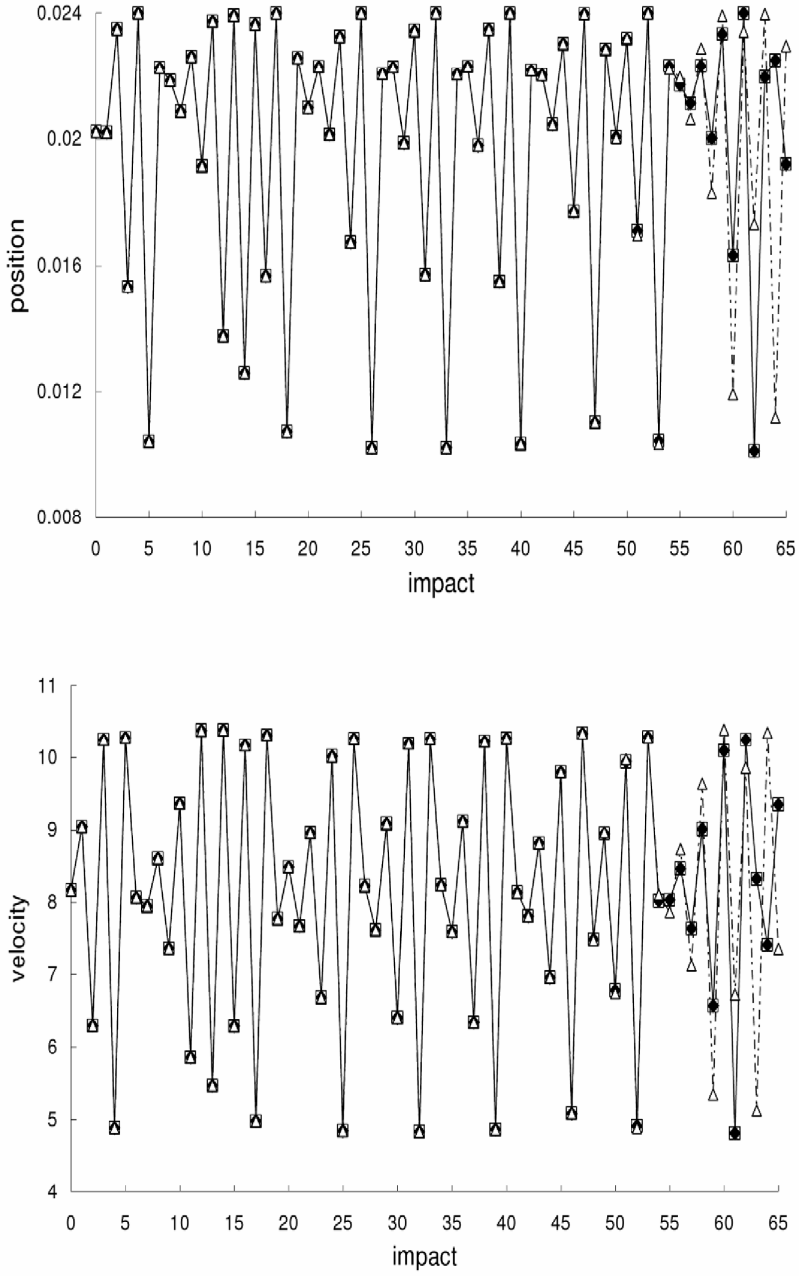

Figure 5. Comparison of trajectories for the second example. Comparison of the Newtonian (squares), special-relativistic (diamonds) and general-relativistic (triangles) positions (top plot) and velocities (bottom plot) for the chaotic second example.
doi:10.1371/journal.pone.0034720.g005

example, the table's frequency and amplitude are 60 Hz and 0.005 cm, and the ball's initial position and velocity are 0.00991 cm and 8.17001 cm/s. The linear growth rates of the magnitude of the position difference and velocity difference are 2×10^{-15} cm and 4×10^{-12} cm/s, respectively, per impact. It would thus require 2.5×10^{10} (!) impacts for the magnitude of the velocity difference to grow to 0.1 cm/s. Similar linear growth rates were found for the difference between the special-relativistic and general-relativistic quasiperiodic trajectories in this example (the special-relativistic trajectory is also plotted in Fig. 9).

In general, the breakdown of agreement between the special-relativistic and general-relativistic trajectories for *weak gravity*, and between the Newtonian and general-relativistic trajectories for *low speed* and *weak gravity* can be further understood as follows.

Firstly, rewriting the general-relativistic impact-phase map [Eq. (5)] and taking the natural logarithm on both sides yield

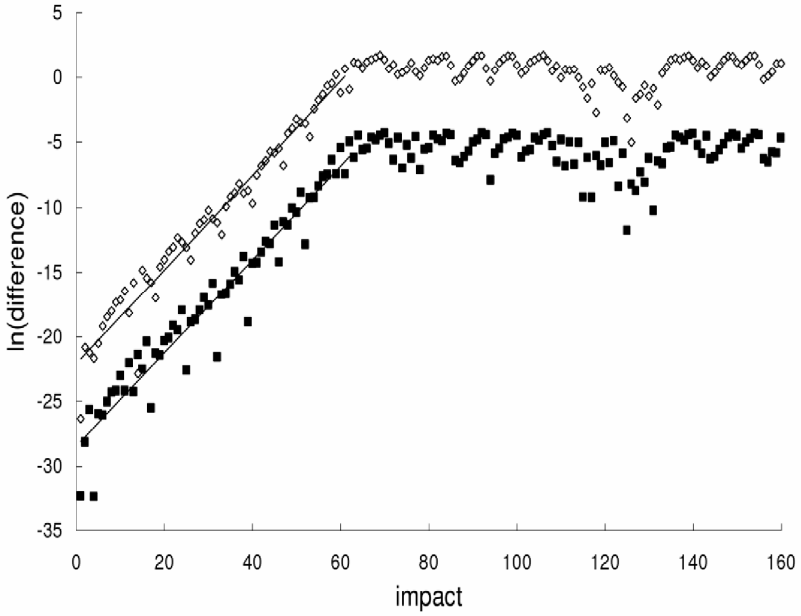

Figure 6. Difference between the special-relativistic and general-relativistic trajectories for the second example. Natural-log of the magnitude of the difference between the special-relativistic and general-relativistic positions (squares) and velocities (diamonds) for the chaotic second example. Straight-line fits up to impact 61 are also plotted.
doi:10.1371/journal.pone.0034720.g006

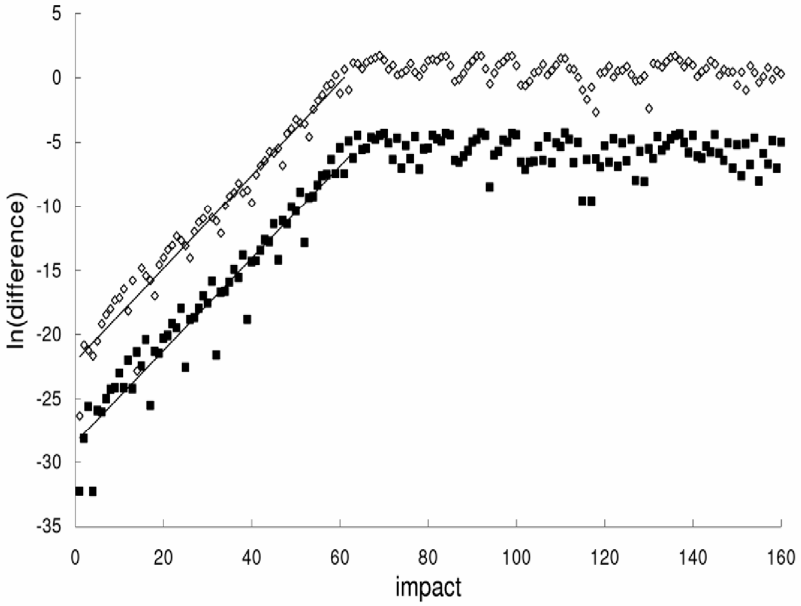

Figure 7. Difference between the Newtonian and general-relativistic trajectories for the second example. Natural-log of the magnitude of the difference between the Newtonian and general-relativistic positions (squares) and velocities (diamonds) for the chaotic second example. Straight-line fits up to impact 61 are also plotted.
doi:10.1371/journal.pone.0034720.g007

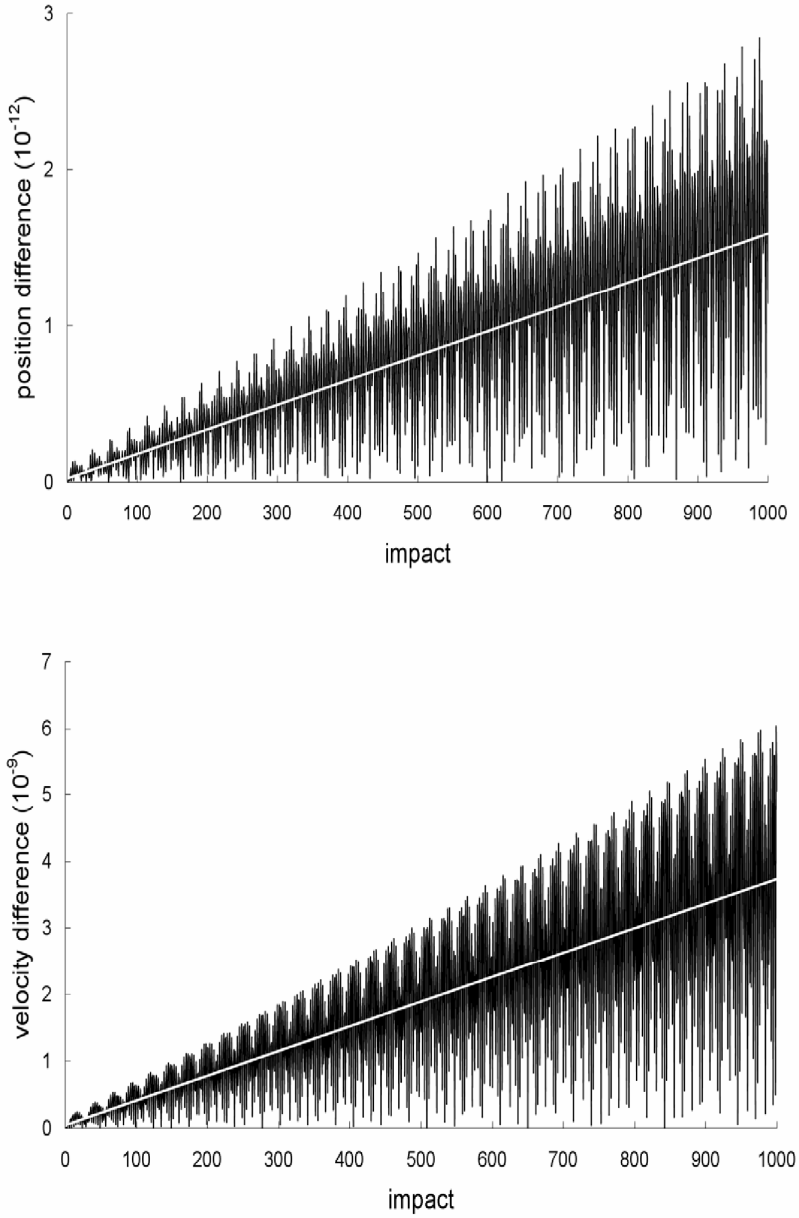

Figure 8. Difference between the Newtonian and general-relativistic trajectories for the third example. Magnitude of the difference between the Newtonian and general-relativistic positions (top plot) and velocities (bottom plot) for the non-chaotic third example. Straight-line fits are also plotted.
doi:10.1371/journal.pone.0034720.g008

$$\ln\left\{1-\left\{1-\frac{2g[R_{\rm TLP}+A[\sin(\theta_k)+1]]}{c^2}\right\}^{-1}\left\{\frac{2gA[\sin(\theta_k)-\sin(\theta_{k+1})]}{c^2}\right\}\right\}$$
$$=-2\ln\left\{\frac{1}{2}\left[(1+\beta_k)e^{-\frac{g}{c}\left(\frac{\theta_{k+1}-\theta_k}{\omega}\right)}+(1-\beta_k)e^{\frac{g}{c}\left(\frac{\theta_{k+1}-\theta_k}{\omega}\right)}\right]\right\}. \quad (8)$$

For *weak* gravity, we have $2g\{R_{TLP}+A[\sin(\theta_k)+1]\}/c^2 \ll 1$ and this implies that the factor $\{1-2g[R_{TLP}+A[\sin(\theta_k)+1]]/c^2\}^{-1}$ in the logarithmic function on the left of Eq. (8) is approximately 1. Furthermore, for *weak* gravity, we have $2g\{R_{TLP}+A[\sin(\theta_{k+1})+1]\}/c^2 \ll 1$, therefore we can use the expansion $\ln(1+x)=x-x^2/2$ for the logarithmic function on the left of Eq. (8) since $|x| \ll 1$. Consequently, Eq. (8) becomes

$$A[\sin(\theta_k)+1]-$$
$$\frac{c^2}{g}\ln\left\{\frac{1}{2}\left[(1+\beta_k)e^{-\frac{g}{c}\left(\frac{\theta_{k+1}-\theta_k}{\omega}\right)}+(1-\beta_k)e^{\frac{g}{c}\left(\frac{\theta_{k+1}-\theta_k}{\omega}\right)}\right]\right\} \quad (9)$$
$$-A[\sin(\theta_{k+1})+1]+\frac{g}{c^2}\{A[\sin(\theta_k)+1]-A[\sin(\theta_{k+1})+1]\}^2=0.$$

The approximate general-relativistic impact-phase map given by Eq. (9) differs from the special-relativistic impact-phase map [Eq.

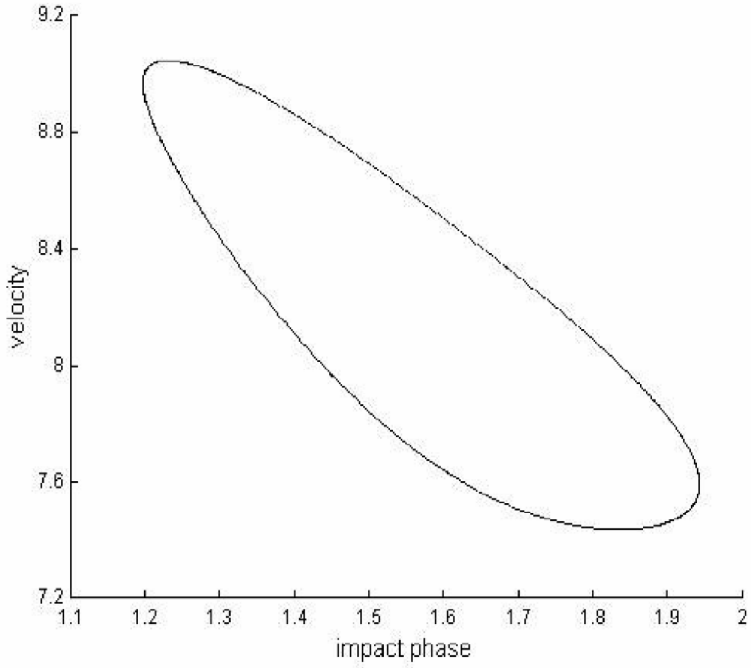

Figure 9. Trajectories for the third example. Quasiperiodic Newtonian, special-relativistic and general-relativistic phase-space trajectories, plotted for the first 1000 impacts, from the non-chaotic third example. The three trajectories are still close to one another at impact 1000 and thus they are indistinguishable in the plot.
doi:10.1371/journal.pone.0034720.g009

(3)] by the last term which involves $1/c^2$. The general-relativistic velocity map is exactly the same as the special-relativistic velocity map [Eq. (4)]. The breakdown of agreement between the special-relativistic and general-relativistic trajectories is thus essentially due to the small $1/c^2$ term in Eq. (9).

Secondly, for *weak* gravity, the factor $\{1-2g[R_{TLP}+A[-\sin(\theta_k)+1]]/c^2\}$ in the general-relativistic impact-phase map [Eq. (5)] is approximately 1. Additionally, for *low* speed, we have $g(\theta_{k+1}-\theta_k)/(c\omega)\ll 1$, therefore we can use the expansion $e^x = 1+x+x^2/2$ for the exponential functions in the term with exponent -2 in Eq. (5) since $|x|\ll 1$. Furthermore, for *low* speed, we have $v_k/c\ll 1$, and hence we can expand the resulting $(1+x)^{-2}$ term as $1-2x+3x^2$ since $|x|\ll 1$. For *low* speed and *weak* gravity, Eq. (5) is thus approximately

$$A[\sin(\theta_k)+1]+v_k\left(\frac{\theta_{k+1}-\theta_k}{\omega}\right)-\frac{g}{2}\left(\frac{\theta_{k+1}-\theta_k}{\omega}\right)^2- A[\sin(\theta_{k+1})+1]+\frac{3g}{2c^2}\left(\frac{\theta_{k+1}-\theta_k}{\omega}\right)^2\left[v_k-\frac{g}{2}\left(\frac{\theta_{k+1}-\theta_k}{\omega}\right)\right]^2=0. \quad (10)$$

Moreover, for *low* speed, $v'_{k+1}/c\ll 1$ and $u_{k+1}/c\ll 1$, and so the general-relativistic velocity map, which is exactly the same as the special-relativistic velocity map [Eq. (4)], is approximately

$$v_{k+1}=(1+\alpha)u_{k+1}-\alpha v'_{k+1}. \quad (11)$$

Furthermore, for *low* speed, we can use the expansion $e^x = 1+x+x^2/2$ for the exponential functions in v'_{k+1} (the expression for v'_{k+1} is given after Eq. 4) since $|x|\ll 1$, and then expand the resulting $(1+x)^{-1}$ term as $(1-x)$ since $|x|\ll 1$. Substituting the resulting approximate expression for v'_{k+1} and $u_{k+1}=A\omega\cos(\theta_{k+1})$ into Eq. (11) yields

$$v_{k+1}=(1+\alpha)A\omega\cos(\theta_{k+1})-\alpha\left[v_k-g\left(\frac{\theta_{k+1}-\theta_k}{\omega}\right)\right]- \frac{\alpha g}{c^2}\left(\frac{\theta_{k+1}-\theta_k}{\omega}\right)\left[v_k^2-v_k g\left(\frac{\theta_{k+1}-\theta_k}{\omega}\right)+\frac{g^2}{2}\left(\frac{\theta_{k+1}-\theta_k}{\omega}\right)^2\right], \quad (12)$$

where terms involving $1/c^4$ are omitted since they are very small. The approximate general-relativistic velocity map given by Eq. (12) differs from the Newtonian velocity map [Eq. (2)] by the last term which involves $1/c^2$. Similarly, the approximate general-relativistic impact-phase map given by Eq. (10) differs from the Newtonian impact-phase map [Eq. (1)] by the last term which involves $1/c^2$. The breakdown of agreement between the Newtonian and general-relativistic trajectories is therefore essentially due to the small $1/c^2$ term in Eq. (10) and Eq. (12).

Discussion

The simplicity of the bouncing ball system allows accurate calculations of the Newtonian, special-relativistic and general-relativistic trajectories for comparison, whereas such accurate calculations would be very difficult to achieve in more complex gravitational systems that can also exhibit chaotic behavior, for example, the three-body problem. Furthermore, the bouncing ball system can be realized experimentally – one realization [15] of the system consists of a steel ball bouncing on a concave lens which is attached to the membrane of a sinusoidally-driven loudspeaker. Because the bouncing ball system is a simple but realistic example of low-speed weak-gravity systems that can exhibit chaotic and non-chaotic behavior – i.e., a prototypical system – the breakdown of agreement of the special-relativistic and Newtonian trajectories

with the general-relativistic trajectory should also occur in other low-speed weak-gravity systems.

The breakdown of agreement of the special-relativistic and Newtonian trajectories with the general-relativistic trajectory for a low-speed weak-gravity system has two important implications. First, general-relativistic mechanics must be used, instead of special-relativistic mechanics, to correctly study the dynamics of a weak-gravity system. Second, general-relativistic mechanics must be used, instead of the standard practice (see, for example, [19]) of using Newtonian mechanics, to correctly study the dynamics of a low-speed weak-gravity system. These paradigm shifts may well lead to new understandings and discoveries for low-speed weak-gravity systems.

Supporting Information

Text S1 Derivation of the special-relativistic and general-relativistic maps.
(DOC)

Text S2 Newtonian and relativistic free-fall motion.
(DOC)

Author Contributions

Conceived and designed the experiments: SNL BLL. Performed the experiments: SNL. Analyzed the data: SNL BLL. Contributed reagents/materials/analysis tools: SNL BLL. Wrote the paper: SNL BLL.

References

1. French AP (1968) Special relativity. Thomas Nelson & Sons.
2. Hartle JB (2003) Gravity: An introduction to Einstein's general relativity. Addison-Wesley.
3. Einstein A (1961) Relativity: The special and the general theory. New York: Random House.
4. Lan BL (2006) Comparison of the Newtonian and relativistic predicted trajectories for a low-speed periodically delta-kicked particle. Chaos 16: 033107.
5. Lan BL (2009) Disagreement between Newtonian and relativistic trajectories for a low-speed kicked dissipative system. In: Skiadas CH, Dimotikalis I, Skiadas C, eds. Topics on chaotic systems.World Scientific. pp 199–203.
6. Lan BL, Cheng HY (2010) Newtonian and special-relativistic predictions for the trajectory of a slow-moving dissipative dynamical system. Commun Nonlinear Sci Numer Simulat 15: 2497–2503.
7. Lan BL, Borondo F (2011) Newtonian and special-relativistic predictions for the trajectories of a low-speed scattering system. Phys Rev E 83: 036201.
8. Lan BL (2009) Implications of the disagreement between Newtonian and relativistic low-speed trajectories. Chaos, Solitons and Fractals 42: 534–537.
9. Davies P (1992) The new physics: A synthesis. In: Davies P, ed. The new physics Cambridge University Press. pp 1–6.
10. Lapidus IR (1972) The falling body problem in general relativity. Am J Phys 40: 1509–1510.
11. Choquet-Bruhat Y (2009) General relativity and the Einstein equations. New York: Oxford University Press.
12. Wald RM (1984) General relativity. Chicago: University Of Chicago Press.
13. de Pater I, Lissauer JJ (2010) Planetary sciences, 2nd edition. New York: Cambridge University Press.
14. Tufillaro NB, Mello TM, Choi YM, Albano AM (1986) Period doubling boundaries of a bouncing ball. J Physique 47: 1477–1482.
15. Tufillaro NB, Abbott T, Reilly J (1992) An experimental approach to nonlinear dynamics and chaos. California: Addison-Wesley.
16. Liang SN, Lan BL (2011) Newtonian versus general-relativistic prediction for the trajectory of a bouncing ball system. Results in Physics 1: 36–39.
17. Lichtenberg AJ, Lieberman MA (1983) Regular and stochastic motion. New York: Springer.
18. Sprott JC (2003) Chaos and time-series analysis. Oxford: Oxford University Press.
19. Lissauer JJ (1999) Chaotic motion in the solar system. Rev Mod Phys 71: 835–845.

Text S1. Derivation of the special-relativistic and general-relativistic maps.

Following [1,2], the earth is assumed to be a uniform sphere of radius R. Furthermore, in between impacts with the table, the ball, which is initially close to the earth's surface ($r_0 \approx R$), undergoes free-fall motion along the radial direction where the distance it travels $|r - r_0|$ is assumed small compared to its initial position r_0 ($|r - r_0|/r_0 \ll 1$). The relativistic position and velocity of the ball between impacts (which are derived in Text S2) are needed in the derivations of the relativistic maps. In the derivations, it is convenient to transform the position r of the ball, which is measured relative to the center of the earth, to y: $y = r - R_{\mathrm{TLP}}$, where R_{TLP} is the distance from the center of the earth to the table's lowest position. The table's position $s(t) = A[\sin(\omega t + \theta_0) + 1]$ is measured relative to R_{TLP}.

In between the kth and (k+1)th impacts, the ball moves with initial velocity v_k and position y_k just after the kth impact. The ball's initial position y_k is the same as the table's position $A[\sin(\theta_k) + 1]$ just after the kth impact, where $\theta_k = \omega t_k + \theta_0$ is the table's phase and t_k is the time just after the kth impact. In the general-relativistic framework, the ball's position at time t after the kth impact is [based on Eq. (B17) in Text S2]

$$y - y_k = -\frac{c^2}{2g}\left\{1 - \frac{2g(R_{\mathrm{TLP}} + y_k)}{c^2}\right\}\left\{1 - \left\{\frac{1}{2}\left[\left(1 + \frac{v_k}{c}\right)e^{-\frac{g(t-t_k)}{c}} + \left(1 - \frac{v_k}{c}\right)e^{\frac{g(t-t_k)}{c}}\right]\right\}^{-2}\right\}, \tag{A1}$$

and the ball's velocity at time t after the kth impact is [based on Eq. (B9) in Text S2]

$$v = c\left[\frac{(1+v_k/c)e^{-g(t-t_k)/c} - (1-v_k/c)e^{g(t-t_k)/c}}{(1+v_k/c)e^{-g(t-t_k)/c} + (1-v_k/c)e^{g(t-t_k)/c}}\right]. \tag{A2}$$

Setting the difference between the ball's position $y(t)$ [Eq. (A1)] and table's position $s(t) = A[\sin(\omega t + \theta_0) + 1]$ at the (k+1)th impact to zero yields the impact-phase map Eq. (5).

Since the collision between the ball and table is inelastic, $\bar{v}'_{k+1}$ and $\bar{v}_{k+1}$, which are respectively the ball's velocity just before and just after the (k+1)th impact in the *table's* reference frame, are related through

$$\bar{v}_{k+1} = -\alpha \bar{v}'_{k+1} \tag{A3}$$

where α is the coefficient of restitution. The ball's velocity just before and just after the (k+1)th impact in the *ground's* reference frame are respectively

$$v'_{k+1} = \frac{\bar{v}'_{k+1} + u_{k+1}}{1 + \frac{\bar{v}'_{k+1} u_{k+1}}{c^2}} \quad \text{and} \quad v_{k+1} = \frac{\bar{v}_{k+1} + u_{k+1}}{1 + \frac{\bar{v}_{k+1} u_{k+1}}{c^2}}, \tag{A4}$$

where u_{k+1} is the table's velocity at the (k+1)th impact in the ground's reference frame. Solving for $\bar{v}'_{k+1}$ and $\bar{v}_{k+1}$ from Eq. (A4) and substituting into Eq. (A3) yields the velocity map Eq. (4). The expression for v'_{k+1} is obtained by substituting $t = t_{k+1}$ into Eq. (A2).

In the derivation of the special-relativistic map, Eq. (A1) is replaced by the special-relativistic position of the ball between the kth and (k+1)th impacts based on

the special-relativistic Eq. (B8) in Text S2. In the derivation [1,2] of the Newtonian map, the Newtonian Eqs. (B5) and (B6) in Text S2 were utilized to obtain the position and velocity of the ball between the kth and (k+1)th impacts, and Eq. (A4) is used without the terms involving c^2.

References

1. Tufillaro NB, Mello TM, Choi YM, Albano AM (1986) Period doubling boundaries of a bouncing ball. J. Physique 47: 1477-1482.

2. Tufillaro NB, Abbott T, Reilly J (1992) An experimental approach to nonlinear dynamics and chaos. California: Addison-Wesley.

Text S2. Newtonian and relativistic free-fall motion.

Here we consider the radial motion of a particle of mass m due to the gravitational field of a uniform sphere of mass M and radius R.

In the Newtonian framework, the change in gravitational potential energy of the particle from an initial position r_0 to a final position r is given by

$$\Delta U = U(r) - U(r_0) = -GMm\left[\frac{1}{r} - \frac{1}{r_0}\right]. \tag{B1}$$

If the distance travelled by the particle is small compared to r_0, that is, $|r - r_0|/r_0 \ll 1$, then $1/r$ is essentially given by

$$\frac{1}{r} = \frac{1}{r_0}\left(1 + \frac{r - r_0}{r_0}\right)^{-1} \approx \frac{1}{r_0}\left(1 - \frac{r - r_0}{r_0}\right) = \frac{1}{r_0} - \frac{r - r_0}{r_0^2}, \tag{B2}$$

since higher-order terms involving $(r - r_0)/r_0$ are negligible. If the particle is initially near the surface of the sphere, that is, $r_0 \approx R$, then

$$GM/r_0^2 \approx GM/R^2 = g. \tag{B3}$$

Substituting Eqs. (B2) and (B3) into Eq. (B1) reduces Eq. (B1) to approximately the change in gravitational potential energy of a particle in a uniform gravitational field

$$\Delta U \approx mgr - mgr_0. \tag{B4}$$

The Newtonian position and velocity of the particle at time t are therefore given by the well-known equations:

$$r - r_0 = v_0(t - t_0) - \frac{1}{2}g(t - t_0)^2, \tag{B5}$$

$$v = v_0 - g(t - t_0). \tag{B6}$$

In the special-relativistic framework, if $|r - r_0|/r_0 \ll 1$ and $r_0 \approx R$, Eqs. (B2) and (B3) reduce the change in gravitational potential energy of the particle to

$$\Delta U = -\frac{GMm}{\sqrt{1-(v/c)^2}}\left[\frac{1}{r} - \frac{1}{r_0}\right] \approx \frac{mgr - mgr_0}{\sqrt{1-(v/c)^2}}. \tag{B7}$$

Solution of the special-relativistic equation of motion with the force derived from the gravitational potential energy $U(r)$ in Eq. (B7) yields [1-3]

$$r - r_0 = -(c^2/g)\ln\left\{\frac{1}{2}\left[\left(1+\frac{v_0}{c}\right)e^{-g(t-t_0)/c} + \left(1-\frac{v_0}{c}\right)e^{g(t-t_0)/c}\right]\right\}, \tag{B8}$$

$$v = c\left[\frac{(1+v_0/c)e^{-g(t-t_0)/c} - (1-v_0/c)e^{g(t-t_0)/c}}{(1+v_0/c)e^{-g(t-t_0)/c} + (1-v_0/c)e^{g(t-t_0)/c}}\right] \tag{B9}$$

for the position and velocity of the particle at time t.

In the general-relativistic framework, the gravitational field outside the uniform sphere is described by the Schwarzschild metric [4] in terms of the Schwarzschild coordinates (ct, r, θ, ϕ)

$$ds^2 = c^2 d\tau^2 = \left(1 - \frac{r_s}{r}\right)c^2 dt^2 - \frac{dr^2}{\left(1 - \frac{r_s}{r}\right)} - r^2\left(d\theta^2 + \sin^2\theta d\phi^2\right), \tag{B10}$$

where ds is the interval between neighboring events, τ is the proper time, and $r_s = 2GM/c^2$ is the Schwarzschild radius. For purely radial motion [3,5] along the line ϕ =constant in the equatorial plane $\theta = \pi/2$, the metric Eq. (B10) is simplified, with $d\phi = d\theta = 0$, to

$$ds^2 = c^2 d\tau^2 = \left(1 - \frac{r_s}{r}\right) c^2 dt^2 - \frac{dr^2}{\left(1 - r_s / r\right)} \tag{B11}$$

and the geodesic equations are reduced to

$$\frac{c d^2 t}{c^2 d\tau^2} + \left(\frac{r_s / r^2}{1 - r_s / r}\right) \frac{c dt}{c d\tau} \frac{dr}{c d\tau} = 0\,, \tag{B12}$$

$$\frac{d^2 r}{c^2 d\tau^2} + \left(1 - \frac{r_s}{r}\right)\left(\frac{r_s}{2r^2}\right)\left(\frac{c dt}{c d\tau}\right)^2 - \left(1 - \frac{r_s}{r}\right)^{-1}\left(\frac{r_s}{2r^2}\right)\left(\frac{dr}{c d\tau}\right)^2 = 0\,. \tag{B13}$$

The local velocity [4,6] of the particle, measured by a local observer who is at rest at a particular Schwarzschild radial coordinate and is next to the particle, is

$$v = \left(1 - \frac{r_s}{r}\right)^{-1} \frac{dr}{dt} = \left(1 - \frac{2GM}{c^2 r}\right)^{-1} \frac{dr}{dt}\,. \tag{B14}$$

The integral of Eq. (B12), which is given by

$$\frac{c dt}{c d\tau} = k\left(1 - \frac{r_s}{r}\right)^{-1}\,, \tag{B15}$$

where k is a constant, and the integral of Eq. (B13), which is given by Eq. (B11), together with the initial condition $v = v_0$ at $r = r_0$, lead to the following expression for dr/dt:

$$\left(\frac{dr}{dt}\right)^2 = \left(1 - \frac{2GM}{c^2 r}\right)^2 \left(1 - \frac{2GM}{c^2 r_0}\right)^{-1} \left[v_0^2 \left(1 - \frac{2GM}{c^2 r}\right) + 2GM\left(\frac{1}{r} - \frac{1}{r_0}\right)\right]. \tag{B16}$$

If $|r - r_0|/r_0 << 1$ and $r_0 \approx R$, substituting Eqs. (B2) and (B3) into Eq. (B16) and integrating it with initial condition $r = r_0$ at $t = t_0$ yields the general-relativistic position of the particle at time t

$$r - r_0 = -\frac{c^2}{2g}\left(1-\frac{2gr_0}{c^2}\right)\left\{1-\left\{\frac{1}{2}\left[\left(1+\frac{v_0}{c}\right)e^{-\frac{g(t-t_0)}{c}}+\left(1-\frac{v_0}{c}\right)e^{\frac{g(t-t_0)}{c}}\right]\right\}^{-2}\right\}. \quad \text{(B17)}$$

In the limit of weak gravity ($2gr/c^2 \ll 1$ and $2gr_0/c^2 \ll 1$), Eq. (B17) reduces to the special-relativistic Eq. (B8). In the limit of weak gravity and low speed ($v/c \ll 1$, $v_0/c \ll 1$ and $g(t - t_0)/c \ll 1$), Eq. (B17) reduces to the Newtonian Eq. (B5).

Substituting Eqs. (B14), (B2), (B3) and (B17) sequentially into Eq. (B16) yields the general-relativistic velocity of the particle at time t, which is the same as the special-relativistic Eq. (B9). In the limit of low speed, Eq. (B9) reduces to the Newtonian Eq. (B6).

References

1. Lapidus IR (1972) The falling body problem in general relativity. Am. J. Phys. 40: 1509-1510.
2. Lapidus IR (1972) Motion of a relativistic particle acted upon by a constant force and a uniform gravitational field. Am. J. Phys. 40: 984-988.
3. Srinivasa Rao KN (1966) The motion of a falling particle in a Schwarzschild field. Ann. Inst. Henri Poincare, Sect. A 5: 227-233.
4. Landau LD, Lifshitz EM (1975) The classical theory of fields. Oxford: Pergamon Press.
5. Srinivasa Rao KN, Gopala Rao AV (1974) Falling body in the theories of

gravitation. J. Phys. A 7**:** 485-488.

6. Zel'dovich YaB, Novikov ID (1996) Relativistic astrophysics vol. 1: Stars and relativity. New York: Dover Publications.

OPEN ACCESS Freely available online

PLoS one

Statistical Predictions for the Dynamics of a Low-Speed System: Newtonian versus Special-Relativistic Mechanics

Shiuan-Ni Liang, Boon Leong Lan*

School of Science, Monash University, Bandar Sunway, Selangor, Malaysia

Abstract

The Newtonian and special-relativistic statistical predictions for the mean, standard deviation and probability density function of the position and momentum are compared for the periodically-delta-kicked particle at low speed. Contrary to expectation, we find that the statistical predictions, which are calculated from the same parameters and initial Gaussian ensemble of trajectories, do not always agree if the initial ensemble is sufficiently well-localized in phase space. Moreover, the breakdown of agreement is very fast if the trajectories in the ensemble are chaotic, but very slow if the trajectories in the ensemble are non-chaotic. The breakdown of agreement implies that special-relativistic mechanics must be used, instead of the standard practice of using Newtonian mechanics, to correctly calculate the statistical predictions for the dynamics of a low-speed system.

Citation: Liang S-N, Lan BL (2012) Statistical Predictions for the Dynamics of a Low-Speed System: Newtonian versus Special-Relativistic Mechanics. PLoS ONE 7(5): e36430. doi:10.1371/journal.pone.0036430

Editor: Gerardo Adesso, University of Nottingham, United Kingdom

Received November 11, 2011; **Accepted** April 2, 2012; **Published** May 11, 2012

Funding: This work was supported by a Fundamental Research Grant Scheme, FRGS/2/2010/ST/MUSM/02/1. The funders had no role in study design, data collection and analysis, decision to publish, or preparation of the manuscript.

Competing Interests: The authors have declared that no competing interests exist.

* E-mail: lan.boon.leong@monash.edu

Introduction

If the speed of a system is low, that is, much less than the speed of light, it is expected [1–3] that the dynamics predicted by special-relativistic mechanics is always well-approximated by the dynamics predicted by Newtonian mechanics for the same parameters and initial conditions. In a recent paper [4], we compared the Newtonian and special-relativistic predicted trajectories for a model Hamiltonian system – the periodically-delta-kicked particle. We found, contrary to expectation, that although the particle speed is low, the Newtonian trajectory does not remain close to the special-relativistic trajectory – the two trajectories eventually become completely different regardless of whether the trajectories are chaotic or non-chaotic. However, the agreement between the Newtonian and special-relativistic trajectories breaks down much faster in the chaotic case compared to the non-chaotic case. Similar breakdown of agreement was also found in a model dissipative system [5,6] and a model scattering system [7]. The loss of agreement means [6–8] that special-relativistic mechanics must be used, instead of the standard practice of using Newtonian mechanics, to correctly calculate the trajectory of a low-speed system.

In this paper, we extend the Newtonian special-relativistic comparison for the low-speed periodically-delta-kicked particle from *single-trajectory* predictions [4] to *statistical* predictions – in particular, the mean, standard deviation and probability density function of the position and momentum – which are calculated from the same parameters and initial ensemble of trajectories. Calculating these statistical quantities directly from an ensemble of trajectories is far easier than solving the Newtonian and special-relativistic Liouville's equations numerically to first obtain the phase-space probability density functions. Details of the model Hamiltonian system and calculation are given next, followed by the results and discussion.

Methods

The model Hamiltonian system is a one-dimensional system where the particle is subjected to a sinusoidal potential which is periodically turned on for an instant. The Newtonian equations of motion for the periodically-delta-kicked particle are easily integrated exactly [9,10] to yield a mapping, which is known as the standard map, of the dimensionless scaled position X and dimensionless scaled momentum P from just before the nth kick to just before the $(n+1)$th kick:

$$P_n = P_{n-1} - \frac{K}{2\pi}\sin(2\pi X_{n-1}) \tag{1}$$

$$X_n = (X_{n-1} + P_n) \bmod 1 \tag{2}$$

where $n = 1,2,\ldots$, and K is a dimensionless positive parameter. For the standard map, the transition from weak (local) chaos to strong (global) chaos occurs at $K \approx 0.917$.

The special-relativistic equations of motion are also easily integrated exactly, producing a mapping known as the relativistic standard map [11,12] for the dimensionless scaled position X and dimensionless scaled momentum P from just before the nth kick to just before the $(n+1)$th kick:

$$P_n = P_{n-1} - \frac{K}{2\pi}\sin(2\pi X_{n-1}) \tag{3}$$

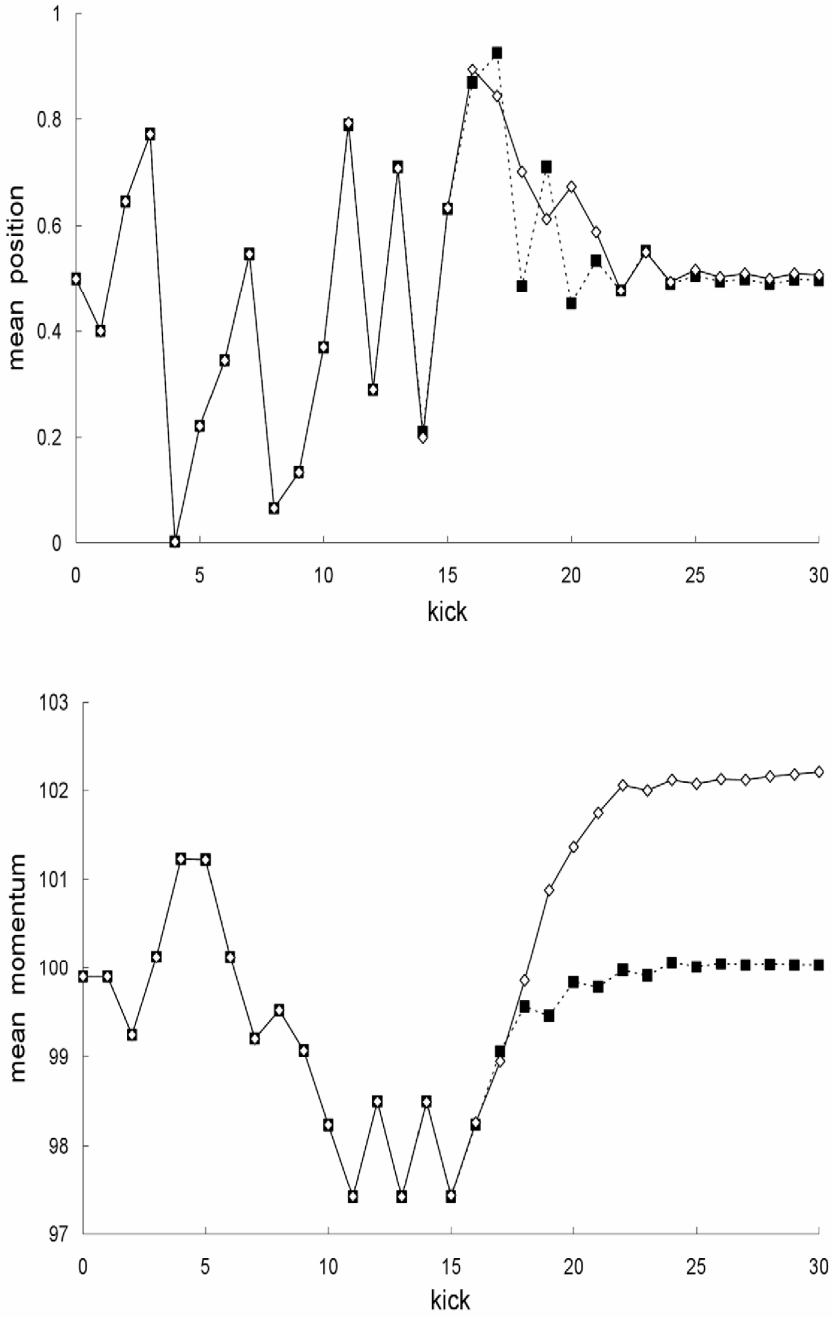

Figure 1. Comparison of mean trajectories for the first example. Newtonian (squares) and special-relativistic (diamonds) mean positions (top plot) and mean momentums (bottom plot) for the first example.
doi:10.1371/journal.pone.0036430.g001

$$X_n = \left(X_{n-1} + \frac{P_n}{\sqrt{1+\beta^2 P_n^2}} \right) \bmod 1 \qquad (4)$$

where $n = 1,2, \ldots$, and β, like K, is a dimensionless positive parameter. Since

$$\frac{v}{c} = \frac{\beta P}{\sqrt{1+(\beta P)^2}}, \qquad (5)$$

$\beta P << 1$ implies $v << c$ (i.e., low speed), where v is the particle speed and c is the speed of light. Ciubotariu et al. [13] have studied a dissipative version of the relativistic standard map to see how weak damping changes the phase-space structure around the

origin described by the relativistic standard map; they did not however compare the dynamical predictions of their dissipative relativistic standard map with the predictions of the dissipative non-relativistic standard map.

For both theories, the ensemble of trajectories is initially Gaussian distributed in position and momentum with means $<X_0>$ and $<P_0>$, and standard deviations σ_{X0} and σ_{P0}:

$$p(X_0,P_0)=\frac{1}{2\pi\sigma_{X0}\sigma_{P0}}\exp\left[-\frac{(X_0-\langle X_0\rangle)^2}{2\sigma_{X0}^2}-\frac{(P_0-\langle P_0\rangle)^2}{2\sigma_{P0}^2}\right]. \quad (6)$$

Each trajectory in the Newtonian (special-relativistic) ensemble is time-evolved using the standard map (relativistic standard map). For each theory, the mean trajectory, i.e., mean position and mean momentum, just before each kick is calculated from the ensemble of trajectories. First, the mean trajectory is calculated using 10^6 trajectories, where the accuracy of the double-precision calculation is determined by comparison with the quadruple-precision calculation. The mean trajectory is then recalculated using 10^7 trajectories with the same accuracy determination. Finally, the accuracy of the mean trajectory is determined by comparing the 10^6-trajectories calculation with the 10^7-trajectories calculation. The position and momentum standard deviations and probability density functions are calculated in the same manner.

Results

In this section, we will present three examples to illustrate the general results. In the first example, the map parameters are $K=7.0$ and $\beta=10^{-7}$. The Newtonian and special-relativistic ensembles are both initially Gaussian distributed in phase space with means $<X_0>=0.5$ and $<P_0>=99.9$, and standard deviations $\sigma_{X0}=\sigma_{P0}=10^{-10}$, and thus initially localized in the chaotic 'sea' in phase space. Figure 1 shows that the Newtonian mean position and mean momentum agree with the special-relativistic mean position and mean momentum for the first 16 kicks only, the two mean trajectories are completely different from kick 17 onwards.

The breakdown of agreement between the Newtonian and special-relativistic mean trajectories in Figure 1 can be understood as follows. In either the Newtonian or special-relativistic case, the position and momentum standard deviations grow [14,15] exponentially initially because the trajectories in the ensemble are chaotic. But as long as the position standard deviation remains small ($<<1$), the mean trajectory is [14,15] well-approximated by the single trajectory with the same initial conditions as the mean trajectory. The agreement between the single trajectory and mean trajectory breaks down when the position standard deviation saturates [14,15], that is, when the position probability density becomes delocalized over the entire position interval. Figure 2 shows that the Newtonian and special-relativistic position standard deviations saturate at kick 19. Thus, in either the Newtonian (see Figure 3) or special-relativistic (see Figure 4) case, the mean trajectory is well-approximated by the single trajectory for the first 18 kicks only. The complete disagreement between the Newtonian and special-relativistic mean trajectories at kick 17 and kick 18 is therefore due to the complete disagreement of the Newtonian single trajectory and the special-relativistic single trajectory, which are both chaotic with Lyapunov exponent of 1.27, from kick 17 onwards. Since the position and momentum difference between the chaotic Newtonian and special-relativistic single trajectories grows exponentially at a rate approximately given by the Lyapunov exponent [4], we can estimate when the agreement between the two single trajectories breaks down and thus when the two mean trajectories breaks down. In particular, the position difference between the two single trajectories with the same initial conditions is 4.99×10^{-9} after 1 kick and, assuming that the exponential growth constant is 1.27, it grows to 0.1 (the maximum possible position difference is 1) after 14 kicks, which is close to the actual 17 kicks.

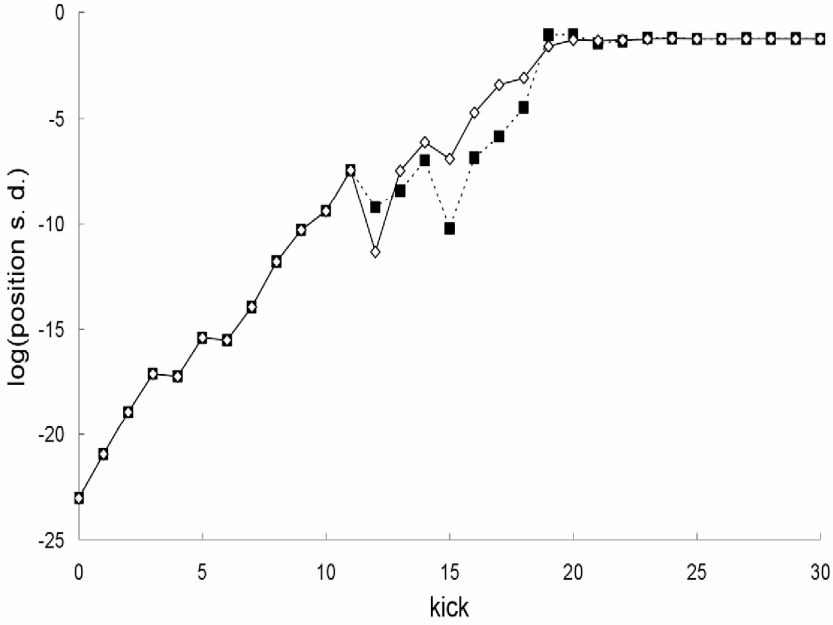

Figure 2. Comparison of position standard deviations for the first example. Natural-log of the Newtonian (squares) and special-relativistic (diamonds) position standard deviations for the first example.
doi:10.1371/journal.pone.0036430.g002

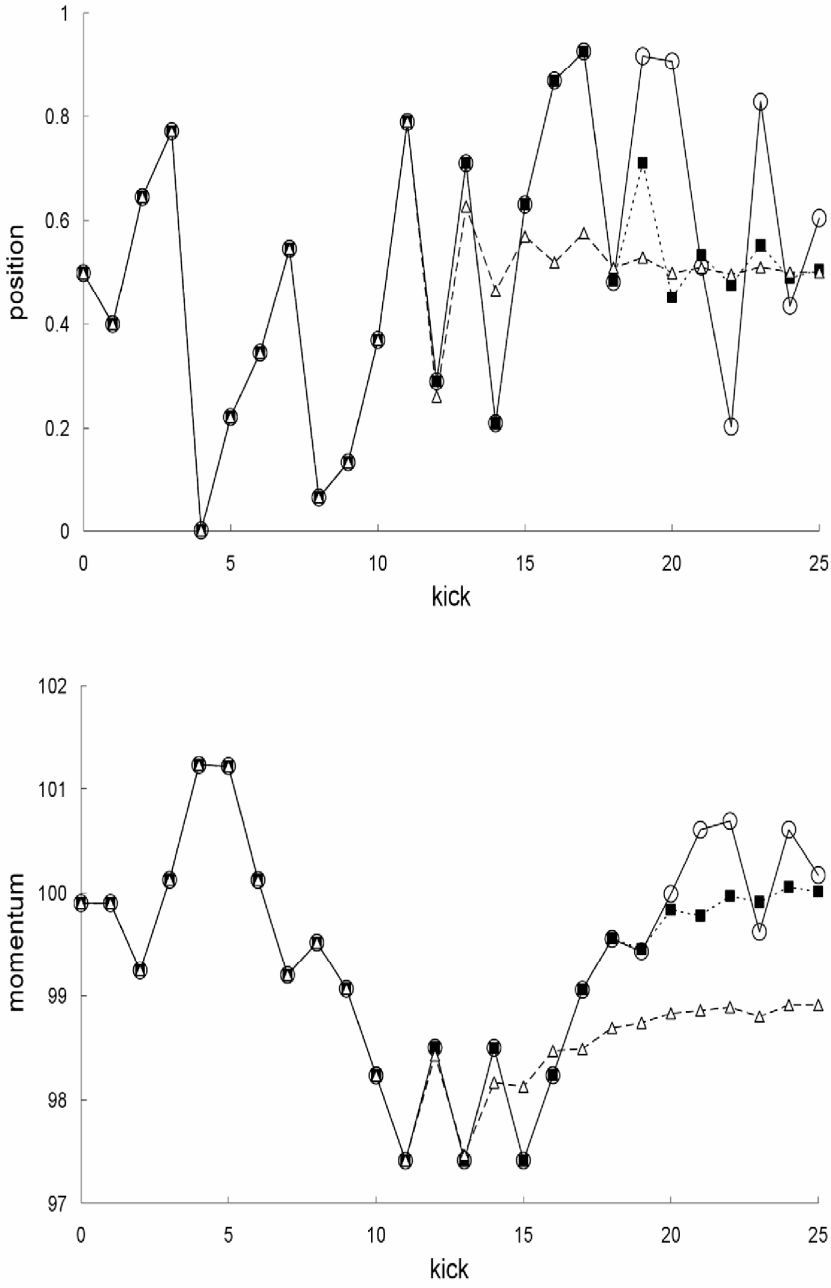

Figure 3. Newtonian single and mean trajectories. Newtonian single trajectory (circles), Newtonian mean trajectory for the first example (squares), and Newtonian mean trajectory for the second example (triangles): positions (top plot) and momentums (bottom plot).
doi:10.1371/journal.pone.0036430.g003

Furthermore, the difference between the Newtonian and special-relativistic mean trajectories grow exponentially up to kick 18 (see Figure 5) because the difference between the Newtonian and special-relativistic chaotic single trajectories grow [4] exponentially. Hence, the breakdown of agreement between the Newtonian and special-relativistic mean trajectories is rapid because of the exponential growth of the difference between the two mean trajectories.

Figure 2 and Figure 6 show that the position and momentum standard deviations predicted by the two theories also do not always agree. The breakdown of agreement occurs at kick 12. This rapid breakdown of agreement is, see Figure 7, due to the exponential growth of the difference between the Newtonian and special-relativistic standard deviations, for both position and momentum, up to kick 12.

Together, Figure 1, Figure 2 and Figure 6 show that the agreement between the statistical predictions of the two theories, Newtonian and special relativistic, for the position and momentum means and standard deviations breaks down from kick 12 onwards even though the mean particle speed is low, only 0.001% of the speed of light since $\beta = 10^{-7}$. Figure 8 shows the different

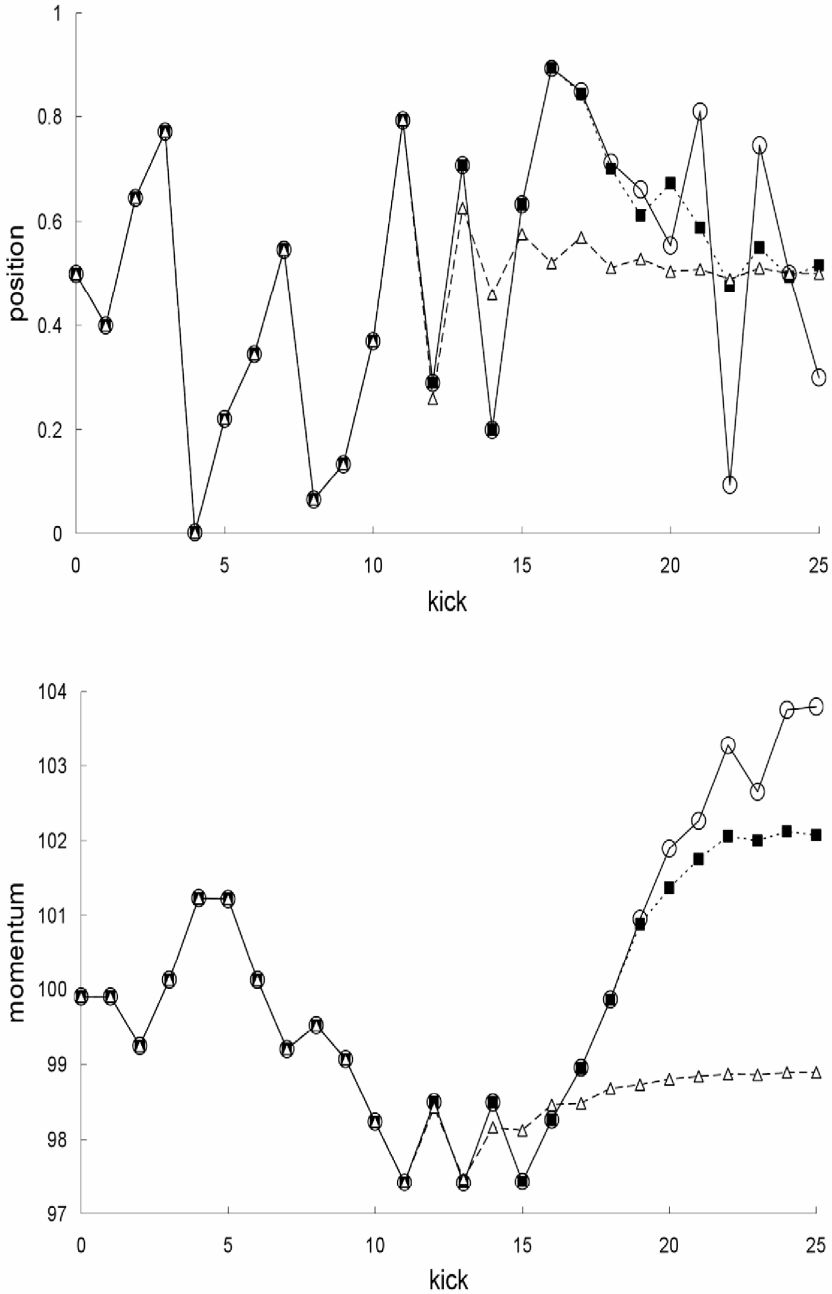

Figure 4. Special-relativistic single and mean trajectories. Special-relativistic single trajectory (circles), special-relativistic mean trajectory for the first example (squares), and special-relativistic mean trajectory for the second example (triangles): positions (top plot) and momentums (bottom plot).
doi:10.1371/journal.pone.0036430.g004

Newtonian and special-relativistic position and momentum probability densities at kick 17.

In the second example, the parameters and initial means are the same as those in the first example but the initial standard deviations are larger: $\sigma_{X0} = \sigma_{P0} = 10^{-8}$. In this case, Figure 9 shows there is no breakdown of agreement between the mean trajectory predictions of the two theories. In addition, Figure 10 shows there is also no breakdown of agreement between the position and momentum standard deviations predicted by the two theories.

The results in Figure 9 and Figure 10 for the second example can be understood as follows. Figure 3 and Figure 4 show that the single trajectory is close to the mean trajectory for the first 12 kicks only, in either the Newtonian or special-relativistic case. Thus, for the first 12 kicks, the Newtonian and special-relativistic mean trajectories are close because the Newtonian and special-relativistic single trajectories are close (recall, the agreement between the

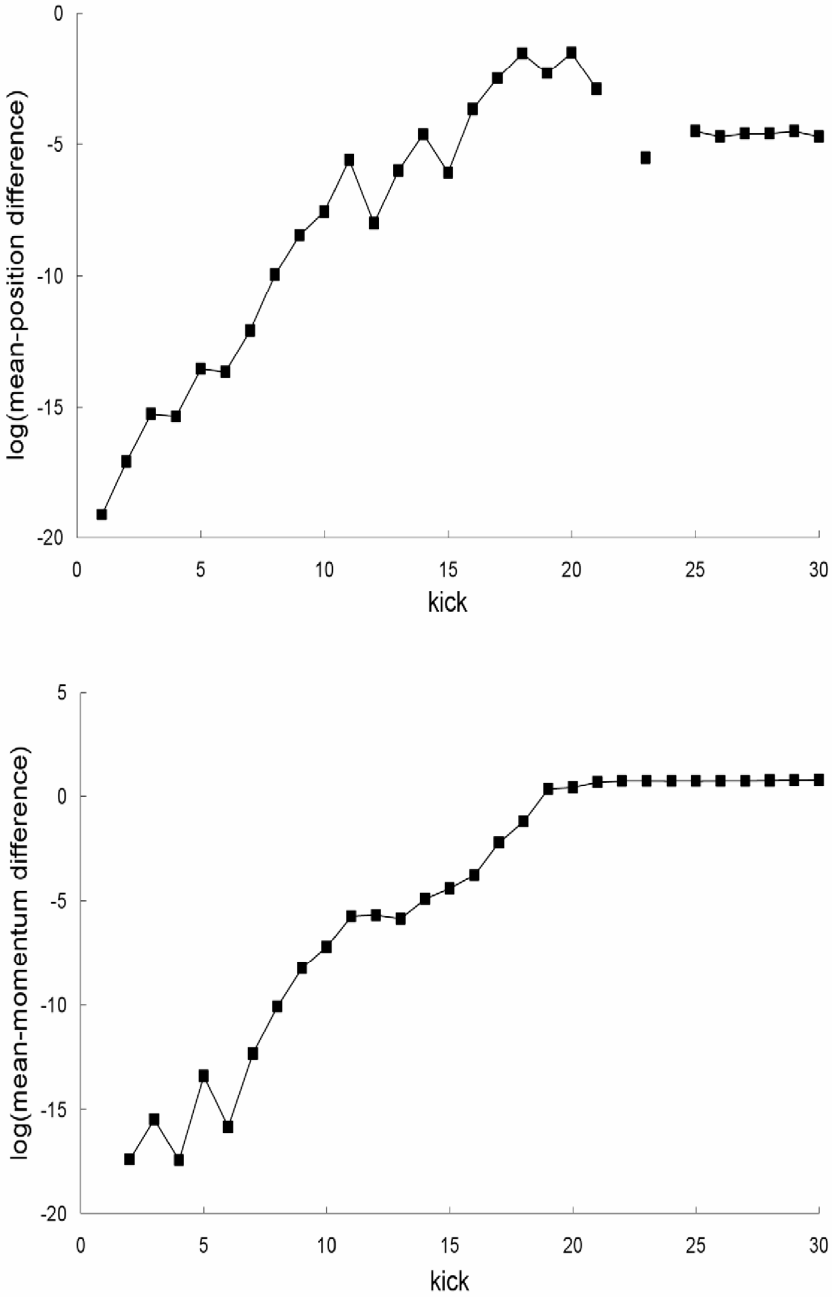

Figure 5. Difference between the mean trajectories for the first example. Natural-log of the absolute value of the difference between the Newtonian and special-relativistic mean positions (top plot) and mean momentums (bottom plot) for the first example. The mean-position differences at kick 22 and 24 cannot be resolved with the accuracy we have for the Newtonian and special-relativistic mean positions at those kicks.
doi:10.1371/journal.pone.0036430.g005

two single trajectories only breaks down at kick 17). Furthermore, the Newtonian and special-relativistic standard deviations are, like the means, still very close at kick 13 when the position standard deviations saturate. In other words, the Newtonian and special-relativistic position and momentum probability densities are essentially the same at kick 13. We have found that the agreement between the statistical predictions of the two theories for the position and momentum means and standard deviations does not break down for an ensemble of trajectories which is initially uniformly distributed (delocalized) in position. Thus, in this example, because the Newtonian and special-relativistic position probability densities are essentially the same and delocalized at kick 13, the statistical predictions of the two theories continue to be close for subsequent kicks.

The results illustrated by the two examples above were also found for other values of the K parameter: 0.9, 3.86, 6.4717, 6.9115 and 10.053.

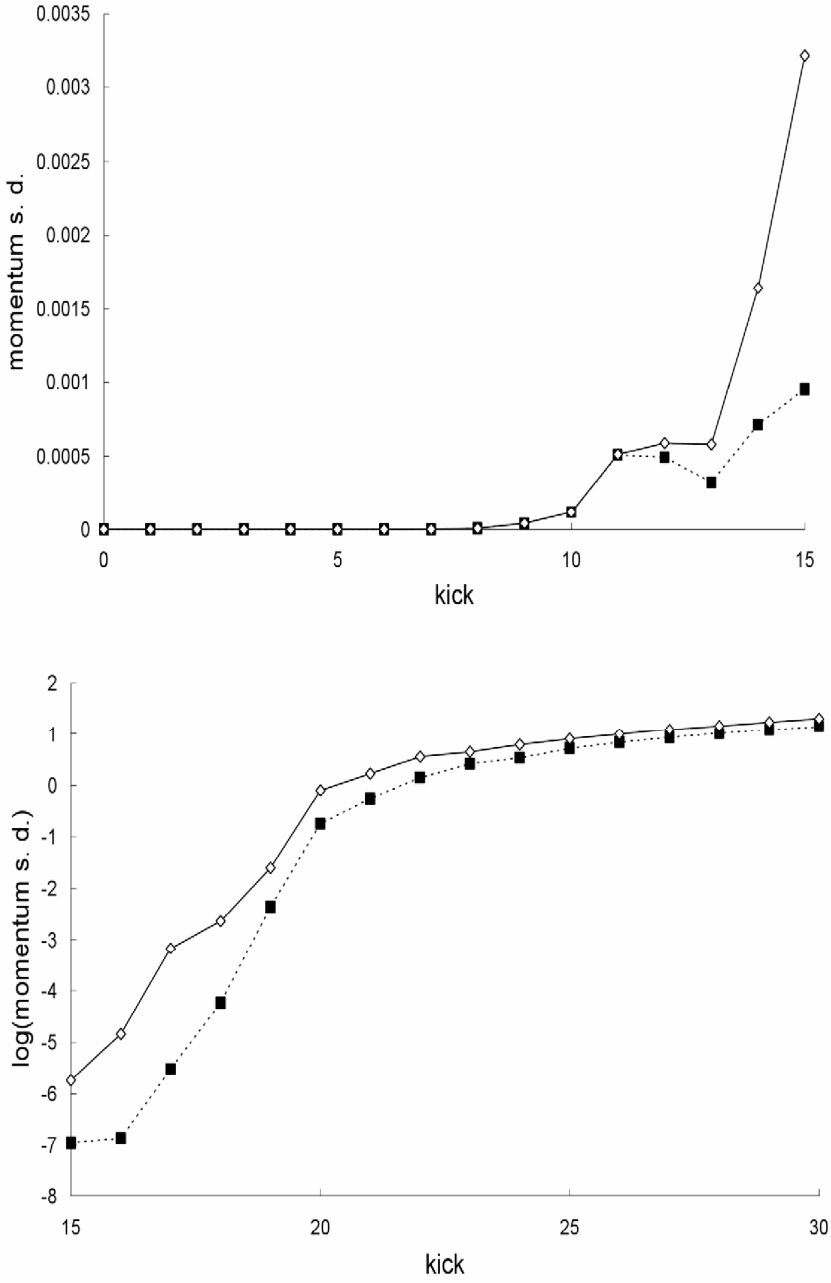

Figure 6. Comparison of momentum standard deviations for the first example. Newtonian (squares) and special-relativistic (diamonds) momentum standard deviations for the first example: first 15 kicks (top plot), kick 15 to 30 (bottom plot). The Newtonian and special-relativistic momentum standard deviations in the bottom plot are completely different from each other - they appear to be close from kick 25 onwards because the natural log of the standard deviations is plotted.
doi:10.1371/journal.pone.0036430.g006

Recall, in the first example (with smaller initial standard deviations), the Newtonian and special-relativistic position standard deviations saturate *after* the agreement between the Newtonian and special-relativistic single trajectories breaks down. However, in the second example (with larger initial standard deviations), the Newtonian and special-relativistic position standard deviations saturate *before* the agreement between the Newtonian and special-relativistic single trajectories breaks down. The first and second examples therefore show that in order for the statistical predictions of the two theories to break down, the initial Gaussian ensemble must be sufficiently well-localized in phase space, that is, the initial standard deviations must be sufficiently small such that the Newtonian and special-relativistic position standard deviations saturate *after* the agreement between the Newtonian and special-relativistic single trajectories breaks down.

If the initial ensemble is localized in the chaotic 'sea' in phase space, in the first example for instance, the agreement between the Newtonian and special-relativistic single trajectories (the initial

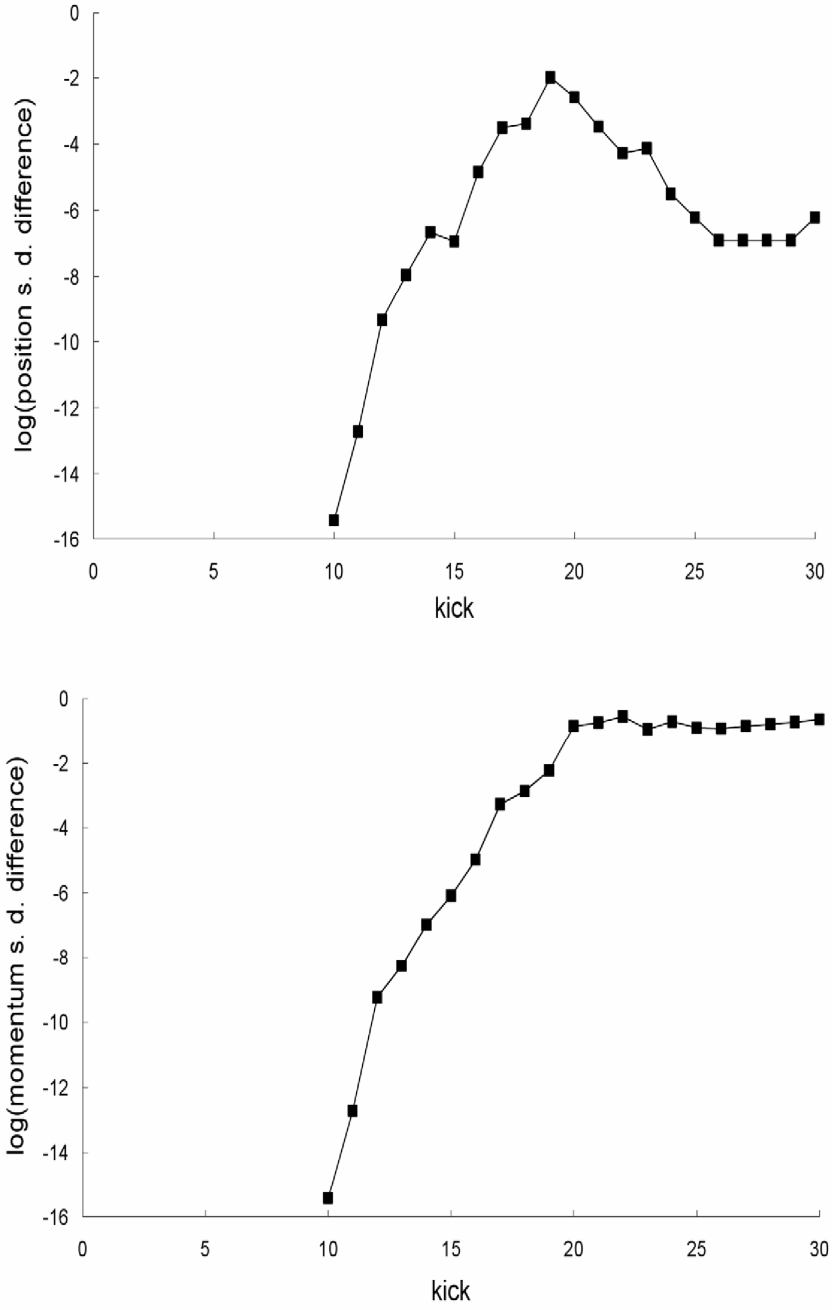

Figure 7. Difference between the standard deviations for the first example. Natural-log of the absolute value of the difference between the Newtonian and special-relativistic position standard deviations (top plot) and momentum standard deviations (bottom plot) for the first example. The standard-deviation differences from kick 1 to 9 cannot be resolved with the accuracy we have for the Newtonian and special-relativistic standard deviations at those kicks.
doi:10.1371/journal.pone.0036430.g007

conditions of the two single trajectories are the same, equal to the initial mean position and mean momentum) breaks down rapidly because the difference between the single trajectories grows [4] exponentially. In contrast, if the initial ensemble is localized in the non-chaotic 'island' in phase space, the difference between the Newtonian and special-relativistic single trajectories only grows [4] linearly, and therefore it takes a very long time for the agreement between the single trajectories to break down. This means that the breakdown of agreement between the statistical predictions of the two theories, Newtonian and special-relativistic, is very fast in the chaotic case, as we saw in the first example, but very slow in the non-chaotic case.

As an example of the non-chaotic case (this is our third example), for map parameters $K = 0.9$ and $\beta = 10^{-7}$, the agreement between the Newtonian and special-relativistic single trajectories with initial conditions $X_0 = 0.7$ and $P_0 = 99.9$ takes

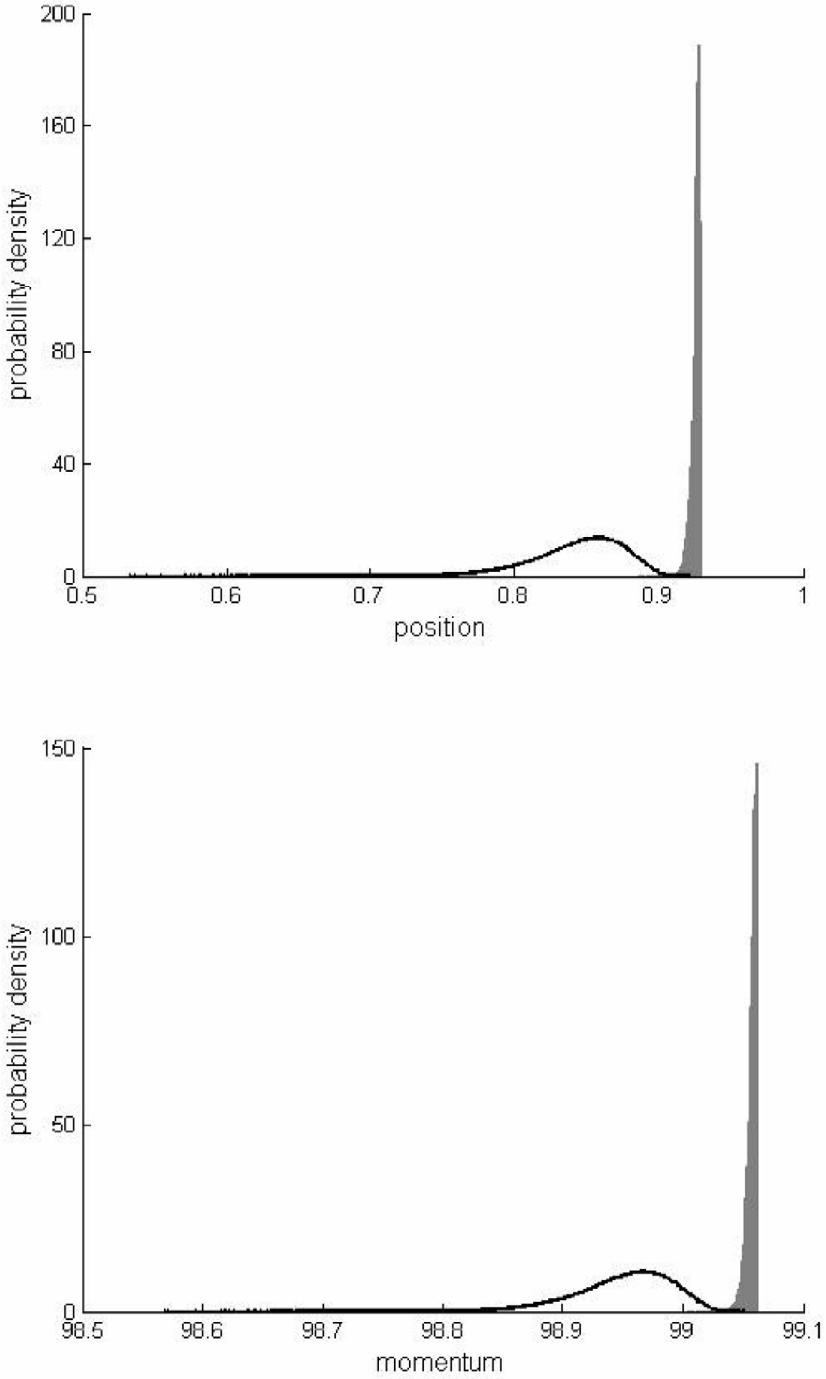

Figure 8. Comparison of probability densities for the first example. Newtonian (shaded grey) and special-relativistic (bold line) position (top plot) and momentum (bottom plot) probability densities for the first example at kick 17.
doi:10.1371/journal.pone.0036430.g008

about 10^8 kicks [4] to break down. The Newtonian and special-relativistic statistical predictions can thus agree for a very long time. Indeed, for initial standard deviations $\sigma_{X0} = \sigma_{P0} = 10^{-9}$, the means still agree to 6 and 9 significant figures respectively for position and momentum at kick 1000. At the same kick, the accuracies we have for both the Newtonian and special-relativistic standard deviations are 3 and 4 significant figures respectively for position and momentum – the Newtonian and special-relativistic standard deviations are the same, 2.67×10^{-7} for position and 2.446×10^{-7} for momentum, within these accuracies. Similar results were found for other non-chaotic cases for other values of the parameter K, 0.5 and 1.5.

Finally, the breakdown of agreement between the Newtonian and special-relativistic statistical predictions for the periodically-

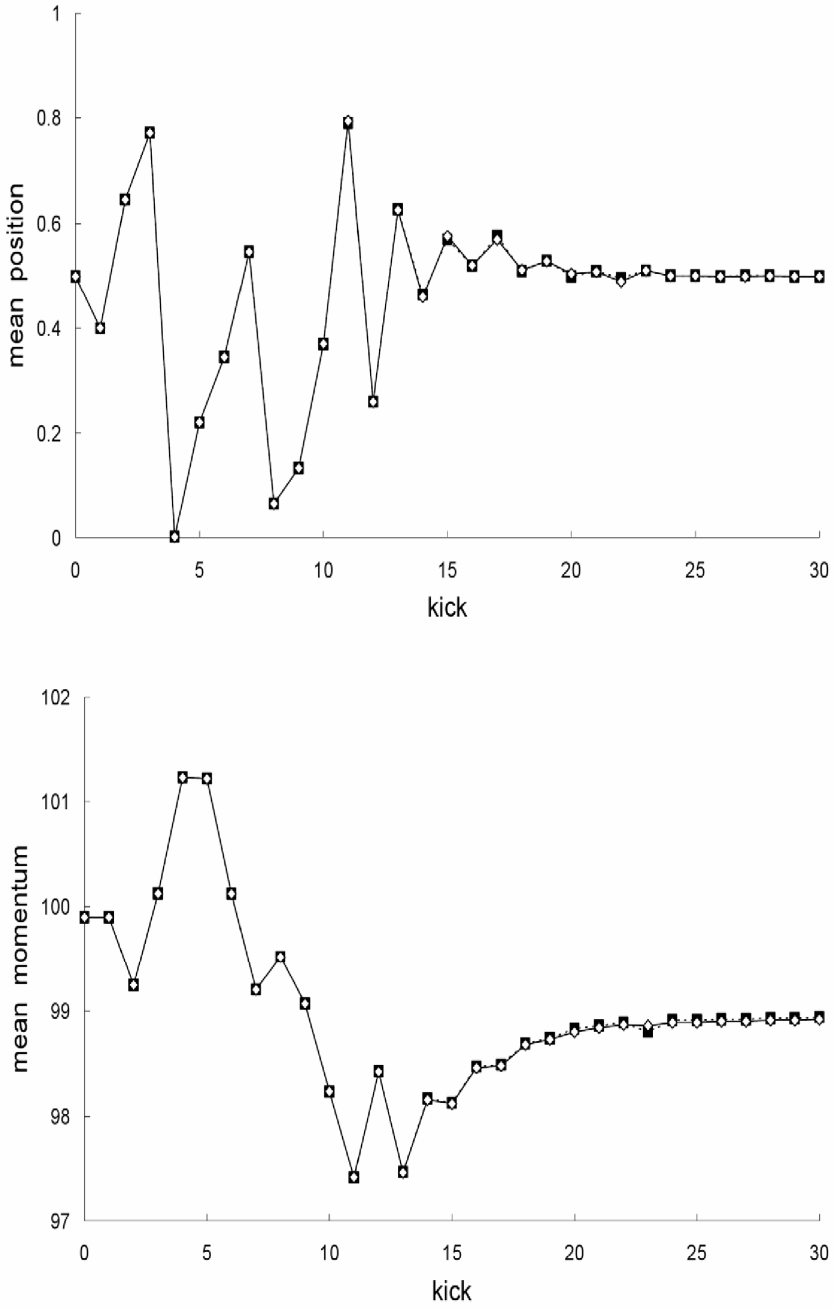

Figure 9. Comparison of mean trajectories for the second example. Newtonian (squares) and special-relativistic (diamonds) mean positions (top plot) and mean momentums (bottom plot) for the second example.
doi:10.1371/journal.pone.0036430.g009

delta-kick particle at low speed can be further understood from a broader perspective by comparing the Newtonian Liouville's equation for the phase-space probability density function $\rho(X,P,t)$

$$\frac{\partial\rho(X,P,t)}{\partial t} = -\left[\frac{P}{T}\right]\left[\frac{\partial\rho}{\partial X}\right] + \left[\frac{K}{2\pi T}\sin(2\pi X)\sum_{j=-\infty}^{\infty} T\delta(jT-t)\right]\left[\frac{\partial\rho}{\partial P}\right] \quad (7)$$

with its special-relativistic counterpart

$$\frac{\partial\rho(X,P,t)}{\partial t} = -\left[\frac{P}{T\left(1+\beta^2P^2\right)^{1/2}}\right]\left[\frac{\partial\rho}{\partial X}\right] + \left[\frac{K}{2\pi T}\sin(2\pi X)\sum_{j=-\infty}^{\infty} T\delta(jT-t)\right]\left[\frac{\partial\rho}{\partial P}\right], \quad (8)$$

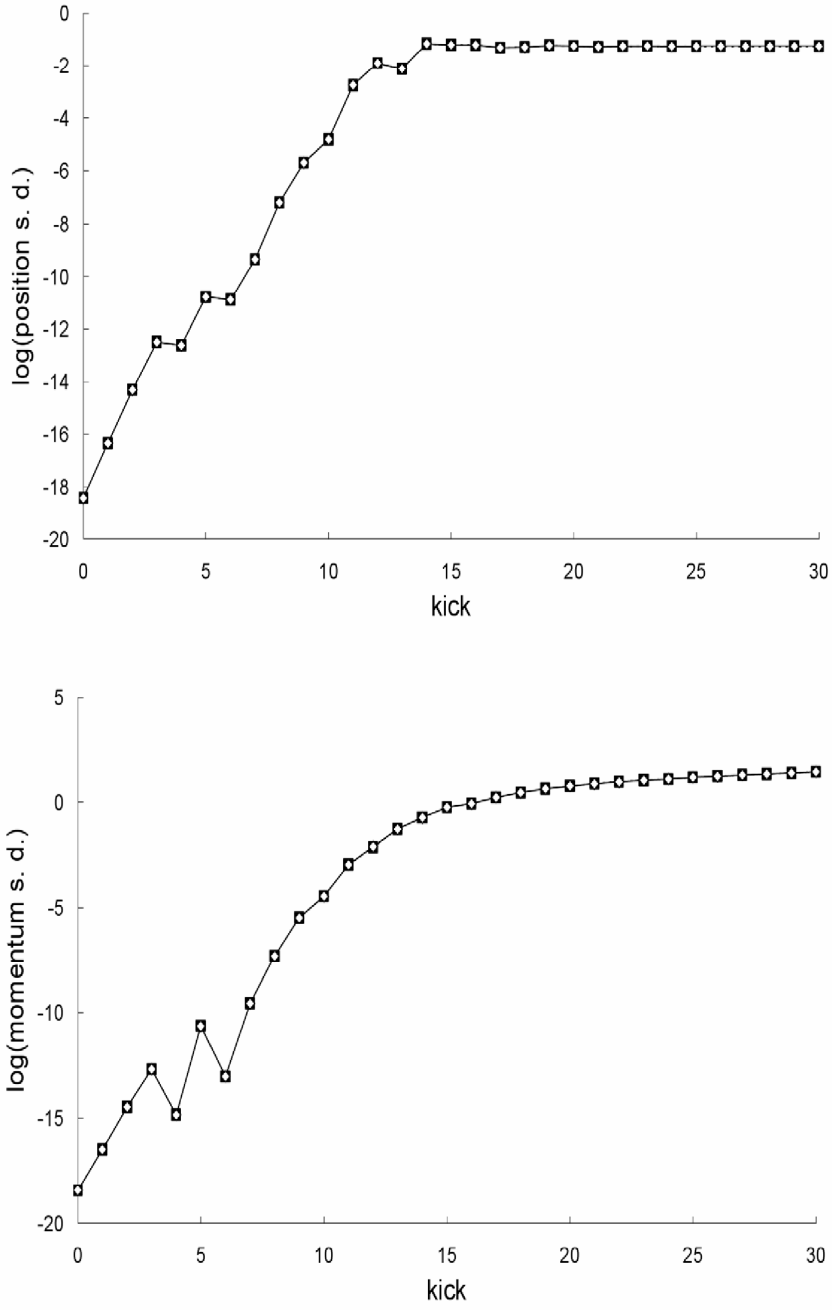

Figure 10. Comparison of standard deviations for the second example. Natural-log of the Newtonian (squares) and special-relativistic (diamonds) position standard deviations (top plot) and momentum standard deviations (bottom plot) for the second example.
doi:10.1371/journal.pone.0036430.g010

where the infinite sum in both equations is the series of periodic delta kicks with period T. For low speed, $\beta P << 1$, therefore

$$\frac{1}{\left(1+\beta^2 P^2\right)^{1/2}} \approx 1-\frac{1}{2}\beta^2 P^2 \qquad (9)$$

in Eq. (8). The breakdown of agreement between the Newtonian and special-relativistic statistical predictions is therefore essentially due to the small $\beta 2P2/2$ term in Eq. (8).

Discussion

Since the periodically-delta-kicked particle is a prototypical [16] Hamiltonian system, we expect the breakdown of agreement between the Newtonian and special-relativistic statistical dynamical predictions to occur in other low-speed Hamiltonian systems.

Our finding raises an important fundamental question: When the Newtonian and special-relativistic statistical dynamical predictions are completely different for a low-speed system, which of the two predictions is empirically correct? Since special relativity

continues to be successfully tested [17] in recent times, we expect the special-relativistic predictions to be correct. The breakdown of agreement therefore implies that special-relativistic mechanics must be used, instead of the standard practice of using Newtonian mechanics, to correctly calculate the statistical predictions for the dynamics of a low-speed system.

We have recently [18,19] shown that the trajectory predicted by general-relativistic mechanics for a *low-speed weak-gravity* system is not always well-approximated by the trajectories predicted by special-relativistic and Newtonian mechanics for the same parameters and initial conditions. We expect similar breakdown of agreement in the statistical predictions for the mean, standard deviation and probability density function of the position and momentum. Finally, it would also be interesting to compare the thermodynamics predictions of classical Newtonian statistical mechanics with the predictions of classical special-relativistic statistical mechanics at low speed.

Author Contributions

Conceived and designed the experiments: SNL BLL. Performed the experiments: SNL. Analyzed the data: SNL BLL. Contributed reagents/materials/analysis tools: SNL BLL. Wrote the paper: SNL BLL.

References

1. French AP (1968) Special relativity. Cambridge: Thomas Nelson & Sons. 167 p.
2. McComb WD (1999) Dynamics and Relativity. Oxford: Oxford University Press. preface.
3. Hartle JB (2003) Gravity: An introduction to Einstein's general relativity. San Francisco: Addison-Wesley. 88 p.
4. Lan BL (2006) Comparison of the Newtonian and relativistic predicted trajectories for a low-speed periodically delta-kicked particle. Chaos 16: 033107.
5. Lan BL (2009) Disagreement between Newtonian and relativistic trajectories for a low-speed kicked dissipative system. In: Skiadas CH, Dimotikalis I, Skiadas C, eds. Topics on chaotic systems World Scientific. pp 199–203.
6. Lan BL, Cheng HY (2010) Newtonian and special-relativistic predictions for the trajectory of a slow-moving dissipative dynamical system. Commun. Nonlinear Sci. Numer. Simulat. 15: 2497–2503.
7. Lan BL, Borondo F (2011) Newtonian and special-relativistic predictions for the trajectories of a low-speed scattering system. Phys. Rev. E 83: 036201.
8. Lan BL (2009) Implications of the disagreement between Newtonian and relativistic low-speed trajectories. Chaos, Solitons and Fractals 42: 534–537.
9. Chirikov BV (1979) A universal instability of many-dimensional oscillator systems. Phys. Rep. 52: 263–379.
10. Casati G, Chirikov BV, Izrailev FM, Ford J (1979) Stochastic behavior of a quantum pendulum under a periodic perturbation. In: Casati G, Ford J, eds. Stochastic Behavior in Classical and Quantum Hamiltonian Systems. Berlin: Springer. pp 334–352.
11. Chernikov AA, Tél T, Vattay G, Zaslavsky GM (1989) Chaos in the relativistic generalization of the standard map. Phys. Rev. A 40: 4072–4076.
12. Nomura Y, Ichikawa YH, Horton W (1992) Nonlinear dynamics of the relativistic standard map. Phys. Rev. A 45: 1103–1115.
13. Ciubotariu C, Badelita L, Stancu V (2002) Chaos in dissipative relativistic standard maps. Chaos, Solitons and Fractals 13: 1253–1267.
14. Fox RF, Elston TC (1994) Chaos and the quantum-classical correspondence in the kicked pendulum. Phys. Rev. E 49: 3683–3696.
15. Lan BL (1994) Wave-packet initial motion, spreading, and energy in the periodically kicked pendulum. Phys. Rev. E 50: 764–769.
16. Campbell DK (1987) Nonlinear science from paradigms to practicalities. Los Alamos Sci. 15: 218–262.
17. Pospelov M, Romalis M (2004) Lorentz invariance on trail. Phys. Today 57: 40–46.
18. Liang SN, Lan BL (2011) Newtonian versus general-relativistic prediction for the trajectory of a bouncing ball system. Results in Physics 1: 36–39.
19. Liang SN, Lan BL (2012) Comparison of Newtonian and special-relativistic trajectories with the general-relativistic trajectory for a low-speed weak-gravity system. PLoS ONE 7(4): e34720.